Evolution of Collective Structure in the rare-earth nuclei on the basis of the Nilsson model

Diploma Thesis

by
Christoph Hinke

December 2005

Prof. Dr. Reiner Krücken
Institut für Experimentalphysik E12
Physik Department, Technische Universität München
James-Franck-Strasse
85748 Garching
Germany

Abstract

Within this thesis we are investigating how recent fit results for well-deformed rare earth nuclei [16, 17] within the Extended Consistent Quadrupole Formalism (ECQF) [14] of the algebraic interacting boson model (IBA) [13, 15] can be understood in terms of the single-particle structure of these nuclei. Particularly the IBA results seem to indicate that the softness of the deformation dependent potential in the γ-degree of freedom, the deformation away from axial symmetry, evolves quite differently along different isotopic chains. Therefore we have concentrated on investigating the evolution of the single-particle structure of the γ-vibrational 2^+ state in well deformed rare earth nuclei. The study was performed on the basis of simplified calculations within the framework of the Random Phase Approximation (RPA) [1, 9-11]. As input, the single particle levels within the deformed shell model (Nilsson model [12]) were used together with experimentally known ground state deformations and excitation energies.
The RPA results clearly show the connection between the quasi-particle structure of the gamma-vibrational state and the fit results of the IBA.

Contents

Chapter 1

Introduction

Within this thesis we are investigating how recent fit results for well-deformed rare earth nuclei [16, 17, 18] within the Extended Consistent Quadrupole Formalism (ECQF) [14] of the algebraic interacting boson model (IBA) [13, 15] can be understood in terms of the single-particle structure of these nuclei. Particularly the IBA resutls seem to indicate that the softness of the deformation dependent potential in the γ-degree of freedom, the deformation away from axial symmetry, evolves quite differently along different isotopic chains. The reason for this quite different behaviour may lie in the single particle structure of these nuclei. It is the aim of this work to investigate the potential connection between the different evolution of the parameters within the IBA to the underlying single-particle structure.
In the first section of the introduction we give a short overview of nuclear models. After that we go into details concerning the aim of this thesis.

1.1 Single-particle versus collective models

In nuclear structure physics we are concerned with a system of particles whose number is neither small enough to allow direct solutions nor large enough so that we are able to apply statistical methods. Furthermore, it was not possible till today to deduce a final form for the interaction between the particles.

The natural choice of the degrees of freedom in the framework of a single-particle model is of course given by adopting the degrees of freedom of all particles in the nucleus. This implies that the wave function depends on all of theses variables. The corresponding Hamilton operator should incorporate a kinetic term and a potential representing the nucleon-nucleon interaction taking into account all degrees of freedom for each pair of nucleons. A further necessity is to include three body inter-

actions, as well. It is obvious that even for the fastest computers it is a tremendous problem to solve the many-body Schrödinger equation directly for nuclei consisting of more than a few nucleons. Such ab initio calculations have only been performed for nuclei up to mass $A \approx 10$ [6]. It is therefore necessary to look for appropriate methods of approximation.

The idea, that a nucleus can be approximately considered as a system of independent nucleons in a spherical average potential which do not interact directly with each other, is known as the shell model [1, 2, 5]. The fundamental insight which made this phenomenological single-particle model to a powerful tool in nuclear physics was the introduction of a strong spin-orbit force in addition to the average potential (Goeppert-Mayer, Jensen). The Nilsson model [12] which will be extensively used and discussed in this work is a phenomenological single particle model describing the energies and wave functions of states in a deformed nucleus [5]. It is an extension of the well known shell model successfully applied in the spherical case. In the Nilsson model the symmetry of the nucleus is reduced from spherical to axial symmetry and the degeneracy of the levels with fixed j (total angular momentum quantum number) is broken with respect to the magnetic substate quantum number m. A related effect of a quadrupole deformation of the nucleus on the energy levels for a growing deformation parameter is the gradual disappearance of the significant energy spacings known in the shell model at the so-called magic numbers. The shape of the potential, in which all the nucleons are moving, is determined by the average field which is generated by the nucleon-nucleon interaction. In the Nilsson model the mean-field potential is basically that of a three dimensional anisotropic harmonic oscillator.
The success of the phenomenologically introduced shell model justifies the assumption that nucleons move independently in an average potential produced by all the nucleons. With the Hartree-Fock method it is possible to extract such a mean field potential out of the sum of two-body interactions. In modern calculations non-relativistic and relativistic self-consistent mean-field models are used for the description of nuclear structure. For recent reviews see Ref. [7, 8].
It was also a theoretical achievement of basic importance in the early 1960s when it was demonstrated that the macroscopic collectivity as observed for instance in vibrational excitations of nuclei could indeed result from the shell model - the standard microscopic model in nuclear physics - with appropriate and reasonable realistic residual interactions (Ref. [20]).

On the other hand collective models play also an important role. These models depend on degrees of freedom which do not belong to single nucleons. Instead they are based on some of the collective properties of a nucleus as a whole. A trivial example for a collective coordinate is the vector of the centre of mass of the nucleus. In this simple case it is relatively easy to express the collective coordinate by the microscopic coordinates which enables us (at least in theory) to shift from one representation to the other. But in most cases the collective coordinates which are introduced are without any obvious connection to the microscopic physics. An

example is the expansion of the surface of the nucleus into spherical harmonics and to use the coefficients as coordinates. In this special case of a geometrical model [1] the nucleus is treated as a liquid drop of an incompressible fluid. Excitations of the surface of the nucleus i.e. oscillations are expressed by a time dependence of the coefficients obeying an equation of motion.

A completely different approach to describe collective motion in nuclei is the interacting boson approximation (IBA) [13, 15], an *algebraic model*, developed by Arima and Iachello in 1974. The basic idea of the IBA is to assume that low-lying collective states in even-even nuclei can be described by a system of interacting s and d bosons carrying angular momenta 0 and 2, respectively. In this model pairs of like nucleons in the valence shell are treated as bosons and the total boson number of the two kinds of nucleons (for protons and neutrons separately counted to the nearest closed shell) is conserved in the system. This restriction originates from the assumption that the s- and d-boson degrees of freedom can be related directly to L=0 and 2 excitations of pairs of fermions[1] in a spherical shell-model basis. These bosons may also interact via one- or two-body interactions with each other. A universal Hamilton Operator is constructed which is indeed able to reproduce the low-lying collective levels in various nuclei by adapting some free parameters.

To complete and to round off the previous discussion one can say that the final destiny will be to unite the microscopic and collective models. The way this is supposed to work is also clear: the collective models should be explained and expressed by the underlying microscopic approaches. Collective models would be used to classify spectra and their structure while microscopic models should explain why collective coordinates of a certain type lead to a valid model.

1.2 Evolution of γ-softness in the deformed rare earth nuclei

Recently, there have been efforts to determine sets of interacting boson model (IBA) parameters that reproduce the properties of all low-lying, positive-parity excitations, including the first excited 0^+ state, for a wide range of even-even, collective nuclei [16,17]. In the rare-earth region detailed fits of isotopic chains were shown to reproduce the energies of positive-parity states and to provide a reasonable description of their transition matrix elements.
The calculations were performed in the framework of the IBA-1. In this model no distinction is made between neutrons and protons. Furthermore the *extended consistent Q formalism* (ECQF) [14] was used applying a simplified version of the IBA

[1] Due to this relation the pairing force is a crucial ingredient for the assumption leading to the IBA.

Hamiltonian. We will go into further details on the IBA in section 3.4.
In this case the Hamiltonian only involves two parameters, ζ and χ, and the corresponding parameter space is traditionally represented by a triangle [19] with one IBA dynamical symmetry at each vertex. The three symmetries are given by $\zeta = 0$, any[2] χ for U(5), $\zeta = 1$, $\chi = -\sqrt{7}/2$ for SU(3), and $\zeta = 1$, $\chi = 0$ for O(6). Nuclei lying in the transition regions between the three symmteries can be described with intermediate parameter values (figure 1.1). For the explicit mapping of the IBA symmtery triangle the parameters ζ and χ are transformed into polar coordinates ρ with $0 < \rho < 1$ and θ with $0° < \theta < 60°$. The angle θ is proportional to the parameter χ in the Hamiltonian and solely depends on this parameter. The explicit transformation formula is given in section 3.4. The slanting lines in the triangle indicate the phase transition region from spherical (nuclei lying close to the U(5) limit) to deformed nuclei.

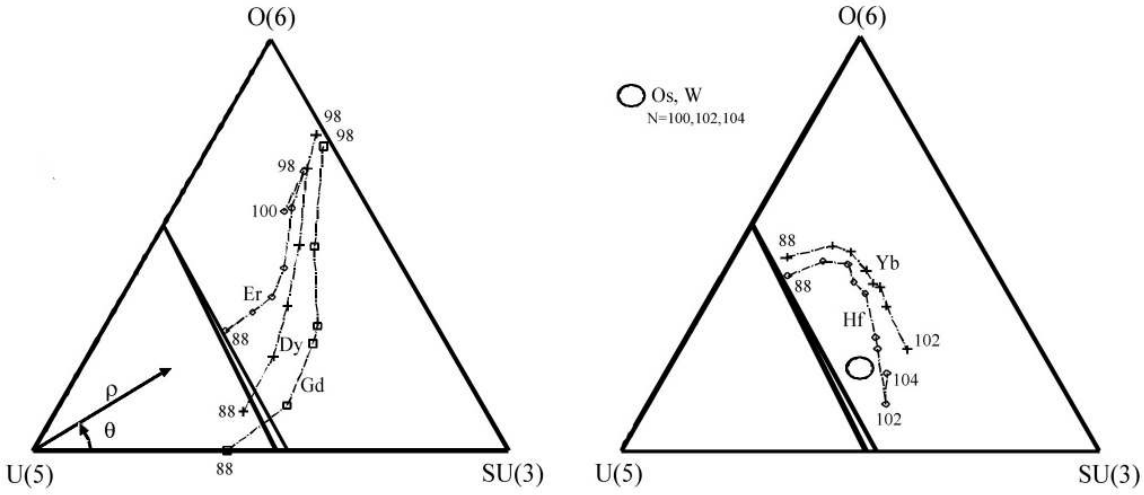

Figure 1.1: Trajectories in the IBA symmetry triangle for the Gd, Dy, Er, Hf, and Yb isotopic chains [16]. The area surrounded by a circle in the triangle on the right side indicates the approximate location of the Os and W isotopes with a neutron number of 100, 102 and 104 [17]. The slanting lines enclose the region of phase coexistence and phase transition from spherical to deformed (corresponding to calculations performed with a boson number equal to ten).

A look at the parameters determined in the IBA fits (shown in figure 1.1) for various rare earth nuclei reveals a crucial difference in the behaviour of the Gd, Dy and Er isotopic chains in comparison to the Yb and Hf isotopic chains. All nuclei cross the phase transition region from spherical to deformed around neutron numbers 88 and 90. Past this region the Gd, Dy isotopes start out at the bottom of the triangle, Er

[2] this is not excactly correct: The U(5) Hamiltonian is indeed independent of the parameter χ, but the E2 operator still depends on χ. Therefore the IBA symmtery triangle should actually be a rectangle.

starts out rather at the center of the triangle, and they all move towards the O(6) limit, while the Yb and Hf isotopes move from a position near the U(5)-O(6) leg of the triangle towards the U(5)-SU(3) leg.
This drastic change of the evolution within the triangle when going from Er to Yb (just adding two protons) seems quite puzzling. The explanation of the trends in the framework of the underlying single-particle structure is the central aim of the present work.
For this purpose it seems to be a reasonable starting point to consider the microscopical composition of the collective gamma-vibrational 2^+ state. We will justify this claim in the following paragraph.

In chapter 2 we will introduce the *geometric collective model* (GCM) [1, 5] in which the surface of the nucleus is expanded into spherical harmonics. The quadrupole deformations consist of five independent degrees of freedom, among those are two surface parameters, describing the β and the γ-degree of freedom, and three angles. In the GCM Hamiltonian the potential V is dependent on β and γ (chapter 2 equation (2.2)). The IBA symmetries just introduced correspond to certain solutions of the GCM determined by the shape of the potential $V(\beta, \gamma)$. For a deformed nucleus the two IBA symmetries SU(3) ($\chi = -\sqrt{7}/2$, $\theta = 0°$ and $\zeta = 1$) and O(6) ($\chi = 0$, $\theta = 60°$ and $\zeta = 1$) are equivalent to the *deformed axially symmetric rotor* and the *gamma-unstable deformed rotor* in the GCM, respectively.
The potential V for the *deformed axially symmetric rotor* has a minimum at a deformation parameter $\beta \neq 0$ and in the γ-direction the potential has a minimum at 0°. For small excursions in the γ-direction away from the minimum the potential shows a steep rise. Nuclei with such a potential are called γ-rigid.
The limit of the *gamma-unstable deformed rotor* is also given by a finite quadrupole distortion, but the potential V is completely independent of the parameter γ (i.e. it has a flat shape in this direction). Consequently the nuclei corresponding to this limit are called γ-soft. The U(5) limit corresponds to the *spherical vibrator* with a potential showing a minimum at $\beta = 0$ and $\gamma = 0°$. In fact for a U(5) nucleus the notion of gamma-softness does not make sense anymore.

This discussion shows that the IBA parameter χ (and the angle θ) are in some way related to the *gamma-softness* of nuclei. Actually nuclei lying on the U(5)-SU(3) leg of the triangle are gamma-rigid and analogously nuclei lying on the U(5)-O(6) leg of the triangle are completely flat in the gamma direction.
The different evolution of the Gd, Dy, Er isotopic chains in contrast to the Yb, Hf isotopic chains can now be classified in terms of increasing and decreasing gamma-softness.
When we speak of gamma-softness in the context of the well-deformed rotational nuclei with $R_{4/2}$ values larger than 2.9 we do not refer to the potential energy surfaces (GCM potentials) that are nearly independent of γ. However, depending on the angle Θ in the IBA triangle the potentials are more ($\Theta \approx 0°$) or less ($\Theta \approx 60°$) stiff in the γ-degree of freedom.

It is the aim of the present work to investigate if the different evolution of the ECQF IBA fit paramters [16, 17] within the symmetry triangle can be understood in terms of a microscopic picture. Since the value of χ and thus the angle Θ is related to the γ-softness we expect that there is some relation to the microscopic structure of the γ-vibrational 2^+_γ state. Thus we will investigate how the structure of the 2^+_γ state evolves within a simplified RPA approach along the isotopic chains.

The chapters of this thesis are organized in the following way: In chapter 2 we start out with a review of the phenomenological description of collective motion in nuclei and introduce the *geometric collective model* (GCM) [1, 5]. After that we focus on the gamma-vibration in the context of the *rotation-vibration model* [1] and finally describe the microscopical properties of collective excitations. Chapter 3, "Description of models", forms the basis for the calculations performed in the present work. We discuss the Nilsson model [12] and pairing correlations [5]. Finally we introduce the *Random Phase Approximation* [1, 9-11] in order to treat the gamma-vibration in deformed nuclei. A short excursion reviewing the basics of the Interacting Boson Model (IBA) [13, 15] is included at the end of the chapter.
In chapter 4 the results concerning the microscopical composition of the gamma-vibrational wave function obtained in our calculations for Gd, Dy, Er, Yb, Hf, Os, W and Pt isotopes are presented. We also discuss various simplifications applied in our approach and their consequences. For some nuclei the composition of the wave function is compared to previous calculations by *Bès et al.* (Ref. [20]) and *Soloviev et al.* (Ref. [24, 27]) showing that our simplified model reproduces the main features obtained by these more sophisticated models. Chapter 5 contains the discussion of our results with regard to the evolution of the rare-earth nuclei in the symmetry triangle determined in the recent IBA fits by *McCutchan et al.* [16,17] as outlined in the introduction.

Chapter 2

Phenomenological description of collective nuclear motion

The most obvious characteristic of nonspherical nuclei is that they can undergo rotations about an axis perpendicular to the symmetry axis. They can, of course, also vibrate and, moreover, rotations can be coupled to vibrational motion. Considering the low-lying energy spectra of deformed even-even nuclei, exactly these collective modes i.e. the corresponding states, can be observed. At higher energies of more than $\approx 2MeV$, starting at about twice the pairing-gap, in deformed even-even nuclei single two-quasiparticle excitations[1] are also observed. These characteristic vibrational and rotational band structures have been for the first time interpreted in the *geometric collective model* [1] which was proposed by Bohr and Mottelson and refers to excitations of the surface of the nucleus. More precisely speaking, the underlying physical picture of the nucleus used here is that of a classical, charged liquid drop. This concept is also leading to the well-known *Bethe-Weizsäcker mass formula* [3]. In the current application it is extended with the feature of dynamical excitations of the nucleus. As already stated, the nuclei are assumed to have a constant mass densitiy (incompressibility of nuclear matter) and a sharply limited surface. The interior structure i.e. the excistence of individual nucleons is neglected in favour of a homogenous, liquid-like nuclear matter.
Along with these assumptions the moving surface of the nucleus can be parameterized by an expansion into spherical harmonics with time-dependent surface parameters as coefficients.

$$R(\theta,\phi,t) = R_0[1 + \sum_{\lambda=0}^{\infty}\sum_{\mu=-\lambda}^{\lambda} \alpha^*_{\lambda\mu}(t) Y_{\lambda\mu}(\theta,\phi)] \tag{2.1}$$

[1] For the moment the two-quasiparticle excitations may be considered as simple particle-hole excitations - they will be discussed extensively later on in the theoretical part about the pairing force.

$R(\theta, \phi, t)$ is the radius of the nucleus in direction (θ, ϕ) at the time t. R_0 denotes the radius of a nucleus with a spherical shape which comes about if all the coefficients $\alpha_{\lambda\mu}$ vanish. These time dependent amplitudes describe the vibration of the nucleus and thus serve as collective coordinates. Their equation of motion is determined by the corresponding Hamilton operator.
The multipole expansion just derived shows that there are several kinds of possible multipole deformation. For $\lambda = 0$ we have the monopole mode which is connected with a change in the radius of the nucleus. An excitation of this mode would require a lot of energy because of the almost incompressible nuclear matter. Dipole deformations $\lambda = 1$ lead in the lowest order just to a translation of the center of mass of the nucleus and thus they should not be considered for nuclear excitations. Finally, *quadrupole deformations* with $\lambda = 2$ (the parity π is given by $(-1)^\lambda$) are one of the most important collective excitation modes of nuclei. Modes with higher angular momentum than $\lambda = 4$ have no further importance[2].
It is possible to show mathematically that there are only five independent degrees of freedom connected with the quadrupole deformations. A transformation[3] of the corresponding coordinates leads to a more convenient interpretation of the expansion coefficients. It yields three Euler angles and two intrinsic variables.
The Euler angles determine the orientation of the nucleus referring to the laboratory system. The two parameters β and γ represent the extent of the quadrupole deformation and the degree of axial asymmetry, respectively. Most deformed nuclei are axially symmetric in their ground states corresponding to $\gamma = 0°$ (completely triaxial shapes have 30°). Prolate nuclei have a deformation parameter $\beta > 0$ and oblate nuclei consequently have a deformation parameter $\beta < 0$ ($\beta \sim \Delta R/R_{av}$ with ΔR being the difference between semi-major and semi-minor axes of the spheroid and $R_{av} = r_0 A^{1/3}$ being the average radius). The larger the value of β the more deformed the nucleus. The essential difference between prolate and oblate shapes is that the former is extended in one direction and squeezed in two, while oblate shapes are extended in two and compressed in one. All of the rare-earth nuclei considered in this work have a prolate shape [5].
The advantage of the transformation just introduced is that rotations and vibrations of the surface are clearly separated from each other. A change in the Euler angles describes a pure rotation of the nucleus without any change of its shape. It should be explicitly mentioned that quantum mechanical symmetry arguments do not permit a spherical nucleus to have any rotational excitations and a nucleus with axial symmetry may not execute rotations around its symmetry axis, only around

[2] Just to be complete: octupole deformations with $\lambda = 3$ are the leading asymmetric modes of the nucleus and are connected with negative parity states. $\lambda = 4$ modes are sometimes observed as admixtures to quadrupole excitations.

[3] definition of β, γ and Ω: $\alpha'_{20} = \beta cos(\gamma)$, $\alpha'_{22} = \beta sin(\gamma)/\sqrt{2}$, $\alpha_{2\mu} = \sum_\nu D^2_{\mu\nu}(\Omega)\alpha'_{2\nu}$ where $D^2_{\mu\nu}$ is a rotation matrix and Ω represents the three Euler angles, $\alpha_{2\mu}$ are the expansion coefficients from formula (2.1)

axis perpendicular to it. The geometric collective model (GCM) Hamiltonian in a simplified form [5] is given by formula (2.2).

$$H = T + V = \frac{1}{B_2}[\pi \times \pi]^{[0]} + C_2'\beta^2 + C_4'\beta^4 - C_3'\beta^3 cos3\gamma \tag{2.2}$$

It contains 4 parameters: B_2 for the kinetic energy and C_2', C_4', C_3' for the potential. π are the conjugated momentum coordinates. This Hamiltonian is able to describe low energy collective motion in nuclei from purely vibrational to axially symmetric rotors as well as transitional nuclei between these extreme limits.

The most important special case of collective surface motions is given by well-deformed nuclei which have a deep energy minimum at an axial deformation ($\beta_0 \neq 0$) like a rigid rotor, but with the additional possibility of small oscillations in the β- and γ- degrees of freedom (all of the rare-earth nuclei considered in this work are such candidates) [1]. In the framework of this *rotation-vibration model* [1] the following formula represents the energy spectrum that is expected.

$$E_{n_\beta n_\gamma IK} = \hbar\omega_\beta(n_\beta + \frac{1}{2}) + \hbar\omega_\gamma(2n_\gamma + \frac{1}{2} \mid K \mid +1) + \frac{\hbar^2}{2J}(I(I+1) - K^2) \tag{2.3}$$

The quantum number K is the projection of the angular momentum I on the symmetry axis of the nucleus. It is obvious that for a given K the quantum number I has to obey the relation $I \geq K$. The angular momentum cannot be less than its projection. n_β and n_γ are the quanta of the vibration in the β- and γ-degree of freedom, respectively. J represents in this context the moment of inertia. The quantum numbers are permitted to take on the following values:

$$K = 0, 2, 4, ... \tag{2.4}$$

$$I = \begin{cases} K, K+1, K+2, ... & for K \neq 0 \\ 0, 2, 4, ... & for K = 0 \end{cases} \tag{2.5}$$

$$n_\gamma = 0, 1, 2, ... \text{ and } n_\beta = 0, 1, 2, ... \tag{2.6}$$

The structure of the spectrum is shown in figure 2.1 on the next page. The bands are characterized by the quantum numbers that have just been introduced. They obey to the $I(I+1)$ rule of the rigid rotator.
The ground state band (g.s.) is shown on the left with an even I of all levels. The β-band with one vibrational quantum in the β-direction starts at an energy of $\hbar\omega_\beta$ above the ground state band (one phonon excitation) and contains also only even angular momenta. From all the other bands that are shown in the illustration the γ-band is of major importance here because the present work is dedicated to investigate the first excited state 2_γ^+ of the gamma-vibrational band.

The γ-band is not, as the name suggests, simply the band with a vibrational quantum in the gamma-direction. Instead the projection of the angular momentum on the symmetry axis, K, is equal to 2. The spectrum of the γ-band starts with a 2^+

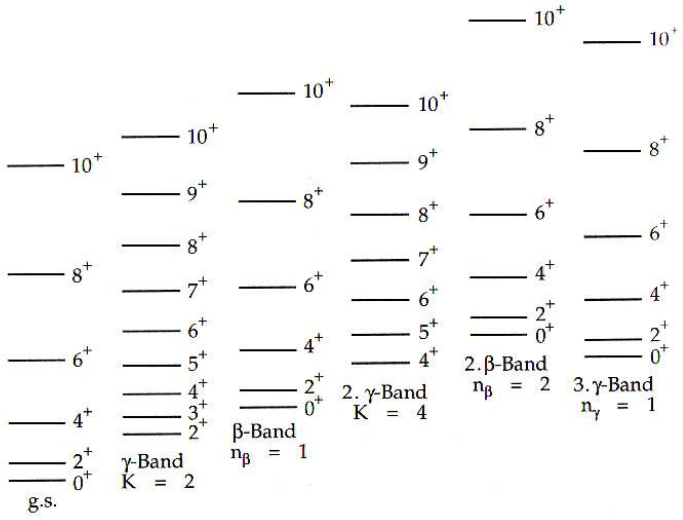

Figure 2.1: Structure of the energy spectrum resulting from the rotation-vibration model. In deformed nuclei the levels near the ground state belong to a rotational band (characteristic $I(I+1)$ energy spacing). However, they exhibit excited states of the vibrational type, the most important ones being the quadrupole β- and γ-vibrational states. The ground state rotational band is accompanied by several other rotational bands which are built upon the vibrational excitations. (Indeed there have been doubts in the last years whether the $K = 0$ band can be really identified with the β-vibration, but this is of minor interest for this work.) This illustration was redrawn from Ref. [1].

state and contains the odd angular momenta, as well.
The band head has an excitation energy of $E_\gamma = \frac{\hbar^2}{J} + \hbar\omega_\gamma$ and therefore it incorporates both a contribution of the rotation and a contribution of the γ-vibration. Indeed there is a strong coupling between the gamma-vibration and rotational motion. Rotations with a non vanishing K value (for the bandhead of the γ-band with $I = K$ this means rotations around the symmetry axis of the nucleus) are only possible in the presence of dynamical triaxial deformations (remember the quantum mechanical limitation just discussed).

Illustrations of the β-vibration and especially the γ-vibrational motion are shown in figure 2.2. The β-vibration with $K = 0$ is aligned along the symmetry axis (fluctuations in the quadrupole deformation β) and therefore it preserves axial symmetry. The $K = 2$ γ-vibrational mode represents a dynamic time-dependent excursion from axial symmetry (osciallations in γ). It has an average value of $\gamma = 0°$ but the values of maximum triaxiality at the turn back points during vibration can be large. However the vibration is a rather complex motion. A pure shape oscillation would not lead to an angular momentum projection of $K = 2$ along the symmetry axis of the nucleus. During the vibrational motion the axial symmetry is broken and that is why additionally a rotation about the former symmetry axis can occur. The superposition of the vibrational and rotational motion is therefore a kind of oscillating

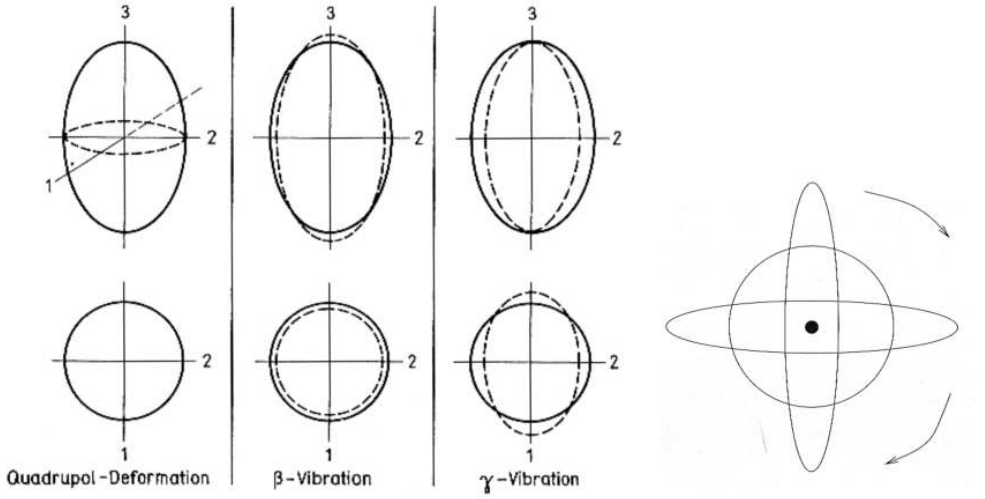

Figure 2.2: Left side: Let us assume that the deformed nucleus has an equilibrium prolate axial symmetric shape (3 denotes the symmetry axis). When the prolate spheroid remains a prolate spheroid and only its degree of deformation changes in course of the oscillation, we have the β-vibration. Similarly, when the prolate spheroid keeps its deformation parameter the same, but acquires a little bit of a triaxial shape during the course of oscillation we have a γ-vibration. This illustation on the left side was taken from Ref. [2].
Right side: This picture shows a schematic illustration of the motion in a γ-vibration. The symmetry axis points out of the page. The circle represents an end-on view of the axially symmetric ground state shape. The ellipses are the extremes of squashing during the vibrational excursions away from axial symmetry. The arrows represent the rotational motion about the symmetry axis which occurs when the nucleus takes on axially asymmetric shapes. This illustration was taken from Ref. [5].

tumbling motion about the symmetry axis of the deformed nucleus in its ground state [5]. The rotational band built on top of the gamma-virbation does not change $K = 2$ because the projection of any rotation perpendicular to the symmetry axis onto this axis is of course zero.

So far we have discussed the geometrical features of the γ-vibration. In this work the microscopic structure of the first excited gamma vibrational state will be examined extensively and thus the last part of this introduction shall illuminate the microscopical properties of collective excitations such as the γ-vibration.

As already mentioned in the last section the nucleus can be described as a many-body system which consists of nucleons moving in an average field. These nucleons are interacting weakly through a residual interaction - in the special case of the γ-vibration particle-holde exciatations are assumed to be generated by the $r^2Y_{2\pm2}$ operator. Of course the pairing force is also taken into consideration by absorbing its

effect into the ground state, which becomes therefore more complex, and by changing the elementary excitation mechanism from particle-hole to two quasi-particle excitations.

It is obvious that such a many-body system will have excited states corresponding to the excitation of one or a few pairs of quasi-particles. This type of excitation mode of the nucleus is well-known near closed shells with single-particle/hole excitations. Moreover, there is an altogether different kind of excitation mode of a many-body system - a mode in which many particles/quasi-particles participate in a coherent manner which is called a collective state. To be more precise, one can say that for an even-even nucleus the elementary non-collective excitation modes of the lowest energies correspond to the creation of a pair of quasi-particles and the microscopic theory of vibration can be built up by the *coherent superposition of many quasi-particle pair states*.

In case of the 2^+_γ state the angular momenta of the two-quasiparticle excitations couple to a total angular momentum of $2\hbar$. Indeed, the simplest explanation for a 2^+ state could be the breaking of only one pair of nucleons[4] and the coupling of these two nucleons to the second energetical favourable configuration with $J^\pi = 2^+$ (according to the Pauli principle two like fermions in the same orbit may only be coupled to an even angular momentum and moreover assuming a reasonable short-range interaction the coupled states are not degenerate anymore - the lowest state is 0^+, followed by 2^+). But the very low energy of the state in question in comparison to the energy of two quasi-particle excitations and measurements of the reduced transition probabilities to the ground state which turn out to be much higher than those for one-particle/two quasi-particle excitations spoil this simple interpretation. They suggest the participation of many nucleons. Indeed it is relatively easy to construct $K = 2$ two quasi-particle states by breaking up many nucleon pairs and elevating one particle of each broken pair to an excited quasi-particle level. Of course only couples of single-particle states that are connected by the $r^2Y_{2\pm2}$ operator and thus have a non-zero transitional matrix element between them can contribute (corresponding to the mechanism just mentioned) to the gamma vibration.

The summarized characteristic features of collective states are thus *low excitation energies*, compared to single two quasi-particle excitations (which have an energy of at least twice the pairing gap with about $1.5 - 2MeV$), and furthermore due to the many contributing components *high electromagnetic reduced transition probabilities* to the ground state which are observed experimentally [3].

In general one can say that the collective correlated wave function consists of a sum of almost equal amplitudes for all particle-hole/two quasi-particle excitations. All of the amplitudes are in phase i.e. they contribute with the same sign. This

[4] The coupling of two like nucleons to a pair with $J = 0^+$ is a consequence of the pairing residual interaction. Furthermore it is responsible for the 0^+ ground state of all even-even nuclei.

means that collective vibrations can be written as a linear combination of two-quasiparticle excitations (in the non-pairing terminology, particle-hole excitations) across the Fermi surface[5] [5].

The microscopic picture of the vibration, as outlined above, apparently seems rather far-fetched from the classical picture of the vibration which consists of a certain dynamical variable oscillating as a function of time. In reality, however, there is indeed an underlying link between these pictures. The nuclear vibrational state, which is a coherent superposition of many elementary excitation modes of the particle-hole (or pair of quasi-particles) type, corresponds to a single-particle densitiy variable that oscillates in time.

In the following chapter the single-particle character of the γ-vibration will be shown more explicitly when we introduce the Random Phase Approximation (RPA).

[5] The Fermi level denotes the highest occupied level in a nucleus. In the context of the pairing force a generalized Fermi energy is defined. This becomes necessary because the occupation probability of the nucleons near the former (shaply defined) Fermi level is now smeared over some states as a consequence of pair scattering.

Chapter 3

Description of the models

In this chapter the appropriate framework for the construction of single-particle states in deformed nuclei is introduced. After that the pairing residual interaction is discussed and we show its crucial impact on the single-particle states. Furthermore the random phase approximation (RPA), a powerful tool in treating collective excitations in nuclei, is derived and the basics of the interacting boson model (IBA) are discussed.

3.1 Nuclear deformation and the Nilsson model

In spherical nuclei, i.e. nuclei with neutron and proton numbers near closed shells, the well-known *shell model* [1, 2] is used to treat the states in order to set up the single-particle wave functions and to classify the corresponding quantum numbers. However, a lot of heavy nuclei are well-deformed with neutron and proton numbers far away from closed shells. The investigation of the impact of the quadrupole deformation on single particle orbits leads to a new approach as a refinement of the shell model, the *Nilsson model* [12] which treats the single-particle states in a deformed potential.
In this work we will concentrate on the well deformed rare earth nuclei (figure 3.1) with $R_{4/2} \equiv \frac{E(4_1^+)}{E(2_1^+)} > 2.90$. We will also treat, for comparison, γ-soft and transitional nuclei, like the Pt isotopes, with $R_{4/2} \approx 2.5$.

In the shape transition region the evolution from spherical nuclei with vibrational character to deformed nuclei is connected with a change in their characteristic low-lying energy levels. For an ideal spherical harmonic vibrator the one phonon excitation yields a 2^+ state and at twice this energy we find the two phonon excitation with three degenerate states with $J^\pi = 0^+$, $J^\pi = 2^+$ and $J^\pi = 4^+$ ($R_{4/2} \approx 2.0$). In the deformed nuclei the ground-state band with $R_{4/2}$ close to 3.33 takes on rota-

tional character. Additionally one finds a low lying $K = 2$, 2^+ level as band-head of the gamma-vibrational band and a $K = 0$, 0^+-band.

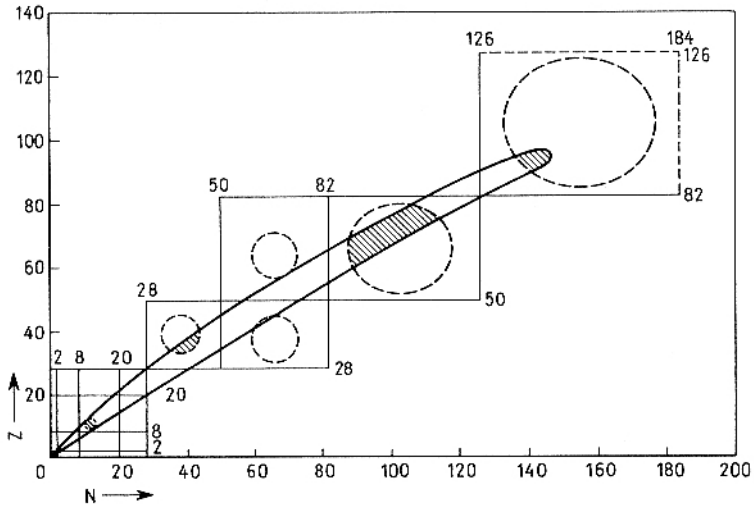

Figure 3.1: Areas of deformed nuclei in the N-Z-plane. The siginficantly deformed regions are marked by surrounding ellipsoids and the hatched area in between denotes stable deformed nuclei. The horizontal and vertical lines denote the magic numbers (closed shells) for neutrons and protons, respectively. The well-deformed rare-earth region is located between 50 and 82 protons and between the neutron numbers of 82 and 126. The illustration comes from the textbook of Mayer-Kuckuk [2].

The average field in which individual nucleons are moving is generated, as already mentioned, exclusively by the interaction with all other nucleons. This implies that the shape of the field is directly related to the density distribution of the nucleons. Since the average field with independent particle motion is only a rough approximation residual interactions have to be taken into account to make a reasonable approach to the physics of the nucleus.
The spherical *shell model* is based on the non-relativistic *Schrödinger equation* for single particles states with a certain potential $V(\vec{r})$.

$$(-\frac{\hbar^2}{2m}\nabla^2 + V(\vec{r}))\psi_i(\vec{r}) = \epsilon_i\psi_i(\vec{r}) \tag{3.1}$$

A reasonable choice of the potential should be a function which has a constant behaviour in the center of heavy nuclei corresponding to the constant mass density of nuclear matter and which decreases rapidly outside the nuclear surface. The best phenomenological potential is the *Woods-Saxon potential* (3.2) which has a shape that is very similar to the measured experimental density distributions of nuclei.

$V_0 \approx 50MeV$ is the depth of the potential, R is the radius of the nucleus defined by $R = 1.3fm \cdot A^{1/3}$ and a is the thickness of the surface $a \approx 0.5fm$.

$$V(r) = -\frac{V_0}{1 + exp[(r - R)/a]} \tag{3.2}$$

Although the *harmonic oscillator potential* (3.3) goes to infinity instead of dropping off to zero for large distances from the center of the nucleus, it is frequently used because of its simple and analytically determinable solutions. Its potential has the form:

$$V(r) = \frac{1}{2}m\omega^2 r^2 \; ; \; \hbar\omega \approx 41MeV/A^{1/3} \tag{3.3}$$

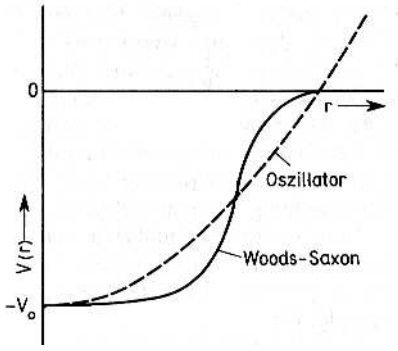

Figure 3.2: Illustration of the Woods-Saxon potential (3.2) and the harmonic oscillator potential (3.3).

Unfortunately all of the suggested potentials are not able to reproduce more than the lowest three magic numbers. It was the introduction of a strong spin-orbit force that couples the spin and the angular momentum of each nucleon which made the nuclear shell model successful (Goeppert-Mayer, Jensen). The additional term in the single particle potential can be written as $C \cdot (\vec{l} \cdot \vec{s})$. C is a constant determining the strength of the spin-orbit force and has a negative sign. Furthermore a $\vec{l}^2$ term is usually incorporated to lower the energies of the single particle states which are closer to the surface of the nucleus. This corrects the steep increase of the harmonic oscillator potential in this area.
The energy levels are characterized by the radial quantum number n, the angular momentum l and the total angular momentum j. The parity of the states is given by the expression $(-1)^l$. Each of these states is degenerate $2j + 1$-times with the magnetic quantum numbers $m_j = -j, -j + 1, ..., j - 1, j$. This approach finally yields the correct magic numbers 2, 8, 20, 28, 50, 82 and 126 both for neutrons and protons i.e. there are big energy gaps in the level scheme to the next empty j-shell for these particle numbers. The ground states of the various nuclei are constructed by simply filling up the single particle states until the Fermi level is reached. The protons differ from the neutrons because of their electric charge and therefore the Coulomb potential should be taken into consideration. In order to get stable nuclei

it is important that the Fermi level of the neutrons is equal to the Fermi level of the protons. Otherwise the difference will be equalized by a β-decay. Hence the proton states which are populated with less particles than the neutron states are lifted by the Coulomb potential. Usually the influence of the Coulomb potential on the energy level sprectrum is ignored and the same level distribution is taken both for neutrons and protons. Of course this yields different Fermi levels for neutrons and protons because the energy levels are filled with a different number of particles.

It is relatively easy to generalize the single particle shell model to treat nuclei with a ground state deformation β_0 which is unequal to zero. The fundamental idea of this extended shell model, the so called *Nilsson model*, is to choose a deformed three dimensional harmonic oscillator potential with different oscillator constants ω_x, ω_y, ω_z in the three directions of space.

$$V(\vec{r}) = \frac{m}{2}(\omega_x^2 x^2 + \omega_y^2 y^2 + \omega_z^2 z^2) \tag{3.4}$$

The geometrical surface of the nucleus is defined as the set of all points (x, y, z) obeying to

$$\frac{1}{2}m\omega_0^2 R^2 = \frac{m}{2}(\omega_x^2 x^2 + \omega_y^2 y^2 + \omega_z^2 z^2), \tag{3.5}$$

where $\hbar\omega_0 = 41MeV/A^{1/3}$ is the oscillator constant of the equivalent spherical nucleus with the radius $R = r_0 A^{1/3}$. It is obvious that equation (3.5) describes an ellipsoid with the axes X, Y and Z given by $\omega_0 R = \omega_x X = \omega_y Y = \omega_z Z$. Furthermore it is necessary to impose the constraint of incompressible nuclear matter which requires the volume of the ellipsoid to be equal to the volume of the corresponding sphere which means $R^3 = XYZ$ and $\omega_0^3 = \omega_x\omega_y\omega_z$, respectively.
Assuming that the nucleus is axially symmetric with respect to the z-axis (a spheroid), i.e. $\omega_x = \omega_y$, and the deviation from a spherical shape is small, it is possible to express the corresponding oscillator constants in the three directions of space in a first order approximation using a deformation variable δ.

$$\omega_x^2 = \omega_y^2 = \omega_0^2(1 + \frac{2}{3}\delta)\ ;\ \omega_z^2 = \omega_0^2(1 - \frac{4}{3}\delta) \tag{3.6}$$

For a prolate deformed spheroid with $\delta > 0$ the frequencies $\omega_{x,y}$ are larger than ω_z. The shape of the potential adopts the assumed nucelar density distribution and thus lowers the energy for oscillations along the symmetry axis z (i.e. making theses oscillations more preferable), while the potential in the x-y-plane perpendicular to the symmetry axis increases. In the introduction the ground-state quadrupole deformation parameter β_0 was used. The parameter δ applied in this chapter and the parameter β introduced in the collective model are almost the same for small deformations. The connection between them is given by $\delta \approx 3/2\sqrt{5/4\pi}\beta \approx 0.95\beta$.
Finally, it is possible to express the appropriate single-particle Hamiltonian for a nucleus with a quadrupole deformed axially symmetric shape around the z-axis as

$$H = T + V = \frac{\vec{p}^2}{2m} + \frac{1}{2}m[\omega_x^2(x^2 + y^2) + \omega_z^2 z^2] + C\vec{l}\cdot\vec{s} + D\vec{l}^2. \tag{3.7}$$

The spin-orbit coupling term is parameterized with a constant C and the strength of the $\vec{l}^2$-term is controlled by a constant D, respectively. The two terms ensure the proper order and energies of the single-particle levels in the spherical limit (the shell model corresponds to $\beta_0 = 0$). The appropriate values of the parameters differ for protons and neutrons and also depend on the nucleon number. Using this deformation-dependent Hamiltonian, the single-particle energies can be calculated as a function of δ. A plot of single-particle energy against deformation is known as a Nilsson diagram, as shown in figure 3.3 for nucleon numbers below 50.

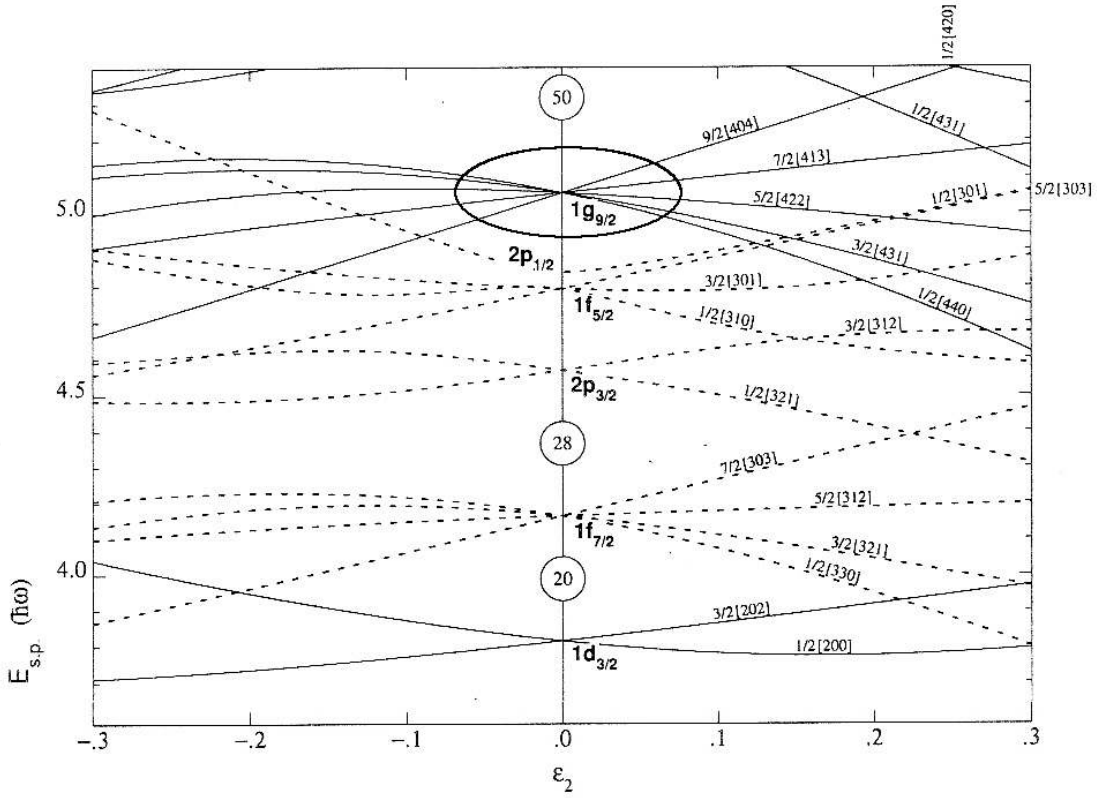

Figure 3.3: Nilsson diagram for protons and neutrons taken from the Nuclear Data Sheets [33]. The deformation paramter ϵ_2 which is used in these diagrams is equal to δ. A prolate deformation is given for $\epsilon_2 > 0$. The diagram starts shortly before the magic number of 20 nucleons and displays states up to the magic number of 50 nucleons. For large deformation parameters the typical gaps known in the spherical shell model between shell closures vanish. For a zero deformation the spherical shell model quantum numbers nlj are given. The deformed states are labled with the asymtotic quantum numbers. The parity of the states is indicated by solid $\pi = +1$ and dashed lines $\pi = -1$. The energy is given in units of $\hbar\omega$ (in our notation $\hbar\omega_0$).

The Nilsson orbitals can be characterised by the so-called asymptotic quantum numbers:

$$K^\pi[N, n_z, \Lambda] \text{ or alternatively } [N, n_z, \Lambda, \Sigma] \,/\, [N, n_z, \Lambda, \pm] \tag{3.8}$$

N is the principal quantum number denoting the major shell (number of the total oscillation quanta), K is the projection of the single-particle angular momentum j (which is no good quantum number anymore for $\beta \neq 0$) onto the symmetry axis z. Furthermore, Λ is the projection of the orbital angular momentum onto the symmetry axis and n_z is the number of oscillator quanta / number of nodes of the wave function along the symmetry axis. The parity π of the state is determined by $(-1)^N$. The projection of the intrinsic spin of the nucleon onto the symmetry axis is $\Sigma = \pm\frac{1}{2}$, thus it is possible to define $K = \Lambda \pm \frac{1}{2}$. The $\pm$ in the last alternative notation just indicates whether the spin aligns or antialigns with the orbital angular momentum. There is another useful condition: If N is even, then $n_z + \Lambda$ must also be even. Similarly, if N is odd, then $n_z + \Lambda$ must also be odd.
The Nilsson diagram in figure 3.3 shows at zero deformation the well known $2j + 1$-fold degeneracy of the spherical shell model. For non-zero deformation the j states split into two-fold degenerate levels. Thus a spherical shell model state j spreads into $j + \frac{1}{2}$ two-fold degenerate levels. In the Nilsson model the former shell model degeneracy is broken according to the orbit orientation (K value / magnetic substate m_j) and each Nilsson orbit can contain only two nucleons corresponding to the two ways ($\pm K$) in which a nucleon can orbit a nucleus (clockwise or counterclockwise). Many properties of the Nilsson model can be understood in simple terms. If one considers the motion of particles around a prolate deformed shape, as shown in figure 3.4, it is possible to define the classical orbit angle θ, as being approximately $\theta = sin^{-1}(K/j)$.

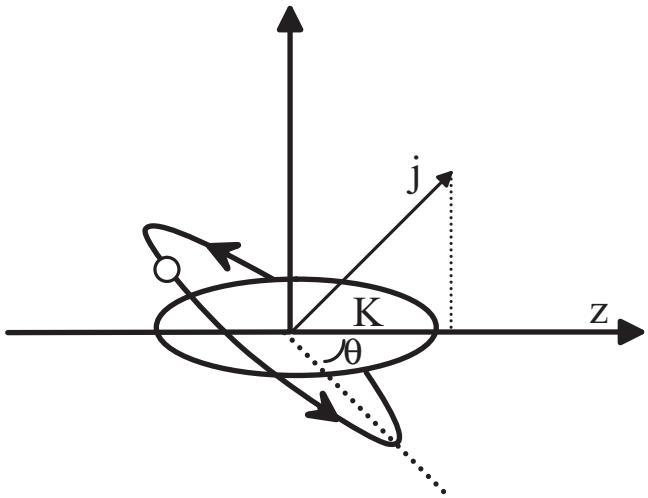

Figure 3.4: Illustration of the bulk of a prolate deformed nucleus with a single particle orbiting in the deformed Nilsson model potential. Furthermore the quantities j, K and θ are defined.

According to the illustration in figure 3.4 it can be seen that low K values correspond to motion around the equator of the nucleus. Since the orbiting nucleon spends more time closer to the bulk of the nuclear matter, these equatorial orbits will be lower

in energy because the nuclear force is attractive and of short range. On the other hand the orbital plane for the highest K values is more or less perpendicular to the symmetry axis and thus the energy of this state will be significantly higher. Consequently, the energy depends on the orientation with respect to the nuclear symmetry axis (K splitting). Moreover, the energies change linearly with increasing deformation δ. In addition, the angle θ changes slowly for low K and more rapidly for higher K (property of the sine-function) and thus the difference in energy between successive K values increases with increasing K. This effect can be seen in the Nilsson diagram in figure 3.3. Especially the $1g_{9/2}$ shell model orbit (emphasized by a circle) is a good example. For oblate deformations ($\delta < 0$) the line of reasoning is basically the same and the energy dependence of the K values is exactly the opposite.
Another interesting feature is given by the fact that orbits with low K values from the shell with the higher j decrease in energy faster with deformation than those from lower j-shells. For the same K a higher j-value leads to a lower angle. Therefore states with the same K and parity can approach each other although the original shell-model energies have a distinct separation.
It is forbidden by the *Pauli Principle* that any two levels with the same quantum numbers may cross (level-level repulsion). Thus we can expect that as an orbit approaches another with the same K^π (in fact K and the partiy π are the only remaining good (i.e. exactly valid) quantum numbers in deformed nuclei) the two levels will repel each other (an infinitesimal interaction will cause them to repel when they get sufficiently close). The interaction between the two orbitals means, however, that although the levels do not cross, the wave function properties are exchanged at the inflection point. This feature can be seen several times in figure 3.5. In the area surrounded by the circle, for example, the $1/2^+[411]$ level originating from the $3s_{1/2}$ state approaches the down sloping $1/2^+[660]$ level originating from somewhere in the 82 to 126 shell. Indeed the levels do not cross but the two states completely mix at the inflection point i.e. for the deformation where the energies of the two states would have crossed the wave function consists of an equal admixture of both states.

Another point to note is that the higher the shell, denoted by the quantum number N, the stronger the effects just discussed will be, since a particle in a higher shell is at larger radius and thus has more to gain energetically upon deformation - if it is located in the equatorial plane.
Neglecting pairing correlations as a rough estimate, in a deformed region the Nilsson orbits are sequentially filled, two protons and neutrons to each successive level until the final neutron / proton number is reached. In order to calculate the total energy of a nucleus a summation of all populated single-particle energies can be made. The steep down-slope of some orbitals as a function of increasing deformation leads to the conclusion that some deformed configurations will have lower energy than a spherical one. Thus, within the framework of the Nilsson model, it is possible to predict stable deformation for nuclei removed from closed shells.
Another important point concerns the separation of rotational and single-particle degrees of freedom. For low spin states it is common to assume that an approximate

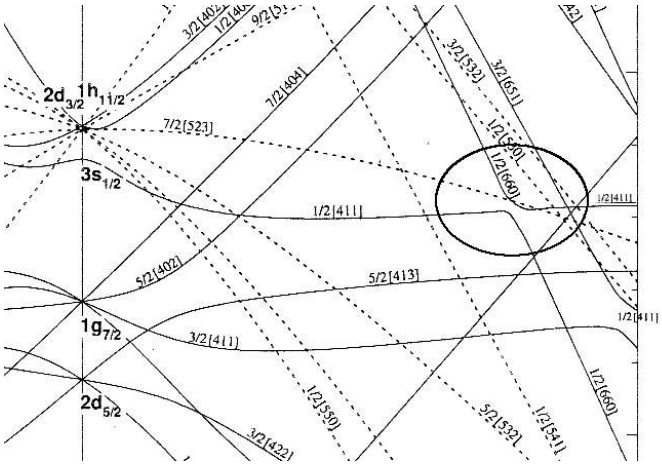

Figure 3.5: This illustration is a part of the 50 to 82 shell of the Nilsson diagram for neutrons. Mainly the part for a prolate deformed nucleus is shown. For a rising nucleon number the level density increases dramatically. Therefore it becomes more likely that levels with the same quantum numbers approach and avoided level crossings can be observed. The diagram was taken from the Nucelar Data Sheets [33].

separation is valid. The single nucleon motion is first evaluated in a body-fixed frame of reference i.e. in the Nilsson model as just derived. Later on the rotational motion is superimposed often neglecting the Coriolis interaction. This way of treatment can only be applied if the nucleus is essentially stationary during a single orbit of the nucleon around the bulk (adiabatic approximation). A model which explicitly incorporates the coupling of single-particle and rotational degrees of freedom is called the *cranked Nilsson model*, but since in this work we are only looking at the first excited state of the gamma-vibrational band these refinements are beyond the scope of this work.

Up to this point in the discussion we have only considered the behaviour for small quadrupole distortions: When deformation sets on, the spherical shell-model quantum number j is no good quantum number anymore. However, it remains an approximately good quantum number for small values of δ. The interaction that leads to configuration mixing of different j shells in the Nilsson model is of quadrupole form and it is not surprising that it increases with deformation. As we have shown, the orbits are characterized by their K quantum numbers and the splitting is linear in δ. Moreover, only K, the parity $\pi = (-1)^N$ and N, respectively, are still good quantum numbers, because their operators commute with the entire Hamlitonian. For large deformations the energies are again linear in δ. This can be easily seen, because the oscillator frequencies are linear in this parameter. The $\vec{l} \cdot \vec{s}$ and $\vec{l}^2$ terms will be negligible in this limit and the Hamiltonian simply reduces to an *anisotropic harmonic oscillator* whose form shows that the motion clearly separates into independent oscillations in the z direction and in the x-y-plane. This also means that the quanta in these directions, n_z and $n_x + n_y$ (with $N = n_x + n_y + n_z$), separately

become good quantum numbers. Since the Hamiltonian is now independent of the angle ϕ around the z axis, the z-projection of both the orbital and spin angular momenta of a particle must be constants of motion. In the limit of large deformations the Λ and Σ asymtotic quantum numbers - as well as n_z - consequently become good quantum numbers. The energies depend on the quantum number n_z now and the lowest lying orbits have $n_z = N, N-1, ...$ while from the midshell region up to the end of a shell $n_z = 2, 1, 0$ orbits predominate (remember that $\omega_z < \omega_{x,y}$ and thus the energy for oscillations with more quanta along the symmetry axis z is lower).

3.1.1 Wave functions and interaction matrix elements

By substituting the single-particle Hamiltonian in equation (3.7) into the eigenvalue equation $\hat{H}\phi_i = E_i\phi_i$, it is possible to determine the energies and wave functions of the deformed single-particle states. For small deformations it is reasonable to expand the wave functions in a *spherical basis* because they involve single-j configuration mixing. Here j is still an approximately good quantum number and one component / expansion coefficient will always be large. Consequently the expansion into shell model orbits specified by their j values implies that the Nilsson wave function ϕ_i can be written in the form [5]:

$$\phi_i = \sum_j C_j^i \psi(j) \tag{3.9}$$

Here $\psi(j)$ are solutions to the spherical independent particle model and the C_j^i are configuration mixing coefficients.
For large deformations (which means that $\delta = 0.6$) it is appropriate to use the analytically determined wave functions which are solutions to the anisotropic three dimensional harmonic oscillator potential [28]. In the limit of large deformations these solutions are exactly valid. In dealing with medium deformed nuclei with $\delta \approx 0.3$ linear combinations of these wave functions have to be considered and n_z is only an approximately good quantum number.

$$\phi_K^N = \sum A_{N,n_z} \psi(N, n_z, K) \tag{3.10}$$

However, even in this case one component of the linear combination is always much larger than any of the rest indicating an almost pure state. In the up-coming calculations for the *transitional matrix elements* between the relevant states it is therefore a reasonable approximation to work with the exact solutions for large deformations.

As already stated in the introduction the quadrupole residual interaction with its operator $r^2 Y_{2\pm 2}$ is responsible for the gamma vibration in deformed nuclei. Certain states have a non vanishing transition matrix element characterized by the following selection rules:

$$\Delta N = 0, \Delta n_z = 0, \Delta\Sigma = 0, \Delta K = \pm 2, \Delta\Lambda = \pm 2, \Delta\pi = +1 \tag{3.11}$$

In order to evaluate the transitional matrix elements between two Nilsson states linked by the quadrupole interaction the single particle wave functions being solutions to the three dimensional anisotropic harmonic oscillator are used.

$$\begin{gathered} H_0 = -(\hbar^2/2m)\nabla'^2 + 0.5m(\omega_r^2 r'^2 + \omega_z^2 z'^2) \\ H_0\psi(N, n_z, \Lambda, \Sigma) = E_{N,n_z}\psi(N, n_z, \Lambda, \Sigma) \end{gathered} \tag{3.12}$$

r' (radial coordinate) and z' (position along the symmetry axis) are the coordinates of the nucleon in a coordinate system fixed in the nucleus. The resulting wave functions are given below in cylindrical coordinates ρ, ϕ and z with $\rho \sim r'$ and $z \sim z'$. The oscillation frequencies in the radial direction and along the z direction depend, as already derived, on the deformation β of the nucleus. One obtains the following eigenvalues E_{N,n_z} and eigenfunctions $\psi(N, n_z, \Lambda, \Sigma)$:

$$\begin{gathered} E_{N,n_z} = \hbar\omega_r(N - n_z + 1) + \hbar\omega_z(n_z + \frac{1}{2}) \\ \psi(N, n_z, \Lambda, \Sigma) = C^{-1} \cdot R_{N,\Lambda} \cdot \Phi_\Lambda \cdot Z_{n_z} \\ |\langle\psi|\psi\rangle|^2 = 1 \end{gathered} \tag{3.13}$$

Here, C is a constant for normalizing the wave function so that the probability to find the nucleon somewhere in space is 1. The expressions for $R_{N,\Lambda}$, Φ_Λ and Z_{n_z} are

$$\begin{gathered} R_{N,\Lambda} = exp(-0.5\rho^2)\rho^{|\Lambda|}(1 + \frac{(|\Lambda| - n_r)\rho^2}{2(1 + |\Lambda|)} + \frac{(|\Lambda| - n_r)(|\Lambda| - n_r + 2)\rho^4}{8(1 + |\Lambda|)(2 + |\Lambda|)} + ...), \\ \Phi_\Lambda = exp(i\Lambda\phi), \\ \text{and } Z_{n_z} = exp(-0.5z^2)h_{n_z}(z), \end{gathered} \tag{3.14}$$

where $h_{n_z}(z)$ are the Hermite polynomials and $n_r = N - n_z$.
The quadrupole operator $r^2Y_{2\pm2}$ written in cylindrical coordinates has the following form:

$$\hat{O} \equiv r^2Y_{2\pm2} = \left(\frac{15}{32\pi}\right)^{1/2} \rho^2 exp(\pm 2i\phi) \tag{3.15}$$

Finally the desired matrix element between two Nilsson states m, i can be calculated with the following integral:

$$\begin{gathered} \langle m|r^2Y_{2\pm2}|i\rangle = \langle\psi((N, n_z, \Lambda, \Sigma)_m)|r^2Y_{2\pm2}|\psi((N, n_z, \Lambda, \Sigma)_i)\rangle = \\ = \int_0^{2\pi}\int_0^{+\infty}\int_{-\infty}^{+\infty} \psi((N, n_z, \Lambda, \Sigma)_m)^* \cdot \hat{O} \cdot \psi((N, n_z, \Lambda, \Sigma)_i) \cdot \rho \cdot dz d\rho d\phi \end{gathered} \tag{3.16}$$

Although it is reasonable to apply in the evaluation of the matrix elements the exact solutions of the Nilsson wave functions for large deformations the admixture of other wave function components near inflection points due to level-level repulsion in the Nilsson diagram still has to be taken into account. For example, a total mixture in the wave function of two states at an inflection point usually leads to a reduction of the transitional matrix element by the factor of 0.5.

In concluding this section it is worth remarking that the importance of the *Nilsson model* arises from the fact that it provides a microscopic basis for the existence of vibrational (and of course rotational) collective motion in deformed nuclei and thus is a refinement to the spherical *shell model*. Single nucleon transfer reactions can be used to determine the dominant states involved in a collective excitation of the nucleus and are therefore an important possibility to confirm the predictions of the deformed shell model [25, 26].

3.2 Pairing correlations

So far we have discussed the deformed shell model considering the nucleons as moving independently in a deformed potential. Indeed this description does not contain all necessary degrees of freedom. It is of major importance to incorporate a short range residual interaction like the *pairing force* [5] in our calculation.
In fact, without pairing correlations, the ground state of a nucleus is of very simple composition. The two-fold degenerate single-particle levels in the Nilsson diagram at a certain deformation are simply filled up until the neutron / proton number of the nucleus under consideration is reached. The highest occupied level for neutrons / protons denotes the neutron / proton *Fermi energy*. In the ground state all single-particle states above this level are empty and consequently all states below the *Fermi level* are occupied.
The elementary excitations in this case are particle-hole excitations. Considering explicitly the gamma-vibration such transitions could happen between two Nilsson states that are connected by the $r^2Y_{2\pm2}$ operator.
In the presence of pairing, however, the situation becomes more complicated. The *BCS theory* [1] treats the pairing as a perturbation of the mean field Hamiltonian of the nucleus. The final effect will be a modification of the former simple ground state leading to a "smearing" out of the Fermi surface and a new mechanism of excitation in even-even nuclei called *two-quasiparticle excitations*.

The pairing force is an attractive force that occurs between identical nucleons in the same j orbit. The interaction is such that the $J = 0$ configuration for the two nucleons is much lower in energy than any other. In the Nilsson model the two nucleons in the degenerate $\pm K$ levels are paired. Before discussing the consequences of pairing correlations explicitly, it is worth to recall the experimental evidence which supports the existence of pairing correlations in the nucleus and therefore proves the essential importance to incorporate pairing into realistic calculations.

- The masses of even-even nuclei in comparison to their odd-mass neighbours are much lower. This fact suggests that the gain in binding energy is much larger when a nucleon is added to an an odd mass nucleus than when a nu-

cleon is added to an even mass nucleus. In the context of pairing this can be understood by the creation of a new pair of nucleons when an appropriate particle is added to an odd mass nucleus and thus lowering its energy.

- The ground-state spin of all even-even nuclei is $0\hbar$. This fact suggests that there is a force that acts to couple nucleons pairwise such that their angular momenta cancel out.

- The energy of the first non-collective state is much higher (clearly above 1 MeV) in even-even nuclei than in odd mass nuclei. We will soon see that as a direct consequence of pairing, in even-even nuclei there is an energy of twice the so called *pairing gap* necessary to create a two-quasiparticle excitation.

- The ground state spin of odd-mass nuclei is determined by the spin of the last nucleon which is unpaired.

- The measured moments of intertia of nuclei are much lower than the rigid-body values. This fact suggests that the nucleus may behave like a "superfluid".

These effects observed in nuclei show similarities to superfluid ^4He and superconductivity in some substances observed for temperatures near $T = 0K$. Nuclei behave as if they consisted of a mixture of normal and superfluid liquid. The superfluid component is probably related to the pairing force. Nuclei with opposite angular momenta couple to $J = 0$ and such a system has a spherical symmetry and thus it cannot contribute to rotational motion (remember the quantum mechanical restriction commented upon in the introduction). In nuclear matter the paired nucleons represent the superfluid component. The creation of pairs can be considered analogously to the binding of electrons in *Cooper pairs* in superconductors accompanied with an energy-gap for breaking up theses objects. Thus basically the same BCS theory can be applied to both nuclei and superconductors.

In the ground state of an even-even nucleus all the nucleons are coupled pairwise. Thus the total angular momentum is $0\hbar$. The strength of the pairing interaction is larger for high j orbits and is dependent upon the spatial overlap of the two nucleons. The strength parameter, denoted by G, therefore decreases with mass, since in heavier nuclei the outer nucleons are further apart. The strength is also lower for protons than for neutrons due to the effect of Coulomb repulsion. The strength is usually given by $G_p = \frac{17}{A} MeV$ for protons and by $G_n = \frac{23}{A} MeV$ for neutrons. Equation (3.17) gives the explicit formula describing the pairing interaction.

$$\langle j_1 j_2 J | V_{pair} | j_3 j_4 J' \rangle = -G \left(j_1 + \frac{1}{2} \right)^{1/2} \left(j_3 + \frac{1}{2} \right)^{1/2} \delta_{j_1 j_2} \delta_{j_3 j_4} \delta_{J0} \delta_{J'0} \qquad (3.17)$$

The pairing interaction not only couples pairs of nucleons in the same state j to $J^\pi = 0^+$ (diagonal interaction), but also contains non diagonal elements connecting different states j, j'. The effect of the non-diagonal matrix elements is that $J^\pi = 0^+$

pairs of nucleons in an orbit j can be scattered into another orbit j', as a pair, still with $J^\pi = 0^+$. Far below the Fermi surface the Pauli principle forbids such scattering to occur since the orbits above j are filled. By the way, this is how it is possible to consider independent particle motion in such a dense object as the nucleus. However, near the Fermi surface this scattering can occur between orbits below and above the Fermi energy. The scattering results in a smearing out of the Fermi surface. As already mentioned, in the absence of pairing the orbits would simply be filled squentially in accordance with the Pauli principle until all A nucleons had been placed in the lowest orbits and thus giving a sharply defined Fermi surface. In figure 3.6 the effect of pairing on the Fermi surface is shown. Altogether the pairing interaction leads, besides lowering the energy of the ground state, also to a more complex ground state in even-even nuclei.

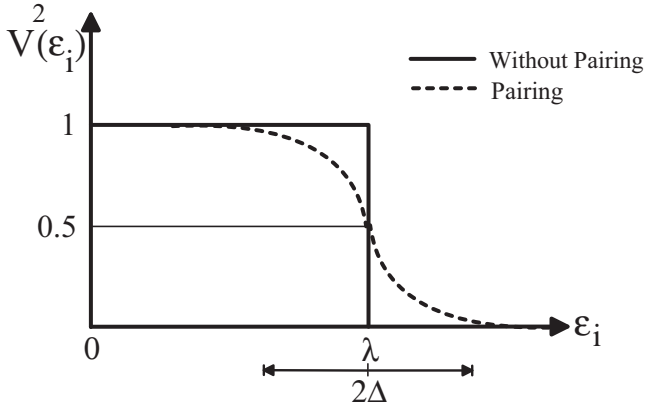

Figure 3.6: Schematic representation of the smearing of the Fermi surface λ due to the pairing interaction. The occupation probability V_i^2 of certain single-particle states i with an energy ϵ_i is shown. The effect of this interaction leads to scattering of pairs of particles in an orbit j to another orbit j'. The scale of the picture does not represent real proportions with $\lambda \approx 50MeV$ and $\Delta \approx 1MeV$.

The probability that a state i is not occupied or that it is occupied by a coupled pair of two nucleons is given by the expressions in equation (3.18) (emptiness and fullness factors).

$$U_i = \frac{1}{\sqrt{2}}\left[1 + \frac{(\epsilon_i - \lambda)}{\sqrt{(\epsilon_i - \lambda)^2 + \Delta^2}}\right]^{\frac{1}{2}} \; ; \; V_i = \frac{1}{\sqrt{2}}\left[1 - \frac{(\epsilon_i - \lambda)}{\sqrt{(\epsilon_i - \lambda)^2 + \Delta^2}}\right]^{\frac{1}{2}} \tag{3.18}$$

U_i^2 is the probability that the orbit i is empty and V_i^2 is the probability that the orbit i is occupied by a coupled pair of two nucleons. It can be seen that far below the Fermi energy ($\epsilon_i << \lambda$) $V_i^2 = 1$ and far above the Fermi energy ($\epsilon_i >> \lambda$) $U_i^2 = 1$. Close to the Fermi energy the probabilities are mixed. ϵ_i is the single particle energy of the two-fold degenerate Nilsson orbit, Δ is the pairing gap paramter and

λ is the (generalized) Fermi energy. The probabilities are of course normalised so that $U_i^2 + V_i^2 = 1$.
In a rough approximation the generalized Fermi energy λ equals to the Fermi energy determined in a nucleus without taking the the pairing interaction into account. To be precise, λ is defined as the energy at which the occupation probability is equal to one half. However, for a nuclear system there is likely to be no state at such a point. The pairing gap parameter Δ denotes the area around the Fermi energy where the occupation probability is significantly different from the extreme cases of 0 and 1, lying somewhere in between, smoothing out the level occupancies, as figure 3.6 shows. The generalized Fermi energy λ and the pairing gap parameter Δ can be determined exactly by solving the *gap-equation* under the condition of conservation of the total number of particles, denoted by n. The single-particle energy levels at a certain deformation have to be used as input data. The gap-equation and the condition of conservation of the total particle number are written down in (3.19).

$$\begin{aligned} \Delta &= \frac{G}{2} \sum_i \frac{\Delta}{\sqrt{(\epsilon_i - \lambda)^2 + \Delta^2}} \\ n &= \sum_i 2V_i^2 \end{aligned} \tag{3.19}$$

Of course these equations have to be solved twice i.e. separately for neutrons and protons. Most important are the single-particle states near the Fermi energy. Levels far away from the Fermi energy become less decisive because their contribution to the *gap-equation* decreases with their distance from λ. It is worth to emphasize that the pairing gap parameter Δ is proportional to G, the strength of the pairing interaction.

Finally, it is necessary to talk about the new mechanism of producing elementary excitations in nuclei when the pairing force is taken into account. The well-known *particle-hole excitations* (refering to the excitement of a particle from a state below the Fermi surface to an unoccupied state above the Fermi surface leaving a hole behind - of course this only works between states that are connected by the $r^2 Y_{2\pm2}$ operator in the case of a γ-vibration and thus leading to a nonvanishing transitional matrix element between them) are replaced by the concept of *two quasi-particle excitations*. Thus the single-particle energies are converted into a quasi-particle energy spectrum [5].

In even-even nuclei (we will not discuss odd mass nuclei) there is no simple excitation below the energy of 2Δ. The simplest quasi-particle excitation[1] consists of breaking one pair of coupled nucleons and raising a particle to another orbit. Without pairing

[1] Scattering of whole pairs from one single particle state to another is already incorporated in the BCS ground state and is not considered to be a simple mode of excitation in even-even nuclei. These excitations would only require about twice the difference in energy between two single-particle states and thus their energy could be much lower than 2Δ in some cases. These excitations are not observed experimentally.

this is clearly a particle-hole excitation, but in the presence of pairing it appears as a two-quasiparticle excitation: the one quasiparticle which is created is the hole that is left behind and the other quasiparticle is the particle excitation newly created. The total excitation energy E_x is given by the sum over the energies needed to create each quasiparticle in a certain single-particle state i and j with the single-particle energy ϵ_i and ϵ_j. The states that are occupied with these quasiparticles are not accessible in the context of pair scattering processes anymore (this is called blocking).

$$E_x = E_i + E_j = \sqrt{(\epsilon_i - \lambda)^2 + \Delta^2} + \sqrt{(\epsilon_j - \lambda)^2 + \Delta^2} \geq 2\Delta \tag{3.20}$$

Equation (3.20) shows that single-particle levels near the generalized Fermi surface λ are energetically favoured. Furthermore the energy for a quasiparticle excitations increases both for higher lying single particle orbits and for lower lying single-particle states in the Nilsson diagram with respect to the Fermi level. If the state coincides with the Fermi level, then the excitation energy of a quasiparticle is minimal, which means $E_i = 1\Delta$. The effect of the pairing gap on the two-quasiparticle excitations causes on the one hand simple two-quasiparticle excitations to appear at energies higher than 2Δ and on the other hand in the region just above twice the pairing gap there is a significant compression of the level density. A lot of states can be found within a small range of the excitation energy.
Apart from the fundamental change in the energy structure of the nucleus, the smearing out of the Fermi surface and thus the partially occupied states with nucleon pairs around λ in the BCS ground state of the nucleus leads to a necessary modification in the interaction matrix element introduced in the last subsection. $M_{im} = \langle m|r^2 Y_{2\pm2}|i\rangle$ is the shape of the former matrix element for a ground state without pairing. The modified matrix element for a BCS ground state (incorporating the pairing interaction) [5] is given in equation (3.21).

$$M_{im}^{BCS} = (V_m \cdot U_i + U_m \cdot V_i) \cdot \langle m|r^2 Y_{2\pm2}|i\rangle \tag{3.21}$$

Indeed, a two-quasiparticle excitation between two Nilsson states i and m which are connected by the quadrupole operator can be realized in two different ways. One possibility is to break a pair sitting in m and transfering one particle to the state i. The other possibility is to break a pair located in the state i and shifting a nucleon to the state m. From the energetical viewpoint these two options are equal.
Finally, it is also important to look at the BCS ground state with the smeared out Fermi surface.
If the single-particle state m is far below the Fermi level and the single particle state i is far above (or the other way round), then the quasiparticle excitation is clearly a particle-hole excitation. Only one level is occupied with the pair of nucleons and thus in this level the hole will be created and one nucleon is excited to the other level which was not occupied by a pair so far - thus the particle is assigned to this level.
If we consider two single-particle states that are located energetically within an area of Δ to both sides of the Fermi level then the situation becomes more complex. It is not possible to distinguish in which level the hole / particle is created. This

important fact shows that a quasi-particle is in general a *mixture of a particle and a hole*. The modification of the transitonal matrix element (3.21) thus incorporates both possibilities:
V_m is connected with the probability to find a pair of nucleons in the state m. In case there is indeed such a pair, it can be broken and if the other level i is not occupied by another pair of nucleons one particle from the broken pair can be moved to this level. The probability that the level i is not occupied by a pair is connected with the factor U_i. This implies that the transitional matrix element has to be modified with a total factor $V_m \cdot U_i$. Furthermore, exactly the same thought can be applied when you exchange the level i with the level m. Therefore a transitional matrix element modfied by the factor $U_m \cdot V_i$ has to be added and finally formula (3.21) is derived within the preceding simple argumentation.

The creation of a particle-hole state for a nucleus without pairing can be written in the operator formalism as $\hat{a}^\dagger_m \hat{a}_i$ with an energy of $|\epsilon_m - \epsilon_i|$ acting on the ground state $|0\rangle$. Consequently the destruction of this state is given by $\hat{a}_m \hat{a}^\dagger_i$. For a two-quasiparticle excitation the creation operator acting on a BCS ground state $|BCS\rangle$ can be written as $\hat{\alpha}^\dagger_m \hat{\alpha}^\dagger_i$ with an excitation energy of $E_m + E_i$ and the corresponding destruction operator is $\hat{\alpha}_m \hat{\alpha}_i$.
The introduction of the quasiparticles is altogether a very elegant concept so that it is possible to consider the nucleus after the incorporation of the pairing force again as a system of independent particles. The complexity is absorbed in the ground state and in the "new" method of creating elementary excitations in such a nucleus. The single-particle energy spectrum is replaced by the quasi-particle energy spectrum $E = \sqrt{(\epsilon - \lambda)^2 + \Delta^2}$.

In the next section of the current chapter we will show that it is indeed possible to have more complex - not "elementary", but collective excitations of even-even nuclei that occur below twice the energy of the pairing gap. They correspond to macroscopic collective vibrations (or rotations) of the nucleus as a whole and can be considered as resulting from the correlation of several two-quasi-particle states.

3.3 Theory of the Random Phase Approximation

The tremendous success of applying the *Random Phase Approximation*[2] (RPA) [1, 9-11] in nuclear physics results from the fact that this method is able to describe collective behaviour (e.g. the gamma-vibration) from the underlying microscopic physics, i.e. from the deformed shell model. This theory is in principle capable of explaining the low energy of the gamma-vibrational state (which is often far below 2Δ, the limit imposed by the pairing force). Furthermore it describes the composition of the collective wave function and of course transition probabilities from the excited state to the ground state can also be calculated.

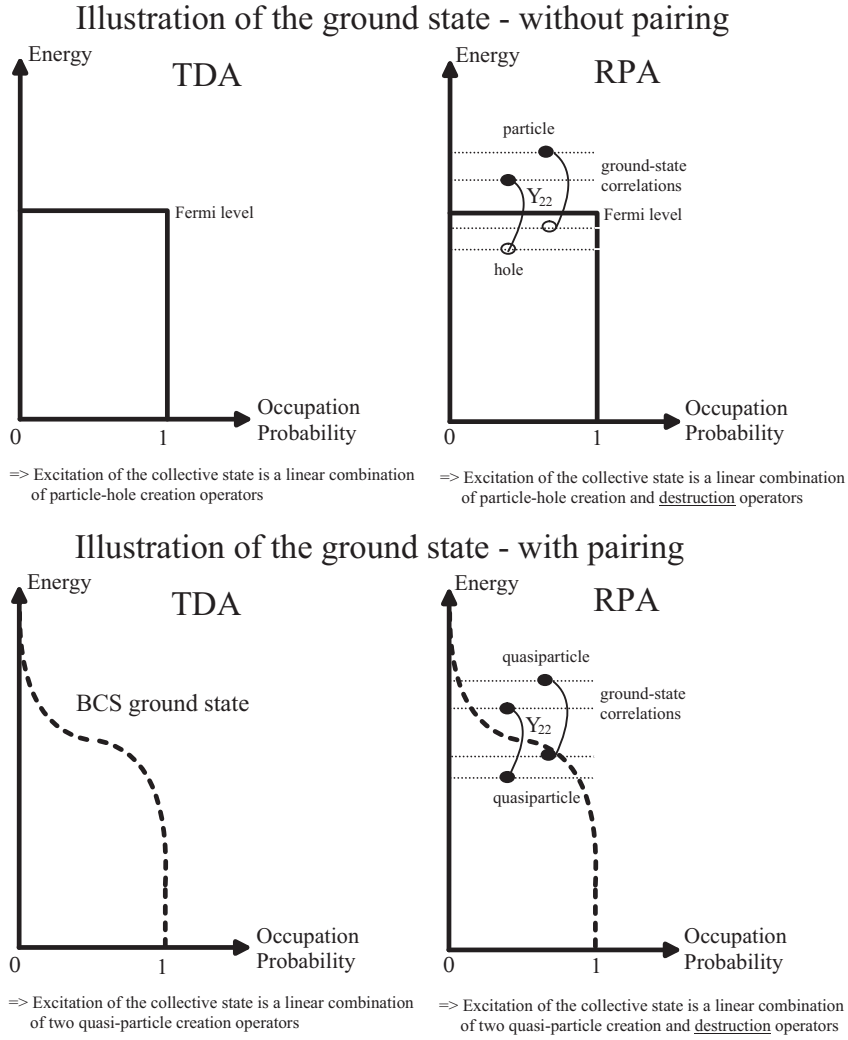

Figure 3.7: Comparison between TDA and RPA, with and without pairing

[2] The name "Random-Phase-Approximation" refers to an approximation which was used in the original derivation of this method.

The underlying idea of the RPA is very simple and will here be outlined in the context of the gamma-vibrational state. The collective vibrational state is assumend to be composed of a coherent linear combination of several particle-hole (in the context of pairing: two quasi-particle) excitations between states connected by the quadrupole residual interaction (the final wave function is a superposition of these fundamental modes of excitation).
There is also another treatment similar to the RPA called the TDA (*Tamm-Dancoff-Approximation*) which will be discussed additionally in the following derivation of the RPA. The difference between these two methods is the ground state which the nucleus is assumed to have before the collective vibrational state is excited.
In the TDA the ground state is very simple, which means that basically for the nucleus without pairing all states up to the Fermi level are filled and all states above the Fermi level are empty. Incorporating pairing we find analogously the unaltered BCS ground state with the smeared out occupation of pairs around the Fermi surface (figure 3.7). Consequently the TDA only involves amplitudes for the creation of elementary excitations to describe the collective vibrational state.
In contrast to the TDA, the RPA intends to make the ground state of the nucleus more complex. Remember that the residual quadrupole interaction connects certain Nilsson model states by the operator $r^2Y_{2\pm2}$. Thus the RPA assumes that already in the ground state there may be some particle-hole or two quasi-particle excitations between states connected by the quadrupole residual interaction. These ground state correlations (or built-in excitations) lead to a far more realistic picture of the physics of the nucleus (figure 3.7).
The consequence will be that the creation of the vibrational collective state in the RPA not only involves amplitudes for the creation of elementary excitations but also (usually much smaller) amplitudes for the destruction of those.
TDA and RPA both lead to a significant lowering of the energy of the vibrational state in comparison to the energy needed to create elementary excitations of the particle-hole / two quasiparticle type. The only difference is that the RPA approach leads to greater collectivity than the TDA approach. Thus the refinement of incorporating ground state correlations yields much higher reduced transition probabilities from the collective state to the ground state.

First of all, for simplicity, we will only work with simple particle-hole excitations and finally the important step to the incorporation of quasi-particles and the pairing force can be done by simply switching to quasi-particle energies and changing the transitional matrix elements according to the BCS ground state with partial occupancies near the Fermi surface as shown in the last section.
Before we will start with the derivation of the RPA following the arguments given in the textbook of Greiner [1], it is already reasonable to list the ingredients needed for a RPA calculation applied to a nucleus:

- Setting up of a model space: usually the model space consists of all single-particle levels connected by the $r^2Y_{2\pm2}$ interaction in a reasonable distance from the Fermi surface. As will be shown soon, the contribution of states far

away from the Fermi surface becomes very small.
In the end we have a set of single-particle energies (taken from the Nilsson diagram at a certain ground state deformation β_0) and transitional matrix elements between them.

- If pairing is incroporated it is necessary to determine the generalized Fermi energies separately for neutrons and protons and the corresponding pairing gaps.

- A realistic assumption about the strength κ of the quadrupole interaction is required. Of course it is also possible, as we will see later, to take the experimental energies of the γ-vibrational state and determine the corresponding strength paramter.
Unfortunately this paramter is not a priori fixed within the framework of RPA.

It seems to be reasonable to start from a nuclear Hamiltonian $H = T + V_{NN}$ where V_{NN} is a realistic nucleon-nucleon interaction potential. Unfortunately the nucleon-nucleon potential V_{NN} is not suitable for direct use in the TDA or RPA because it usually has a strong repulsive core at small distances. So the first step is to transform $H = T + V_{NN}$ into some effective Hamiltonian (3.22).

$$H_{eff} = H_0 + V = \sum_{k_1 k_2} t_{k_1 k_2} a^\dagger_{k_1} a_{k_2} + \frac{1}{2} \sum_{k_1 k_2 k_3 k_4} \nu_{k_1 k_2 k_3 k_4} a^\dagger_{k_1} a^\dagger_{k_2} a_{k_4} a_{k_3} \tag{3.22}$$

H_0 is the effective one-body Hamiltonian and V is assumed to be an effective two-body interaction[3]. The model space in which TDA and RPA calculations are usually performed is composed of all the Nilsson single-particle states within a certain distance from the Fermi level in a given nucleus. The collective gamma-vibrational state $|c\rangle$ solves the *Schrödinger-Equation*

$$H|c\rangle = E_c|c\rangle \tag{3.23}$$

and an operator can be defined, which acts on the ground state, creating the collective state as shown in (3.24). This operator creates a vibrational quantum and is therefore called phonon creation operator. The adjoint operator represents the corresponding annihilation of the excited collective state.

$$O^\dagger_c|0\rangle = |c\rangle \ ; \ O_c|0\rangle = 0 \ ; \ O_c|c\rangle = |0\rangle \tag{3.24}$$

An approximation for the creation operator is based on a principle of variations.

$$0 = \delta\langle c|H - E_c|c\rangle = \delta\langle 0|O_c H O^\dagger_c - E_c O_c O^\dagger_c|0\rangle \tag{3.25}$$

[3] The Hamiltonian can also be split up into a part H_0 incorporating the kinetic term and an average attractive potential V for each nucleon plus the potential $V_{residual}$. The difference between V_{NN} and the potential V gives the residual interaction $V_{residual}$ that can not be included in the average potential. In fact the whole treatment of the nucleus in the Nilsson model plus resdiual interactions is based on this separation.

The operator $O_c^\dagger$ and the adjoint operator O_c can be varied independently from each other and the energy of the ground state is denoted by E_0. After using the obvious commutation relation $HO_c^\dagger|0\rangle = \left[H, O_c^\dagger\right]|0\rangle + E_0 O_c^\dagger|0\rangle$ and the properties of the introduced operators, the following fomula (3.26) can be easily derived.

$$\langle 0|\left[\delta O_c, \left[H, O_c^\dagger\right]\right]|0\rangle = (E_c - E_0)\cdot\langle 0|\left[\delta O_c, O_c^\dagger\right]|0\rangle \tag{3.26}$$

As already mentioned one big advantage in the use of the RPA instead of the TDA is the fact that the ground state itself may already contain excitations due to some residual interaction.
The ground state $|0\rangle$ without pairing in the TDA consists simply of occupied levels below and empty levels above the Fermi surface. Applying the more realistic RPA then the ground state $|0\rangle$ has already some built in correlations i.e. particle-hole excitations, as already mentioned (figure 3.7).
Therefore excited states are constructed by the use of usual particle-hole creation operators $a_m^\dagger a_i$ and in addition by the use of operators which remove particle-hole excitations $a_i^\dagger a_m$ from the ground state. In the TDA the $a_i^\dagger a_m$ contribution is canceled (there are no ground-state correlations that can be removed).
The single particle energy of states denoted by m, n shall be above the Fermi surface and the energy of states i, j shall be below the Fermi level. This restriction is not necessary if the pairing force and thus quasi-particle energies are considered.
If the pairing force is taken into account the ground state $|0\rangle$ in the TDA is the BCS ground-state with a smeared out Fermi surface. Using the more complicated RPA in this case leads to a ground state $|0\rangle$ which has already some built in two quasi-particle excitations (figure 3.7).
Applying the RPA, the two quasi-particle creation $\alpha_i^\dagger\alpha_j^\dagger$ and destruction $\alpha_i\alpha_j$ operators have to be used to form the collective state. Analogously in the TDA the $\alpha_i\alpha_j$ contribution is canceled.
Thus the operator for the creation of the collective state (in the RPA but without pairing) finally has the following form.

$$O_c^\dagger = \sum_{m,i}\left(x_{mi}^c a_m^\dagger a_i - y_{mi}^c a_i^\dagger a_m\right) \tag{3.27}$$

In equation (3.27) the coefficients/amplitudes x_{mi}^c and y_{mi}^c are real numbers. Applying the principle of variations to the operator (3.27) means either to vary the coefficients x_{mi}^c or to vary the coefficients y_{mi}^c. This yields, in connection with the formula (3.26) just derived above, two equations whose commutators have to be evaluated in the RPA ground state. Assuming that only a few particles are lifted above the Fermi energy and consequently only a few holes exist below the Fermi level due to the residual quadrupole interaction the so called $quasi-boson-approximation$ is applied. It permits to evaluate the commutators as if the ground state contained no built in excitations. This is equivalent to the interpretation that the particle-hole creation operators behave as if they satisfied boson commutation relations.
The application of the *schematic model* (being based on a rank-one separability ap-

proximation for the interacting potential matrix elements $\bar{\nu}_{mnij} = \kappa \cdot \langle m|r^2 Y_{2\pm2}|i\rangle \cdot \langle n|r^2 Y_{2\pm2}|j\rangle$) leads to the final form of the RPA equations.

$$\begin{aligned} I)\ \sum_{nj} \left(A_{mi,nj} x^c_{nj} + B_{mi,nj} y^c_{nj}\right) &= (E_c - E_0) \cdot x^c_{mi} \\ II)\ \sum_{nj} \left(B^*_{mi,nj} x^c_{nj} + A^*_{mi,nj} y^c_{nj}\right) &= -(E_c - E_0) \cdot y^c_{mi} \end{aligned} \tag{3.28}$$

$$\begin{aligned} A_{mi,nj} &= (\epsilon_m - \epsilon_i) \cdot \delta_{mn} \cdot \delta_{ij} + \kappa \cdot \langle m|r^2 Y_{2\pm2}|i\rangle \cdot \langle n|r^2 Y_{2\pm2}|j\rangle \\ B_{mi,nj} &= \kappa \cdot \langle m|r^2 Y_{2\pm2}|i\rangle \cdot \langle n|r^2 Y_{2\pm2}|j\rangle \end{aligned} \tag{3.29}$$

The simpler TDA in the case of particle-hole excitations (i.e. without pairing) is also described by the equations (3.28) and (3.29) if equation II) is removed and y^c_{nj} is set equal to zero (no ground-state correlations or vacuum fluctuations). In the TDA the operator exciting the collective state has the following shape $O^\dagger_c = \sum_{m,i} x^c_{mi} a^\dagger_m a_i$. The solution of equation I) for the TDA is similar to the up-coming procedure in the RPA and will not be treated in the present work.
The further assumption that the interaction matrices contain real numbers and are symmetric is a reasonable refinement. κ is the paramter which classifies the strength of the residual quadrupole $r^2 Y_{2\pm2}$ interaction. For an attractive interaction the sign is negative. Unfortunately this strength parameter is a free parameter in the RPA and TDA respectively.
The pairing residual interaction is completely incorporated by applying the following modifications [5]:

- The RPA ground state $|0\rangle$ is built upon the BCS ground state
- $\epsilon_m - \epsilon_i \ \rightarrow\ E_m + E_i$ with the quasi-particle energy $E_k = \sqrt{(\epsilon_k - \lambda)^2 + \Delta^2}$
- For the transitional matrix element between Nilsson states:
  $\langle m|r^2 Y_{2\pm2}|i\rangle \ \rightarrow\ (V_m \cdot U_i + U_m \cdot V_i) \cdot \langle m|r^2 Y_{2\pm2}|i\rangle$

U^2_m and V^2_i are the well known BCS emptiness and fullness factors due to pair scattering describing the probability that a certain state is occupied by a pair of nucleons or not. For states far above or below the Fermi energy it is obvious that the pairing interaction has no effect. In this case the expression for the matrix element is not changed.
Turning again to the RPA equations I) and II) a solution for the unknown coefficients x^c_{mi} and y^c_{mi} can be found after recognizing that the same sum S appears in both equations.

$$S = \sum_{nj} \left((U_n V_j + U_j V_n) \cdot \langle n|r^2 Y_{2\pm2}|j\rangle \cdot x^c_{nj} + (U_n V_j + U_j V_n) \cdot \langle n|r^2 Y_{2\pm2}|j\rangle \cdot y^c_{nj}\right) \tag{3.30}$$

$$
\begin{aligned}
x^c_{mi} &= \frac{\kappa \cdot S \cdot (U_m V_i + U_i V_m) \cdot \langle m|r^2 Y_{2\pm2}|i\rangle}{(E_c - E_0) - (E_m + E_i)} \\
y^c_{mi} &= \frac{-\kappa \cdot S \cdot (U_m V_i + U_i V_m) \cdot \langle m|r^2 Y_{2\pm2}|i\rangle}{(E_c - E_0) + (E_m + E_i)}
\end{aligned}
\tag{3.31}
$$

E_0 can be set equal to zero because it is possible to make an arbitrary choice for the energy of the ground state. The coefficients (3.31) are the amplitudes of the two quasi-particle states making up the collective vibrational wave function.

The combination of the Nilsson single-particle states m, i connected by the quadrupole residual interaction can be considered as basis states. Due to the existence of the residual interaction these states are not eigenstates of the Hamilton operator, but they can be used as a basis for the preceding procedure of variational calculus.
The coefficients of course fulfil the normalisation condition and thus are normalised to 1 (3.32). The x_{mi} are called the *forward amplitudes*, because they describe the creation of a particle-hole (or two quasi-particle) excitation. The y_{mi} are called the *backward amplitudes* describing the destruction of an elementary excitation.

$$
\begin{aligned}
\sum_{mi} \left(|x^c_{mi}|^2 - |y^c_{mi}|^2\right) &\equiv \sum_{mi} C_{mi} = 1 \\
\text{with pairing: } |c\rangle &= \sum_{mi} \left(x_{mi}\alpha^\dagger_m \alpha^\dagger_i |0\rangle - y_{mi}\alpha_m \alpha_i |0\rangle\right)
\end{aligned}
\tag{3.32}
$$

In general the collective correlated wave function consists of a sum of almost equal amplitudes for all particle-hole / two quasi-particle excitations with all amplitudes in phase i.e. contributing with the same sign.
Finally, the C_{mi}, defined in (3.32), show the contribution of the basis states in the collective vibrational state. Said in other words the C_{mi} represent the fraction of the collective vibrational wave function a certain combination of Nilsson states carries.

Substituting the solutions for the amplitudes into the definition of the sum S the result is an equation (3.33) which is suitable for calculating the energy of the collective gamma vibrational state.
From the several solutions of the equation one just has to take the solution with the lowest energy. The energy value $E_c \equiv E_\gamma$ corresponding to the collective vibrational state is indeed appearing significantly lowered in energy for an attractive interaction in comparison to the other solutions of the equation.

$$
-1/\kappa = \sum_{mi} \frac{-\left(U_m V_i + U_i V_m\right)^2 \cdot |\langle n|r^2 Y_{2\pm2}|j\rangle|^2 \cdot (E_m + E_i)}{\left(E_c - E_0\right)^2 - \left(E_m + E_i\right)^2}
\tag{3.33}
$$

Equation (3.33), the so-called *dispersion relation*, is solved graphically to find the collective solution E_c. This is shown in figure 3.8. It is seen that all solutions except one lie between the unperturbed energies. If the interaction is sufficiently strong ($1/\kappa$ small), the lowest solution is pushed farther away than the others from the corresponding unperturbed energy and thus representing the collective state. For a sufficiently strong quadrupole force (κ large and negative) there may be no real solution of the RPA equations.

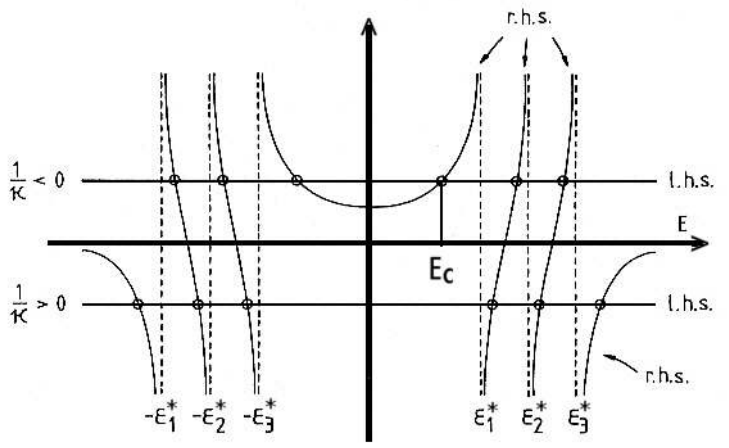

Figure 3.8: This illustration shows the so-called *dipersion relation* (equation (3.33)) in the RPA. The energies ϵ_x^* denote particle-hole states with $\epsilon_x^* = \epsilon_m - \epsilon_i$ and if pairing is incorporated two quasi-particle states with $\epsilon_x^* = E_m + E_i$. For an attractive interaction $1/\kappa < 0$ the collective solution E_c is pushed down below the unperturbed energies. If the quadrupole interaction is too strong, then there might be no real solution for the energy E_c of the collective state.

Finally, it is an interesting point to calculate the reduced transition probability from the collective state to the ground state via the operator $E2$ corresponding to an electromagnetic quadrupole transition. The following equations listed in (3.34) show the principal way this calculation works [5, 10]. $|0\rangle$ denotes the correlated ground state (vacuum) and $|c\rangle$ denotes the collective gamma-vibrational state.

$$\begin{aligned}
\text{no pairing: } |c\rangle &= \sum_{mi} \left(x_{mi}^c a_m^\dagger a_i |0\rangle - y_{mi}^c a_i^\dagger a_m |0\rangle \right) \equiv \sum_{mi} \left(x_{mi}^c |im\rangle - y_{mi}^c |im^{-1}\rangle \right) \\
\text{transition amplitude: } \langle c|E2|0\rangle &= \sum_{mi} \left(x_{mi}^c \cdot \langle im|E2|0\rangle + y_{mi}^c \cdot \langle im^{-1}|E2|0\rangle \right) = \\
&= \sum_{mi} \left(x_{mi}^c \cdot \langle m|E2|i\rangle + y_{mi}^c \cdot \langle i|E2|m\rangle \right) \\
\text{transition probability: } B(E2) &\propto |\langle c|E2|0\rangle|^2 = \\
&= |\sum_{mi} \left(x_{mi}^c \cdot \langle m|E2|i\rangle + y_{mi}^c \cdot \langle i|E2|m\rangle \right)|^2
\end{aligned} \tag{3.34}$$

We will continue the discussion of the calculation of electromagnetic reduced transition probabilties at the beginning of the next chapter.

In the last part of this section we emphasize explicitly the important equations in the RPA determining the collective wave function in the case of pairing and discuss which components may be dominant depending on their location in the Nilsson diagram [5]. The BCS ground state including vacuum fluctuations is now

denoted explicitly by $|RPA\rangle$. Furthermore the operators create and destroy two quasi-particle excitations.

$$\begin{aligned} |c\rangle &= \sum_{mi} \left(x_{mi}\alpha_m^\dagger \alpha_i^\dagger |RPA\rangle - y_{mi}\alpha_m \alpha_i |RPA\rangle \right) \\ \sum_{mi} C_{mi} &= \sum_{mi} \left(|x_{mi}|^2 - |y_{mi}|^2 \right) = 1 \\ C_{mi}^{\pi,\nu} &\propto \left| \langle m|r^2 Y_{2\pm 2}|i\rangle \right|^2 \cdot (U_m V_i + U_i V_m)^2 \cdot \\ \cdot \left[(E_\gamma - (E_m + E_i))^{-2} - (E_\gamma + (E_m + E_i))^{-2} \right] & \end{aligned} \tag{3.35}$$

In formula (3.35) we distinguish the neutron and proton contribution denoted by π and ν, respectively.
It can be easily seen that the forward amplitudes x_{mi} (- in the denominator) usually are the dominant contributions and the backward amplitudes y_{mi} (+ in the denominator) are rather small. Therefore the importance, denoted by C_{mi}, of the Nilsson states connected by the quadrupole operator in the vibrational wave function mainly depends on the forward amplitudes.
However, in the next subsection it will be shown that the "small" backward amplitudes are an essential ingredient to obtain high reduced transition probabilities and thus they are by no means negligible.
Assuming a pairing gap of about $0.8MeV$ and an energy of the gamma-vibrational state of about $1.0MeV$, which is a typical value for the nuclei under consideration, the C_{mi} are large if the two states are located as close as possible to the generalized Fermi energy which means that the excitation energy of two quasi-particle excitations between these states is near its minimum value of twice the pairing gap. For states away from the Fermi level the participation in the collective wave function decreases rapidly with the distance.
Furthermore, the contribution is proportional to the value of the transitional matrix element. The part consisting of emptiness and fullness factors clearly prefers two single-particle Nilsson states lying symmetrical on opposite sides of the generalized Fermi level. This means that the occupation probability of the one Nilsson orbit has to correspond to the non-occupation probability of the other orbit and the other way round, respectively.
In this work istopic chains of nuclei are considered. It is obvious that the distrbution of the C_{mi} for the proton states will hardly change. The constant proton number implies an almost constant proton Fermi surface. For the neutrons the Fermi level mainly changes due to the different neutron number of the nuclei lying on the isotopic chain. The distribution of the contribution of the neutron states does not change rapidly but changes occur rather smoothly with the neutron number.
The energy of the gamma-vibration generally decreases with the number of contributing orbits. Therefore nuclei with semi filled shells, which implies Fermi levels lying in a very dense region of the Nilsson diagram with a lot of Nilsson states close together, have on average lower energies of the gamma-vibration in comparison to nuclei far from midshell.

3.3.1 Explicit comparison between TDA and RPA for degenerate single-particle states

It is fruitful to compare the *Tamm-Dancoff-Approximation* and the more realistic *Random-Phase-Approximation* which incorporates ground state correlations for degenerate single-particle states (for simplicity we neglect pairing here) with a single-particle energy difference (and thus excitation energy) of $\epsilon \equiv \epsilon_m - \epsilon_i$.

If pairing is negelected the collective state in the TDA has an energy of $E_c = \epsilon + \kappa \sum_{mi} |\langle m|r^2 Y_{2\pm 2}|i\rangle|^2$. If the interaction is attractive ($\kappa < 0$) the collective state decreases in energy with the number of contributing states as long as their matrix elements are approximately equal. The transition probability from the excited collective state to the ground state is given by $|\langle c|E2|0\rangle|^2 = \sum_{mi} |\langle m|E2|i\rangle|^2$. It is just the sum of the transition probabilities for all unperturbed states.
One can summarize the results as follows: For degenerate unperturbed particle-hole energies, a single collective state is produced and pushed away from its unperturbed energy by the sum of all particle-hole matrix elements and carries all the transition strength. This is just a quantitative statement of the fact that all the particle-hole configurations connected by the transitional matrix elements contribute coherently to the collective vibrational state.
The same investigation in the context of the RPA with equal assumptions and also degenerate input single-particle states delivers for the energy of the collective state $E_c^2 = \epsilon^2 + 2\epsilon\kappa \sum_{mi} |\langle m|r^2 Y_{2\pm 2}|i\rangle|^2$. The collective RPA solution is always lower in energy than the collective TDA solution ($\kappa < 0$): $E_c^2(RPA) = E_c^2(TDA) - \kappa^2 \left(\sum_{mi} |\langle m|r^2 Y_{2\pm 2}|i\rangle|^2\right)^2$. The energy shift is larger the stronger the interaction is. The difference between TDA and RPA also shows up in the transition probability form the excited collective state to the ground state via the $E2$ operator. The transition probability in the RPA is given by $|\langle c|E2|0\rangle|^2 = \frac{\epsilon}{E_c} \left(\sum_{mi} |\langle m|E2|i\rangle|^2\right)$. The transition probability in the RPA turns out to be energy dependent in contrast to what was the case for the TDA. Thus for a sufficiently attractive quadrupole force (and consequently $E_c << \epsilon$) the transition probability may considerably exceed the TDA value. The difference in magnitude of the RPA and TDA transition probabilities is due to the presence of ground-state correlations in the RPA. In fact the assumption that already in the ground state elementary particle-hole excitations induced by the quadrupole force are present is very important to be able to reproduce the high experimentally observerd reduced transition probabilities for collective states.
Although the degenerate case is clearly an idealization, it serves to illustrate the mechanism behind collective, coherent states.

3.4 The Interacting Boson Approximation (IBA)

It was already mentioned that the IBA is an algebraic model capable of describing low-lying collective states in deformed nuclei. The simplest version of the interacting boson model (Ref. [13, 15]), referred to as IBM-1 or IBA-1 (Interacting Boson Approximation and Interacting Boson Model mean the same), is defined as a system of N bosons, each of which may have angular momentum 0 or 2 (called s or d bosons) and which interact with one-body and two-body interactions. This simple model does not distinguish between neutrons and protons. For a given nucleus the number of N bosons is fixed by the number of nucleons in the valence shell of the nucleus (for protons and neutrons the boson number is separately counted to the nearest closed shell which means that past midshell holes are counted). The lower lying closed shells are neglected.
In the shell model the consideration of all possible couplings of the valence nucleons spread over the various states in the valence shell, yielding for example a 2^+ state, is an intractable enterprise. Indeed the number of possible combinations for nuclei with a few fermions off a closed shell rapidly rises to about 10^{14}-10^{18}. This is a tremendous problem in the shell model. The approach of the IBA, having the pairing interaction in mind, and thus forming two different kinds of bosons constructed of couples of valence shell nucleons, is a vast simplification and reduces the possibilities to form a 2^+ state dramatically. The number of bosons is fixed for a certain nucleus and thus the results are boson number dependent.
The ground-state in this model, corresponding to the lowest 0^+ state, consists only of s bosons. The energy of the s bosons is set to zero. Excited states are produced by the annihilation of s bosons and the creation of d bosons, thus conserving the total boson number. Furthermore the bosons interact with each other. The Hamiltonian is expressed by using the boson creation operators $s^\dagger$, $d^\dagger$ and the boson annihilation operators s, d up to second order. The IBA basis states, making up the low-lying excited collective positive parity nuclear levels, can be denoted by the following set of quantum numbers:

$$|n_d, \sigma, \tau, J^\pi\rangle$$

In this expression n_d is the number of d bosons, σ is the number of d bosons coupled pairwise to $J = 0$, similarly τ denotes the number of d bosons coupled triplewise to $J = 0$ and finally J^π is the total angular momentum and parity resulting from the coupling of all the d bosons.
A fundamental feature of the IBA is its group theoretical structure. Since an s boson ($J = 0$) has only one magnetic substate and a d boson ($J = 2$) has five, the s-d boson system can be looked at mathematically as a six dimensional space. Such a system can be described in terms of the algebraic group structure U(6). There are various subgroups of U(6) leading to different dynamical symmetries. Three of these symmetries are physically interesting (U(5),O(6) and SU(3)), figure 3.9. Each

has specific characteristic properties and a geometric analogue as already mentioned in the introduction. The U(5) symmetry corresponds to the limit of the *spherical vibrator* in the geometric collective model. For a deformed nucleus the two IBA symmetries SU(3) and O(6) are equivalent to the *deformed axially symmetric rotor* and the *gamma-unstable deformed rotor* in the GCM, respectively.

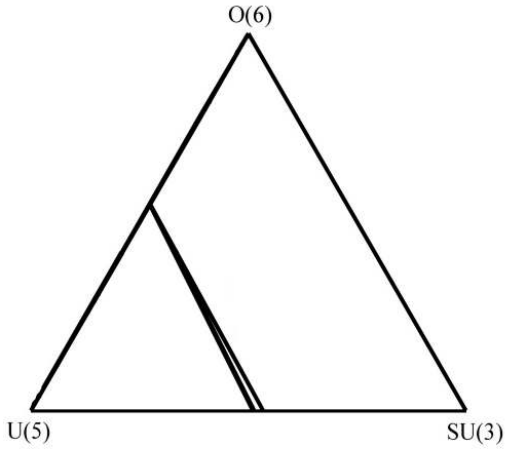

Figure 3.9: Illustration of the three dynamical symmetries in the IBA symmetry triangle. In the Extended Consistent Q Formalism the three symmetries are expressed by the following Hamiltonian parameters: U(5) corresponds to any χ and $\zeta = 0$, SU(3) corresponds to $\chi = -\sqrt{7}/2$, $\zeta = 1$ and O(6) corresponds to $\chi = 0$, $\zeta = 1$.

A very useful simplified version of the Hamiltonian of the IBA-1 written in the *Extended Consitent Q Formlism* (ECQF) (Ref. [14]) has the following shape.

$$H(\zeta,\chi) = c \cdot \left[(1-\zeta)\hat{n}_d - \frac{\zeta}{4n}\hat{Q}^\chi \cdot \hat{Q}^\chi\right] \qquad \text{with } \hat{Q}^\chi = (s^\dagger d + d^\dagger s) + \chi(d^\dagger d)^{(2)} \tag{3.36}$$

ζ $(0 \leq \zeta \leq 1)$ and χ $(-\sqrt{(}7)/2 \leq \chi \leq 0)$ are the two free parameters of the simplified Hamiltonian. In the paper of *McCutchan et al.* [16] it was shown that a reasonable treatment of rare-earth nuclei can be achieved within this simple framework. Here c is an arbitrary scaling factor of the energies. Usually, when fits to experimental data are done, c is determined so that the calculated energy of the 2^+ state of the ground-state band matches with the experimental value. $\hat{n}_d = d^\dagger d$ is the d boson particle number operator and $\hat{Q}^\chi$ is the quadrupole operator. The same quadrupole operator is used in the Hamiltonian and the E2 operator, which is given by $T(E2) = e_B Q$, where e_B is a free parameter, called the effective boson charge, which is used as a scaling factor for the reduced quadrupole transition probabilities.

In the limit U(5), corresponding to the spherical vibrator, with $\zeta = 0$ and an arbitrary χ, only the boson number operator in the Hamiltonian is left leading to an equally spaced energy spectrum as expected for a vibrator with multiple phonon excitations. In the two deformed limits only the quadrupole operator contributes ($\zeta = 1$). This operator mixes different basis states with quantum number n_d. In the O(6) limit corresponding to a gamma-unstable deformed rotor with $\zeta = 1$ and $\chi = 0$ the quadrupole operator creates an s boson and destroys a d boson or it creates a d boson and destroys an s boson instead. In the SU(3) limit of the deformed axially symmetric rotor with $\zeta = 1$ and $\chi = -\sqrt{7}/2$ a maximum contribution of the term, which destroys a d boson somewhere and creates another d boson, is present in addition to the interaction in case of the O(6) limit. The parameter χ determines the relative strength of the $s^\dagger d + d^\dagger s$ and $(d^\dagger d)^{(2)}$ parts of the quadrupole operator.

It is possible to map the IBA parameters into the symmtery triangle (figure 3.9) by a simple formula. This mapping converts the parameters ζ and χ in the Hamiltonian into radial and angular coordinates ρ and θ.

$$\begin{aligned} \rho &= \frac{\sqrt{3}\zeta}{\sqrt{3}cos\theta_\chi - sin\theta_\chi} \\ \theta &= \frac{\pi}{3} + \theta_\chi \\ \theta_\chi &= (2/\sqrt{7}) \cdot \chi \cdot \frac{\pi}{3} \end{aligned} \tag{3.37}$$

These coordinates allow for a simple and convenient description of the entire IBA symmtery triangle, with θ ranging from 0° to 60° and ρ acting as a standard radial coordinate from 0 to 1. The polar coordinates are defined in the following way: ρ is the distance from the U(5) limit to the point under consideration inside the triangle and θ denotes the angle between the U(5)-SU(3) leg and the distance vector.
Equation (3.37) was used in Ref. [16, 17] to map the IBA fits for the rare earth nuclei into the triangle, as shown in figure 1.1.

Chapter 4

Application to the γ-vibration in well-deformed even-even rare earth nuclei

The theoretical model discussed in the previous chapter is applied to several well-deformed even-even rare-earth nuclei. Before presenting the results it is necessary to go into details concerning the origin of the various input parameters that are used and to discuss the simplifications applied in our calculations. Restrictions arising from the simplified treatment will be emphasized. In the last section of this chapter an explicit comparison of our results with previous calculations for some of the nuclei considered here in the so called *Quasiparticle-Phonon Nuclear model* [21-23] by *Soloviev et al.* is shown to support the reliability of our results.

4.1 Input parameters and simplifications applied in our calculations

Our microscopical treatment of the gamma-vibrational state is based on the Nilsson model (deformed shell model). Thus we use the Nilsson diagrams for neutrons and protons taken from the Nuclear Data sheets [33] due to the lack of an available Nilsson shell model code. These diagrams show the energy of the single-particle Nilsson states as a function of the ground state quadrupole deformation parameter β_0 / δ_0. The appropriate quadrupole deformation of the various nuclei was looked up at the Website of the National Nuclear Data Center [34] and taken from the Raman compilation [29], respectively. Of course the energy eigenvalues taken from the diagrams are afflicted with minor errors due to the modest reading accuracy and possible inaccuracies in the ground state deformation parameter.

For the wave functions used to calculate the interaction matrix elements between certain Nilsson states it is a good approximation to take the exact solutions in the case of large deformations. For medium deformation parameters a linear combination of several of these wave functions should be considered, but fortunately one component is always highly dominant justifying our approximation. Solely for the transitional Pt isotopes with a deformation paramter β_0 close to 0.1 the results of our calculation obtained within the simplification of pure wave functions should be handled with care.
Furthermore, the mixtures of Nilsson states with the same exact quantum numbers K^π were only roughly taken into consideration i.e. either no mixture of two states is assumed or a complete mixture of two states in the area close to the point in the Nilsson diagram where the energy levels of these two states would have crossed (inflection point).
In the previous chapter it was shown that the amplitude of a two quasi-particle excitation is most likely to be important in the entire wave function if the single particle energies of the two Nilsson states which are involved are as close as possible to the Fermi energy. Moreover the states should be placed symmetrical to the Fermi level (one above, one below). To get an idea which states could be important we determined the Fermi level in a first order approximation by successively filling the Nilsson states according to the Pauli principle until the neutron / proton number of the nucleus under consideration was reached. Besides we also looked at the paper by *Bès et al.* [20] and used the results as a guideline. *Bès et al.* have done calculations concerning the gamma-vibrational wave function in some nuclei of the rare-earth region and written down all components with a contribution greater than 0.5 percent to the entire collective wave function (usually about 20 states for protons and neutrons together). The many small components that were not given explicitly represent a constant fraction of about ten percent of the collective wave function. Indeed in our calculations these components are beyond the scope, but it is important that their entire contribution to the wave function is approximately constant for the whole rare-earth region.
We only concentrate on the structural evolution of the major components of the wave function along an isotpic chain and compare this behaviour for various nuclei. It would be a tedious task to incorporate all these small amplitudes by manually extracting the information for so many single-particle levels from the Nilsson diagram.
This is also the reason why the generalized Fermi energy used in the BCS theory in our calculations was approximated by the Fermi energy determined by the highest occupied level in the Nilsson model neglecting pairing correlations. Indeed in some cases this first order approximation was altered a little bit by solving the *Gap-equation* under the condition of particle number conservation, but only the levels lying close to the expected Fermi surface were taken into consideration for this refinement. For a precise result a lot more single-particle energy levels would have to be incorporated exeeding the frame of this diploma thesis.
The pairing gaps for the neutrons and the protons were calculated by comparison

of the experimental *nucleon separation energies* (taken from the National Nuclear Data center) in adjacent nuclei using the following formula.

$$\begin{aligned} \text{for neutrons: } \Delta_{N,Z} &= \frac{1}{4}\left(2 \cdot S_n\left(N,Z\right) - S_n\left(N+1,Z\right) - S_n\left(N-1,Z\right)\right) \\ \text{for protons: } \Delta_{N,Z} &= \frac{1}{4}\left(2 \cdot S_p\left(N,Z\right) - S_p\left(N,Z+1\right) - S_p\left(N,Z-1\right)\right) \end{aligned} \tag{4.1}$$

Finally the applied simplifications can be justified by the fact that a qualitative comparison between the results for the amplitudes of the two quasi-particle excitations obtained in our model for the rare-earth nuclei and the amplitudes published in the paper by *Bès et al.* show a good agreement. In this context the reader is refered to the last section of this chapter where an explicit comparision of our results with previous calculations for some of the nuclei of interest is shown.

In the present work the energies for the gamma-vibrational state were not calculated using the dispersion relation (3.33) introduced in the RPA section of the last chapter. Instead the experimental values of the energy (also taken from the National Nuclear Data center) were used to obtain the desired amplitudes of the orbital combinations involved in the collective wave function.
There are two main reasons for proceeding like this:
First, a correct result for the vibrational energy can only be calculated if the many small components which make up a tenth of the collective wave function (according to *Bès et al.*) are also well known. The dispersion relation has to be solved graphically and the lowest solution determining the energy of the collective state is very sensitive to small variations in the contributing states even if they are very small. This is due to the nearly horizontal course (for higher collective energies rather prabolic than horizontal) of the right hand side of equation (3.33) and the problem arising when the intersection with the left hand side, determined by the strength paramter κ, has to be found. A small upward shift of the right hand side caused by some small components could lead to a significant lowering in the collective gamma-vibrational energy.
Second, we do not have a model that tells us something about the strength parameter κ of the quadrupole interaction. In our RPA derivation this is a free paramter. Of course another unsatisfying possibility would be to feed the equation with experimental energies of the gamma-vibrational states and calculate κ separately for each nucleus. After that a mean value of the paramter κ for all nuclei could be derived. Finally reapplying this mean value to the dispersion relation some pseudo theoretical values of the energy of the gamma-vibrational state would result. Of course this procedure would only make at best a limited sense if at least the many small components were exactly known and taken into consideration.

In our simple model it is also not possible to determine *reduced electromagnetic transition probabilities*. According to equation (3.34) in the last chapter the calculation of the B(E2) value for the transition from the excited gamma-vibrational state to the BCS ground state could be done theoretically in the following way: the

corresponding entire amplitude is composed of a sum over the amplitudes of all the single-particle E2 transitions each weighed by the amplitude X_{mi} and Y_{mi} of the corresponding two Nilsson states in the collective vibrational state. The phases of the amplitudes all have the same sign in the collective state which is a compostion consisting of a coherent superposition of single-particle excitations. To get finally the transition probability the entire amplitude has to be squared.
The problem with our model arises again from the many small components of the wave function. Their contribution in comparison to the contribution of the large components of the wave function can easily be of the same magnitude making a calculation only involving the major components of the wave function absurd. For reduced transition probabilities the detailed structure of the vibrational wave function down to the smallest components is of major importance. Furthermore according to the paper of *Bès et al.* a theory which is dedicated to deliver realistic B(E2) values should incorporate the *Coriolis interaction* (mixing states with $\Delta K = \pm 1$) in any case. In our work only the interaction based on the $r^2 Y_{2\pm 2}$ operator was taken into account.
Although the model was applied to the well deformed rare earth nuclei with $R_{4/2} > 2.9$, this selection includes some nuclei near the phase/-shape transition region from spherical to deformed: ^{152}Sm, ^{154}Gd, ^{156}Dy and ^{162}Yb. The results for those nuclei should be taken with some caution, since large fluctuations in the deformation parameter β are to be expected, making the assignment of two quasi-particle structure of the involved states unreliable. However, these results are helpful in following the trends for the isotopic chain.

To summarize the previous discussion one can say that our model is suitable to reproduce the qualitative behaviour of the distribution of the major amplitudes for the gamma vibrational state along an istopic chain, although the absolute values of the amplitudes should be handled with some care.
In fact the reason for performing own calculations was that neither *Bès et al.* nor *Soloviev et al.* have done calculations for all nuclei being of interest in our investigation. Therefore it was not possible to use these previous results in the systematic analysis of isotopic chains for various nuclei.

On the following pages the results of the calculations for the various rare-earth nuclei are shown. The squares of the amplitudes $C_{m,i} = (|x_{mi}|^2 - |y_{mi}|^2)$ of the dominant states connected by the selection rules of the $r^2 Y_{2\pm 2}$ operator making up the collective wave function are displayed separately for neutrons and protons. To be precise, according to the last chapter, the value of the square of the forward amplitude x_{mi} minus the square of the backward amplitude y_{mi} considered separately for each contributing orbital combination is the indicator for the dominance of those states in the wave function.
In the table below the plots, the percent value of each state in the collective wave function is printed. As additional information the overall sum of the percent values separately for all of the neutron states and all of the proton states is also shown. Of course, the sum incorporating all these values for a nucleus is normalized to 100

percent.
In calculations for the Pt isotopes, a lot of states with no importance are included. This was an arbitrary choice which depends on the circumstance that later on in this paper the results for different nuclei shall be compared. Therefore dealing with nearly the same number of basis states displayed in all illustrations is more convenient.

4.2 Presentation of the results

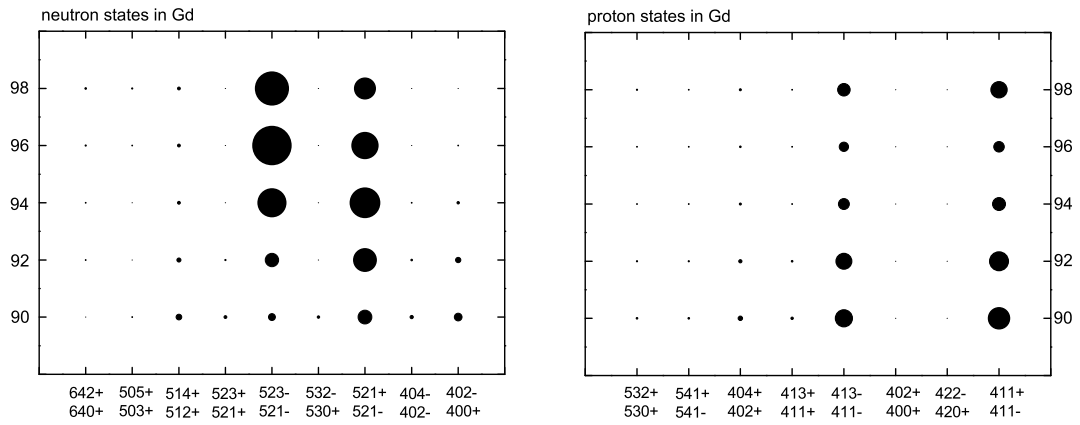

Figure 4.1: Most relevant two quasi-particle amplitudes for the 2^+_γ state in well deformed even-even Gd isotopes. The radius of the circles indicates the fraction of each wave-function component with respect to the total wave function. Eeach row is classified by the neutron number of the isotope.

Nilsson states	N = 88	N = 90	N = 92	N = 94	N = 96	N = 98
642+ 640+	0,04	0,44	0,73	0,94	1,27	1,63
505+ 503+	3,78	0,90	0,54	0,40	0,77	1,36
514+ 512+	5,75	6,28	4,67	2,99	2,78	3,04
523+ 521+	4,10	2,88	1,28	0,36	0,15	0,10
523- 521-	1,52	7,59	14,58	29,70	40,22	34,86
532- 530+	45,15	2,53	0,54	0,10	0,05	0,03
521+ 521-	3,45	14,76	24,16	31,47	27,67	22,21
404- 402-	1,35	3,37	1,77	0,64	0,23	0,15
402- 400+	6,98	8,39	5,77	2,43	0,68	0,38
neutrons total	72,10	47,15	54,04	69,02	73,81	63,76
532+ 530+	0,50	1,70	1,43	0,93	0,86	1,04
541+ 541-	0,61	1,71	1,30	0,80	0,73	0,82
404+ 402+	3,52	4,82	3,31	1,95	1,81	2,09
413+ 411+	1,39	2,36	1,72	1,03	0,96	0,83
413- 411-	9,79	18,73	17,51	12,06	10,02	13,71
402+ 400+	0,64	0,13	0,05	0,02	0,02	0,03
422- 420+	1,98	0,54	0,21	0,09	0,09	0,07
411+ 411-	9,46	22,88	20,41	14,09	11,70	17,64
protons total	27,90	52,85	45,96	30,98	26,19	36,24

Table 4.1: The composition of the **neutron part (upper table)** and the **proton part (lower table)** of the γ-vibrational wave function in Gd in terms of two quasi-particle excitations between Nilsson states which are connected by the $r^2Y_{2\pm2}$ operator.

Although we have made calculations for 88 neutrons they are not shown in figure 4.1 because for further evalutation only well-deformed nuclei with a stable ground state deformation and a ratio $R_{4/2} > 2.9$ are considered.

Results for Dy isotopes

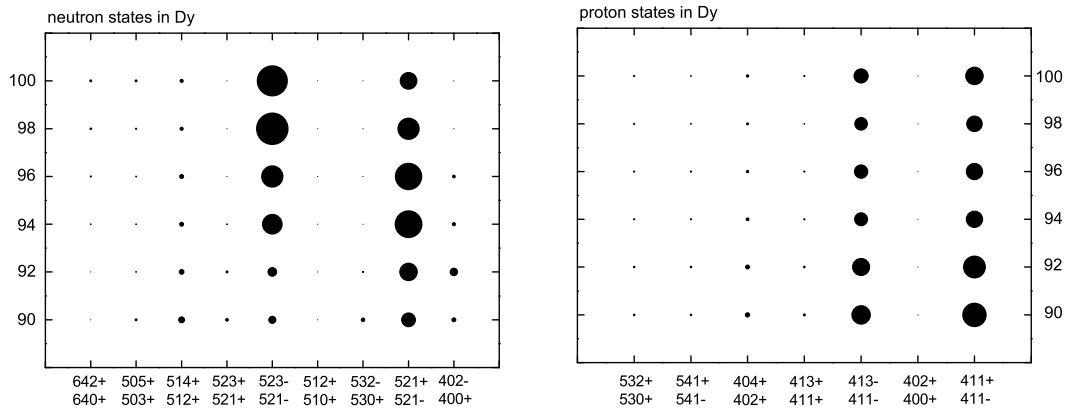

Figure 4.2: Most relevant two quasi-particle amplitudes for the 2^+_γ state in well deformed even-even Dy isotopes. The radius of the circles indicates the fraction of each wave-function component with respect to the total wave function. Eeach row is classified by the neutron number of the isotope.

Nilsson states	N = 88	N = 90	N = 92	N = 94	N = 96	N = 98	N = 100
642+ 640+	0,23	0,36	0,52	0,95	1,04	1,6	2,06
505+ 503+	5,92	1,86	0,68	0,69	0,62	1,26	2,19
514+ 512+	7,13	6,52	5,56	4,25	3,95	3,11	3,38
523+ 521+	2,56	2,88	2,13	0,74	0,56	0,12	0,06
523- 521-	12,28	7,98	9,62	21,48	23,1	33,99	32,42
512+ 510+	1,05	0,44	0,11	0,11	0,11	0,2	0,39
532- 530+	6,72	3,62	1,28	0,26	0,18	0,04	0,02
521+ 521-	23,11	15,39	19,5	28,73	28,51	22,97	18,51
402- 400+	3,29	4,73	8,42	3,38	2,92	0,45	0,2
neutrons total	62,28	43,78	47,81	60,60	60,98	63,74	59,24
532+ 530+	0,84	1,56	1,62	1,25	1,21	1,08	1,17
541+ 541-	1,01	1,61	1,49	1,09	1,04	0,87	0,94
404+ 402+	4,61	5,1	4,01	2,83	2,59	2,19	2,37
413+ 411+	1,83	2,1	1,78	1,26	1,18	0,98	1,06
413- 411-	12,78	20,23	19,16	14,63	14,68	13,97	15,79
402+ 400+	0,29	0,11	0,09	0,05	0,04	0,02	0,03
411+ 411-	16,34	25,53	24,04	18,28	18,29	17,14	19,4
protons total	37,72	56,22	52,19	39,40	39,02	36,26	40,76

Table 4.2: The composition of the **neutron part (upper table)** and the **proton part (lower table)** of the γ-vibrational wave function in Dy in terms of two quasi-particle excitations between Nilsson states which are connected by the $r^2Y_{2\pm2}$ operator.

Although we have made calculations for 88 neutrons they are not shown in figure 4.2 because for further evalutation only well-deformed nuclei with a stable ground state deformation and a ratio $R_{4/2} > 2.9$ are considered.

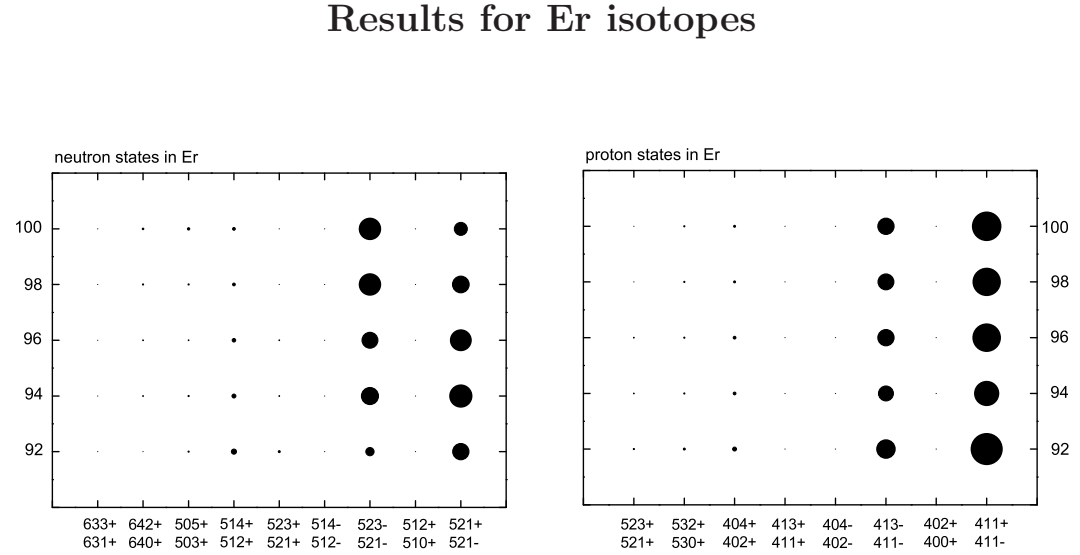

Figure 4.3: Most relevant two quasi-particle amplitudes for the 2^+_γ state in well deformed even-even Er isotopes. The radius of the circles indicates the fraction of each wave-function component with respect to the total wave function. Eeach row is classified by the neutron number of the isotope.

Nilsson state	N = 92	N = 94	N = 96	N = 98	N = 100
633+ 631+	0,08	0,12	0,10	0,21	0,41
642+ 640+	0,40	0,84	0,88	1,33	1,77
505+ 503+	1,44	1,35	0,80	1,24	2,39
514+ 512+	5,77	4,14	3,82	2,92	2,99
523+ 521+	2,20	0,66	0,64	0,17	0,06
514- 512-	0,13	0,14	0,10	0,15	0,27
523- 521-	9,29	19,13	17,62	23,37	23,64
512+ 510+	0,35	0,40	0,13	0,23	0,46
521+ 521-	18,12	24,56	22,71	18,53	14,53
neutrons total	37,77	51,35	46,79	48,16	46,51
523+ 521+	1,06	0,76	0,72	0,59	0,60
532+ 530+	1,97	1,43	1,43	1,20	1,17
404+ 402+	4,09	2,84	2,90	2,24	2,27
413+ 411+	0,46	0,33	0,30	0,25	0,22
404- 402-	0,53	0,24	0,16	0,08	0,09
413- 411-	20,29	16,40	18,02	17,77	18,20
402+ 400+	0,50	0,23	0,15	0,08	0,09
411+ 411-	33,34	26,42	29,53	29,63	30,85
protons total	62,23	48,65	53,21	51,84	53,49

Table 4.3: The composition of the **neutron part (upper table)** and the **proton part (lower table)** of the γ-vibrational wave function in Er in terms of two quasi-particle excitations between Nilsson states which are connected by the $r^2Y_{2\pm2}$ operator.

Results for Hf isotopes

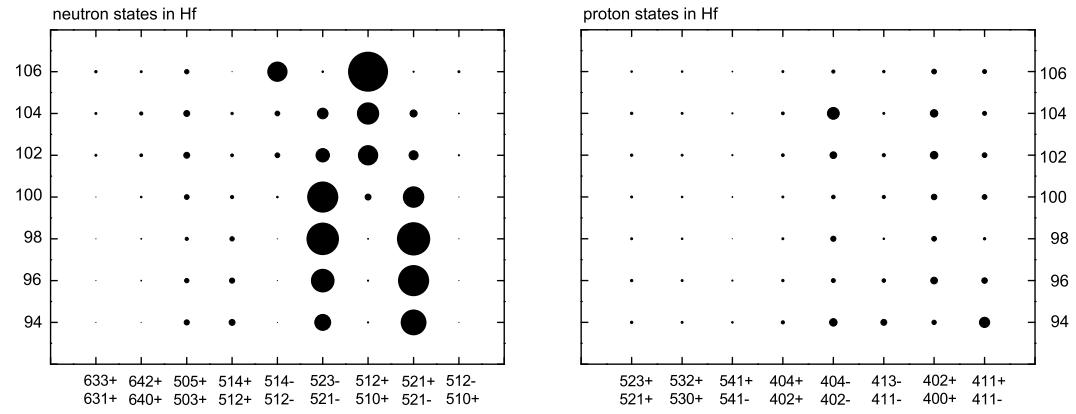

Figure 4.4: Most relevant two quasi-particle amplitudes for the 2^+_γ state in well deformed even-even Hf isotopes. The radius of the circles indicates the fraction of each wave-function component with respect to the total wave function. Eeach row is classified by the neutron number of the isotope.

Nilsson states	N = 94	N = 96	N = 98	N = 100	N = 102	N = 104	N = 106
633+ 631+	0,13	0,16	0,16	0,6	1,96	2,04	2,54
642+ 640+	0,4	0,67	0,98	1,85	3,06	3,18	2,26
505+ 503+	5,79	4,57	3,2	5,17	6,55	6,66	4,95
514+ 512+	6,73	5,84	4,56	3,31	2,84	2,63	0,54
514- 512-	0,46	0,39	0,25	1,8	5,57	5,24	21,02
523- 521-	17,62	24,85	34,06	32,59	14,78	12,17	1,78
512+ 510+	1,34	1,14	0,82	6,75	20,96	23,1	41,75
521+ 521-	27,03	32,44	34,54	22,25	9,97	8,05	1,36
512- 510+	0,21	0,17	0,11	0,44	1,09	0,86	2,09
neutrons total	59,71	70,23	78,67	74,77	66,77	63,91	78,29
523+ 521+	2,35	2,28	1,87	1,88	2,64	2,53	1,73
532+ 530+	2,18	1,99	1,56	1,62	2,24	2,06	1,48
541+ 541-	1,46	1,15	0,61	0,99	1,28	1,07	0,91
404+ 402+	3,18	2,63	1,98	2,23	2,99	2,76	2,12
404- 402-	8,17	4,01	5,59	3,73	7,28	13,33	3,36
413- 411-	6,79	3,83	1,65	3,11	3,13	2,27	2,39
402+ 400+	4,47	7,52	5,4	6,32	8,45	8,1	5,5
411+ 411-	11,7	6,38	2,66	5,35	5,23	3,96	4,22
protons total	40,29	29,77	21,33	25,23	33,23	36,09	21,71

Table 4.4: The composition of the **neutron part (upper table)** and the **proton part (lower table)** of the γ-vibrational wave function in Hf in terms of two quasi-particle excitations between Nilsson states which are connected by the $r^2Y_{2\pm2}$ operator.

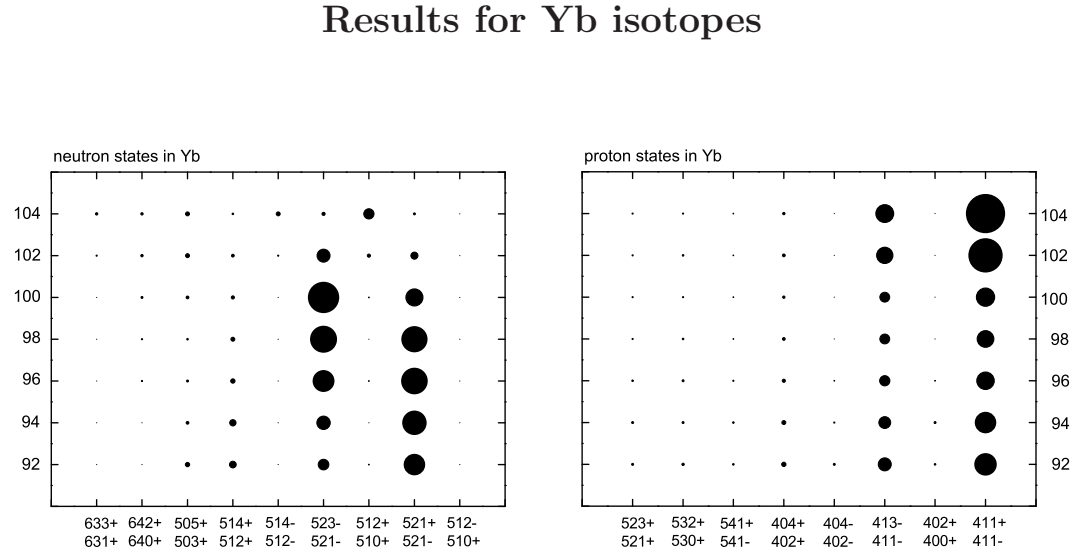

Figure 4.5: Most relevant two quasi-particle amplitudes for the 2^+_γ state in well deformed even-even Yb isotopes. The radius of the circles indicates the fraction of each wave-function component with respect to the total wave function. Eeach row is classified by the neutron number of the isotope.

Nilsson state	N = 92	N = 94	N = 96	N = 98	N = 100	N = 102	N = 104
633+ 631+	0,1	0,11	0,19	0,18	0,5	1,44	2,44
642+ 640+	0,3	0,49	1,09	1,21	1,89	2,54	2,59
505+ 503+	4,51	2,82	2,1	1,66	3,06	4,24	4,33
514+ 512+	7,31	6,87	4,93	4,03	3,37	3,04	1,72
514- 512-	0,27	0,2	0,24	0,18	0,42	1,32	3,98
523- 521-	11,98	14,8	22,56	28,14	32,8	14,32	3,44
512+ 510+	0,75	0,57	0,69	0,28	0,87	3,51	11,47
521+ 521-	22,39	25,75	27,55	27,3	19,07	7,78	2,12
512- 510+	0,13	0,11	0,06	0,04	0,07	0,14	0,23
neutrons total	47,74	51,73	59,41	63,02	62,05	38,32	32,32
523+ 521+	2,04	1,93	1,6	1,32	1,18	1,35	1,22
532+ 530+	2,29	2,21	1,87	1,54	1,37	1,57	1,44
541+ 541-	1,61	1,48	1,1	0,92	0,83	0,99	0,92
404+ 402+	4,45	4,27	3,51	2,86	2,54	2,91	2,67
404- 402-	1,98	1,08	0,89	0,52	0,42	0,42	0,4
413- 411-	14,48	13,12	11,56	10,79	11,22	18,25	19,77
402+ 400+	1,79	1,95	0,81	0,45	0,35	0,35	0,32
411+ 411-	23,62	22,22	19,26	18,57	20,04	35,83	40,94
protons total	52,26	48,27	40,59	36,98	37,95	61,68	67,68

Table 4.5: The composition of the **neutron part (upper table)** and the **proton part (lower table)** of the γ-vibrational wave function in Yb in terms of two quasi-particle excitations between Nilsson states which are connected by the $r^2Y_{2\pm2}$ operator.

Results for Sm isotopes

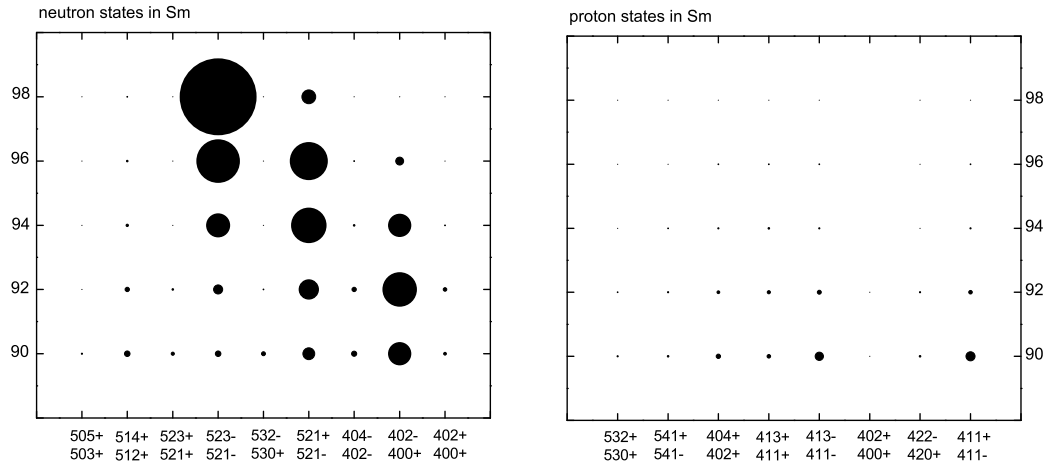

Figure 4.6: Most relevant two quasi-particle amplitudes for the 2^+_γ state in well deformed even-even Sm isotopes. The radius of the circles indicates the fraction of each wave-function component with respect to the total wave function. Eeach row is classified by the neutron number of the isotope.

Nilsson states	N = 90	N = 92	N = 94	N = 96	N = 98
505+ 503+	1,23	0,33	0,16	0,1	0,35
514+ 512+	6,4	4,81	2,66	1,53	0,92
523+ 521+	3,27	1,83	0,46	0,17	0,02
523- 521-	6,36	9,97	25,33	45,3	80,5
532- 530+	4,21	0,77	0,11	0,04	0,01
521+ 521-	13,37	21,1	37,14	39,5	15,47
404- 402-	5,9	4,35	1,84	0,62	0,05
402- 400+	24,4	35,75	24,42	8,79	0,32
402+ 400+	2,75	3,92	0,96	0,31	0,04
neutrons total	67,89	82,83	93,08	96,34	97,68
532+ 530+	1,04	0,78	0,4	0,21	0,13
541+ 541-	1,54	1,35	0,7	0,36	0,23
404+ 402+	4,82	2,77	1,25	0,64	0,41
413+ 411+	3,72	3,36	1,76	0,91	0,57
413- 411-	9,24	4,07	1,25	0,68	0,43
402+ 400+	0,08	0,02	0	0	0
422- 420+	1,79	1,08	0,41	0,23	0,15
411+ 411-	9,88	3,74	1,14	0,63	0,4
protons total	32,11	17,17	6,92	3,66	2,32

Table 4.6: The composition of the **neutron part (upper table)** and the **proton part (lower table)** of the γ-vibrational wave function in Sm in terms of two quasi-particle excitations between Nilsson states which are connected by the $r^2Y_{2\pm2}$ operator.

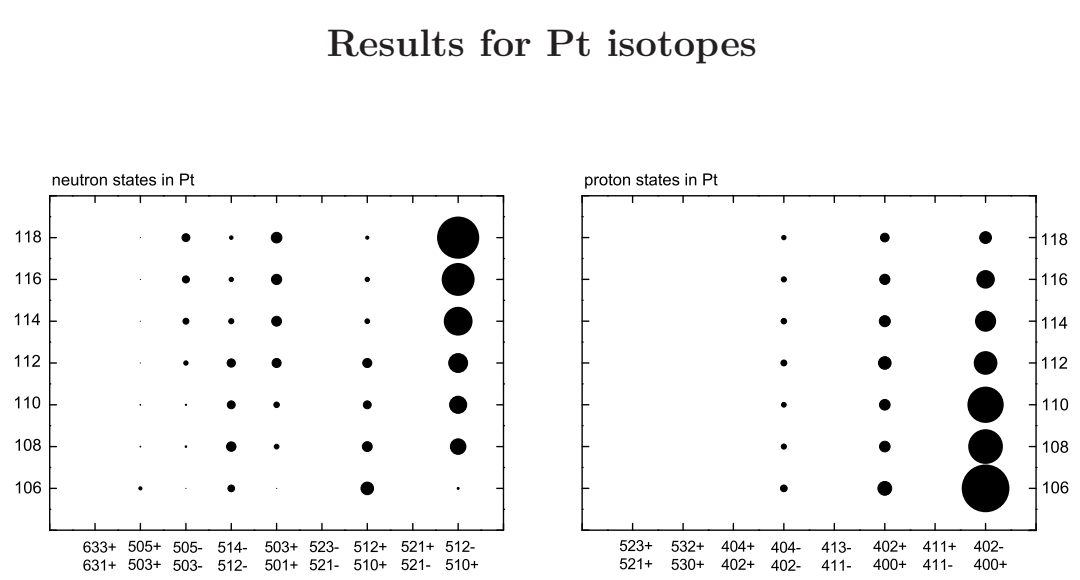

Figure 4.7: Most relevant two quasi-particle amplitudes for the 2^+_γ state in well deformed even-even Pt isotopes. The radius of the circles indicates the fraction of each wave-function component with respect to the total wave function. Eeach row is classified by the neutron number of the isotope.

Nilsson states	N = 106	N = 108	N = 110	N = 112	N = 114	N = 116	N = 118
633+ 631+	0	0	0	0	0	0	0
505+ 503+	3,18	1,02	0,7	0,52	0,24	0,14	0,07
505- 503-	0,21	1,68	1,32	4,48	6,57	7,78	8,86
514- 512-	7,55	10,35	8,79	9,22	5,85	4,94	3,84
503+ 501+	0,36	5,28	6,32	10	11,27	11,41	11,96
523- 521-	0	0	0	0	0	0	0
512+ 510+	13,85	10,56	8,64	9,73	5,56	4,46	3,44
521+ 521-	0	0	0	0	0	0	0
512- 510+	2,11	17,29	18,86	20,74	30,07	34,33	44,02
neutrons total	27,26	46,19	44,63	54,69	59,56	63,07	72,18
523+ 521+	0	0	0	0	0	0	0
532+ 530+	0	0	0	0	0	0	0
404+ 402+	0	0	0	0	0	0	0
404- 402-	7,31	5,67	5,44	6,76	6,09	5,69	4,97
413- 411-	0	0	0	0	0	0	0
402+ 400+	15,46	11,86	11,91	13,9	12,47	11,71	9,64
411+ 411-	0	0	0	0	0	0	0
402- 400+	49,97	36,29	38,02	24,65	21,88	19,53	13,2
protons total	72,74	53,81	55,37	45,31	40,44	36,93	27,82

Table 4.7: The composition of the **neutron part (upper table)** and the **proton part (lower table)** of the γ-vibrational wave function in Pt in terms of two quasi-particle excitations between Nilsson states which are connected by the $r^2Y_{2\pm2}$ operator.

Results for Os isotopes

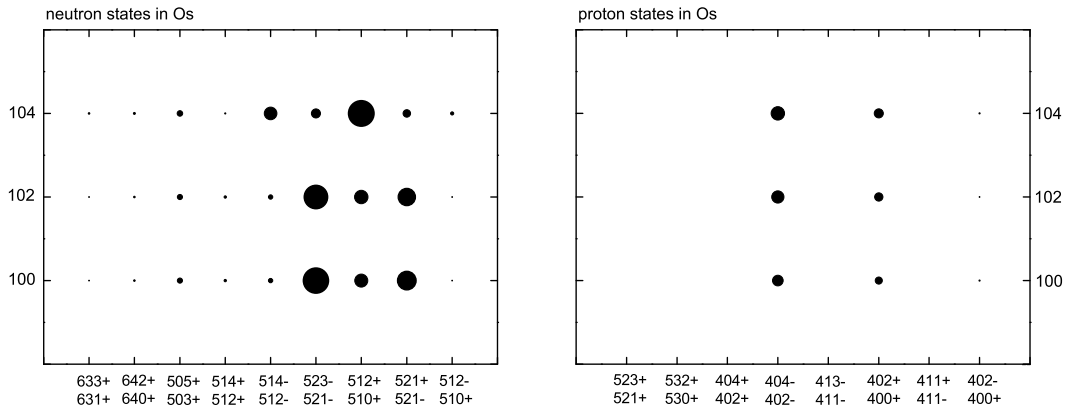

Figure 4.8: Most relevant two quasi-particle amplitudes for the 2^+_γ state in well deformed even-even Os isotopes. The radius of the circles indicates the fraction of each wave-function component with respect to the total wave function. Eeach row is classified by the neutron number of the isotope.

Nilsson states	N = 100	N = 102	N = 104
633+ 631+	0,67	0,69	1,47
642+ 640+	1,56	1,57	1,99
505+ 503+	5,97	5,85	6,08
514+ 512+	2,45	2,3	1,14
514- 512-	4,54	4,77	14,14
523- 521-	27,58	25,91	9,98
512+ 510+	14,47	15,01	28,05
521+ 521-	20,63	19,3	8,19
512- 510+	0,96	0,99	3,16
neutrons total	78,83	76,39	74,2
523+ 521+	0	0	0
532+ 530+	0	0	0
404+ 402+	0	0	0
404- 402-	12,07	13,61	14,76
413- 411-	0	0	0
402+ 400+	8,03	9,03	9,85
411+ 411-	0	0	0
402- 400+	1,07	0,97	1,19
protons total	21,17	23,61	25,8

Table 4.8: The composition of the **neutron part (upper table)** and the **proton part (lower table)** of the γ-vibrational wave function in Os in terms of two quasi-particle excitations between Nilsson states which are connected by the $r^2Y_{2\pm2}$ operator.

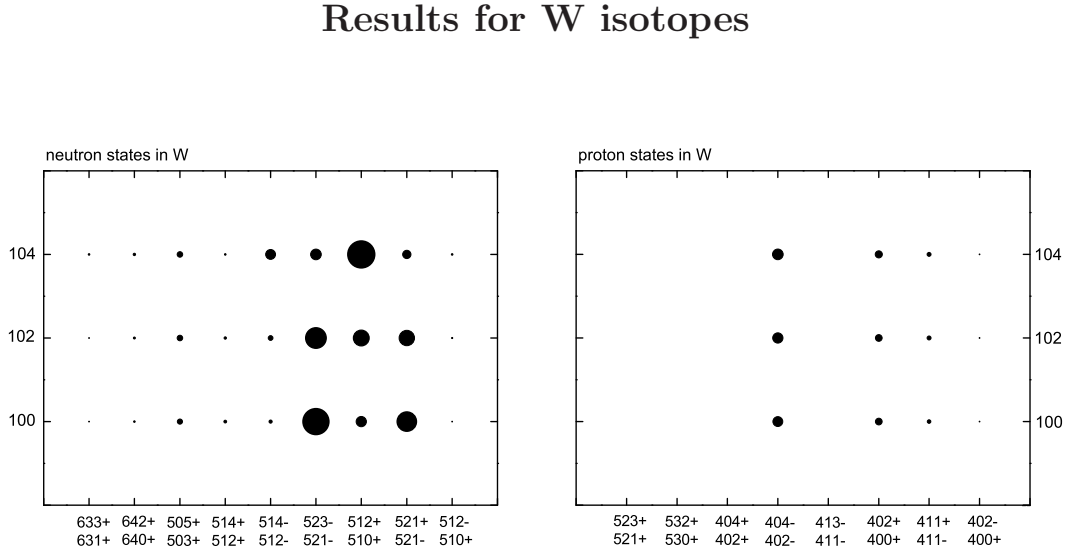

Figure 4.9: Most relevant two quasi-particle amplitudes for the 2^+_γ state in well deformed even-even W isotopes. The radius of the circles indicates the fraction of each wave-function component with respect to the total wave function. Eeach row is classified by the neutron number of the isotope.

Nilsson states	N = 100	N = 102	N = 104
633+ 631+	0,69	1,02	1,64
642+ 640+	1,73	2,09	2,38
505+ 503+	5,87	6,32	6,39
514+ 512+	2,92	2,47	1,54
514- 512-	3,22	5,27	10,8
523- 521-	28,52	22,92	12,06
512+ 510+	11,41	17,92	29,87
521+ 521-	21,61	16,98	9,05
512- 510+	0,76	1,07	1,79
neutrons total	76,73	76,06	75,52
523+ 521+	0	0	0
532+ 530+	0	0	0
404+ 402+	0	0	0
404- 402-	11,28	11,53	11,86
413- 411-	0	0	0
402+ 400+	7,41	7,6	7,81
411+ 411-	3,89	4,08	4,09
402- 400+	0,69	0,73	0,72
protons total	23,27	23,94	24,48

Table 4.9: The composition of the **neutron part (upper table)** and the **proton part (lower table)** of the γ-vibrational wave function in W in terms of two quasi-particle excitations between Nilsson states which are connected by the $r^2Y_{2\pm2}$ operator.

4.2.1 Comparison with other calculations

It it is important to verify that the results shown in this work which were calculated in the framework of the Random Phase Approximation incorporating the quadrupole and the pairing residual interaction are reasonable in view of the simplifications entering in our calculation. With regard to the various simplifications applied in our calculations (illustrated at the beginning of this chapter) at least the qualitative distribution of the wave function on the various basis states should roughly correspond with results from calculations performed in other papers and results that were obtained experimentally.

As already mentioned in 1964 similar calculations have been performed by *Bès et al.* [20] concerning the composition of the gamma-vibrational state in deformed even-even rare earth nuclei. Actually we have taken these results as a guideline to determine the most important two quasi-particle Nilsson states to be taken into consideration in our calculations. Therefore it does not surprise that the quasiparticle composition obtained in this paper - if our model is correct and the simplifications are appropriate - resembles those results. Due to the many small components which we do not treat it is quite clear that our results focused on the major components are usually overpredicted (because of their normalization to 1). Indeed, as already mentioned, the small components make up a constant value of about ten percent of the vibrational wave function according to the calculations carried out by *Bès et al.* for the rare earth nuclei.
Altogether a detailed comparison of our results and the results of *Bès et al.* for the Gd, Dy, Er, Yb and Hf isotopes - especially focused on the qualitative evolution of the structure of the wave-function as moving along an isotopic chain - shows a good agreement. Thus the various simplifications applied in our model seem to be justified.
For some Gd, Dy, Er isotopes and the Hf isotope with 106 neutrons calculations by *Soloviev et al.* [24, 27] have been performed in the context of the *quasiparticle-phonon nuclear model* (QPNM) [21-23]. In comparison to our simple model the QPNM is rather complicated. The initial QPNM Hamiltonian for nonrotational states of deformed nuclei consists of the average field of the neutron and proton systems in the form of the axialy symmetric Woods-Saxon potential, monopole pairing, and in addition also isoscalar and isovector particle-hole and particle-particle multipole, spin-multipole, and tensor interactions between the quasiparticles.
Nevertheless, the results from the present work plotted together with the results of *Soloviev et al.* and *Bès et al.* in figures 4.10-4.13 show an overall reasonable agreement, although the admixture of two quasi-particle states that cannot be connected by the $r^2Y_{2\pm2}$ operator is in some cases significant, in particular in calculations by *Soloviev et al.*. However, the agreement seems sufficiently good to give confidence to the schematic calculation of this work, that is primarily interested in the investigations of trends in the contributions of those two quasi-particle states that can be connected by the $r^2Y_{2\pm2}$ operator.

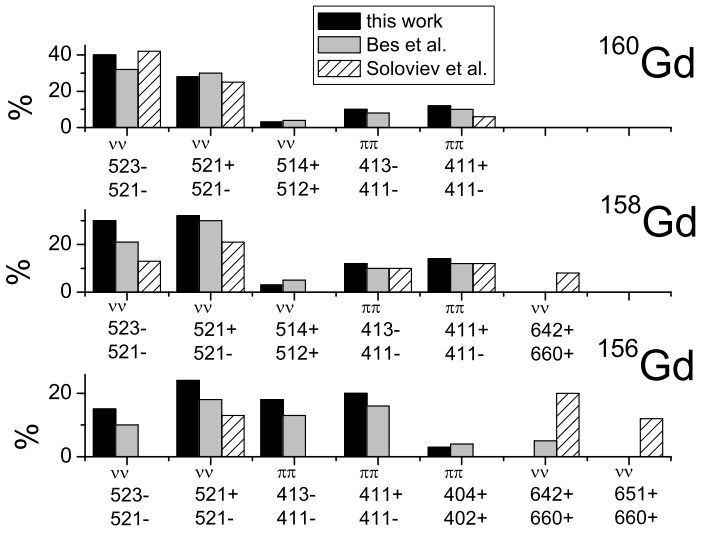

Figure 4.10: Comparison of the strongest two-quasiparticle components in the wave function of the 2^+_γ state (in percent) in Gd isotopes in the calculations from this work with those by *Bès et al.* [20] and by *Soloviev et al.* [24].

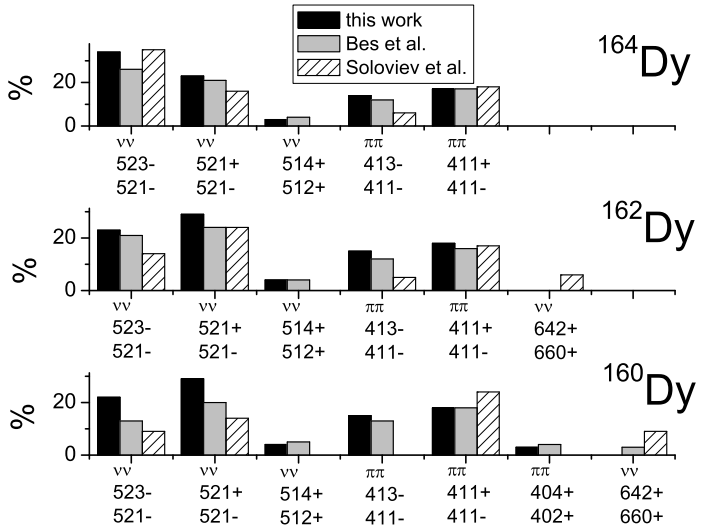

Figure 4.11: Comparison of the strongest two-quasiparticle components in the wave function of the 2^+_γ state (in percent) in Dy isotopes in the calculations from this work with those by *Bès et al.* [20] and by *Soloviev et al.* [24].

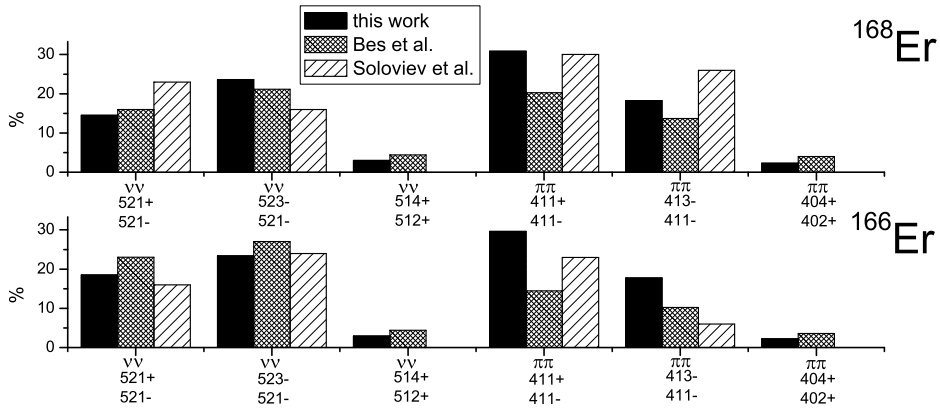

Figure 4.12: Comparison of the strongest two-quasiparticle components in the wave function of the 2^+_γ state (in percent) in Er isotopes in the calculations from this work with those by *Bès et al.* [20] and by *Soloviev et al.* [24].

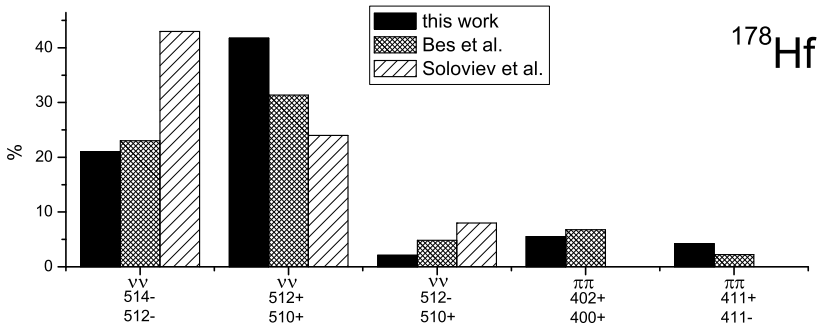

Figure 4.13: Comparison of the strongest two-quasiparticle components in the wave function of the 2^+_γ state (in percent) in the ^{178}Hf isotope in the calculations from this work with those by *Bès et al.* [20] and by *Soloviev et al.* [27].

Chapter 5

Discussion of the results

In this chapter we show that structural evolution obtained in the Interacting Boson Model (IBA) for the rare-earth region can indeed be linked to the qualitative behaviour of the distribution of the gamma vibrational wave-function among the basis states as calculated in our microscopic approach.
We explicitly refer to the trajectories of the rare-earth nuclei in the IBA symmetry triangle [16, 17] as illustrated in section 1.2.
Finally, a formula is presented which shows that even a quantitative correlation of the results from the microscopical calculations with the paramter χ in the IBA Hamiltonian is present.

5.1 The distribution function S and the gamma correlation function Γ

Considering the results presented in chapter 4 it can be seen that the number of important components of the collective wave function is limited to a maximum value of nine orbital combinations for the neutrons and eight orbital combinations for the protons in the rare-earth region. In order to make a reasonable comparison between different distributions of the wave function among the basis states, it is necessary to work with a fixed number of basis states for all nuclei. Thus we normalize the calculation to the maximum quantity of contributing orbits separately for neutrons and protons. This means, for example, if our calculations yielded only five important proton states it would be necessary to take another three states with zero contribution into account.
A *distribution function* $S_\alpha(k)$ is now constructed to make it possible to distinguish in a quantitative way whether the collective wave function is mainly carried by a few dominant Nilsson states representing a large part of the collective wave function, or

whether the collective wave function is distributed in more or less equal parts over a large number of basis states:

$$S_\alpha(k) = \frac{\sum_{h=1}^{k-1}\sum_{l>h}|C_{mi}^{(h)} - C_{mi}^{(l)}|}{(k-1)} \; ; \; \sum_{h=0}^{k} C_{mi}^{(h)} = 1 \tag{5.1}$$

The total number of contributing states is denoted by k. The index $\alpha = n, p$ distinguishes between neutrons and protons. It is of course necessary that the sum of the squares of the amplitudes entering formula (5.1) are normalized to 1. Thus the results from chapter 4 have to be modified first to be suitable for the calculation if the neutron or proton parts are analysed separately.
The distribtion function S can have values between 0 and 1. For the case that exactly one two-quasiparticle excitation conributes to the gamma-vibrational wave function one obtains $S_\alpha(k) = 1$ while $S_\alpha(k) = 0$ is reached in the case that all k two-quasiparticle excitations contribute exactly with the same squared amplitudes. Due to the normalization to a fixed number of basis states for all rare-earth nuclei under consideration it is possible to skip the previous notation $S_\alpha(k)$ and simplify it to S_α.

In figure 5.1 an illustration is shown to verify that the distribution function works in the way indicated above. We choose a set of eight contributing states and determine all possbile values of the squared amplitudes, in the order of their magnitude from left to right, which lead to the same value of the distribution function S. Each possible combination of the eight values is connected by straight lines. It can be seen that the distribution function indeed delivers a reasonable classifaction for distributions lying between the limiting cases of $S = 1$ and $S = 0$.

Besides the distribution functions S_n and S_p we can, within the framework of our model, also determine the fractions f_p and f_n of the proton and neutron quasiparticles to the wave function of the gamma-vibrational state ($f_n + f_p = 1$). These values were already presented in the previous chapter in tables 4.1-4.9. Figures 5.3-5.10 show the distribution functions S_n, S_p, as well as the fraction f_n for well deformed Sm, Gd, Dy, Er, Yb, Hf and Os, W isotopes. Also shown is the distribution function S for which all squared amplitudes were considered without distinguishing between neutrons and protons.

One can observe some general feature for the distribution functions. The proton distribution function S_p remains almost constant as a function of neutron number for most elements. Exceptions to this behaviour occur only, e.g. in ^{174}Hf, due to a variation of the quadrupole deformation causing variations in the occupation of quasiparticle states. For the neutron distribution function S_n there are significant variations as a function of neutron number due to changes of the Fermi energy as one moves along an isotopic chain. Therefore the development of the neuton distribution function S_n is of prime interest and the total distribution function S, characterizing the distribution of the wave function among all basis states without distinguishing

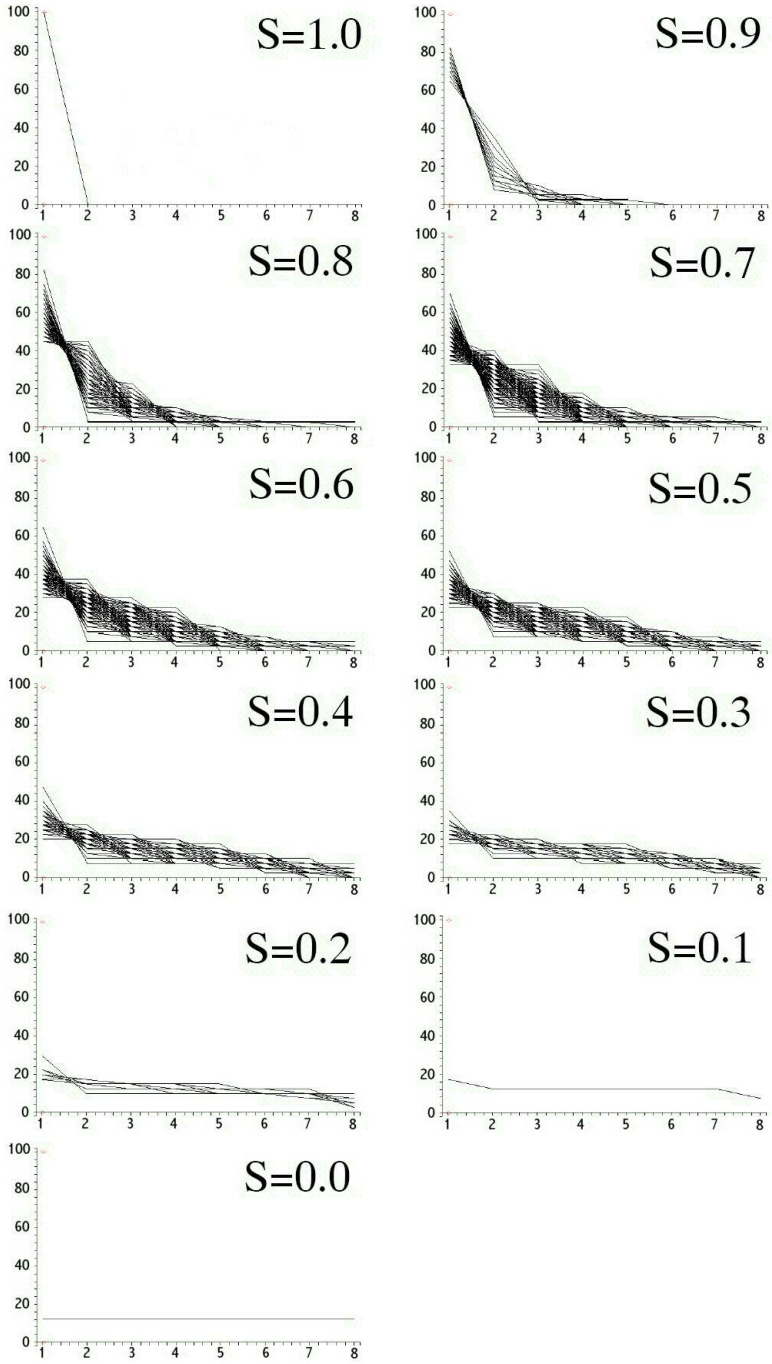

Figure 5.1: Illustration of the distribution function for eight contributing states. The states are given in the order of their magnitude from left to right. The vertical axis is in percent.

between neutrons and protons, correlates mostly with S_n.
Another remarkable feature is the strong correlation in most nuclei between S_n and f_n, the fraction of the entire collective wave function carried by all the neutron states together. To avoid any misunderstandings it should be reemphasized that S_n only

takes the distribution among the neutron states into account. Due to its construction it is completely independent of the neutron fraction of the wave function. However, the evaluated data shows that the process of building up a few highly dominant neutron basis states when moving along the isotopic chain is most often connected with the transfer of weight in the entire wave function from the proton states to the neutron states.

Finally all the information gathered so far is combined into one value which we denote *gamma correlation function* Γ.

$$\Gamma = \frac{1}{4}\left[f_p \cdot S_p \cdot f_n \cdot S_n\right] \tag{5.2}$$

It is obvious that the possible values of Γ are located in the interval $[0, 1]$. The value of Γ is close to 1 if both for neutrons and protons the collective wave function is only carried by a few dominant states. Furthermore the wave function should be equally distributed among both kinds of nucleons.
In figure 5.2 we show the gamma-correlation function as a function of the neutron number for the rare-earth nuclei. The Γ values for the gamma-soft Pt isotopes for which the application of our model is certainly questionable are also inlcuded (see section 5.6 for further details). These results should only be taken as some general guidance.

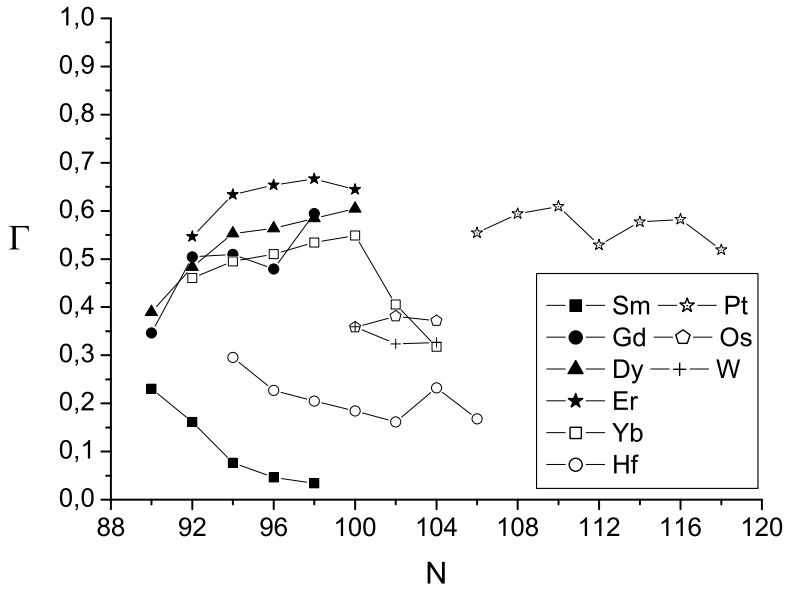

Figure 5.2: Gamma-correlation function Γ as a function of neutron number.

The IBA calculations presented in the introduction show quite different trajectories for Gd, Dy and Er on one side and for Yb, Hf on the other. Here we want to

concentrate on the behaviour of the polar angle θ, which was defined in the IBA section of this work. The angle is related to the gamma-softness of the various nuclei. Table 5.1 explicitly summarizes the angles θ that were obtained in the IBA fits [16].

N	θ (Gd)	θ (Dy)	θ (Er)	θ (Yb)	θ (Hf)
90	10.1	21.5			
92	21.0	29.6	32.8	41.0	39.6
94	23.7	37.8	36.0	36.4	36.0
96	36.0	45.9	43.2	33.7	32.8
98	46.4	48.2	45.9	32.3	24.2
100			43.7	28.7^a	21.9
102				19.6^a	10.1
104					16.5

Table 5.1: Angle $\theta = (180°/\pi) \cdot (\pi/3 + (2/\sqrt{7})\chi(\pi/3))$ in the IBA symmetry triangle for the well deformed Gd, Dy, Er, Yb, and Hf as a function of neutron number. The marking ^{a} means that the corresponding parameter χ was obtained by considering the second excited 0^+ state as the first excited collective 0^+ state.

The detailed discussion of the nuclei on the following pages is supposed to relate their behaviour in the symmetry triangle to the gamma-correlation function and the underlying distribution functions.

5.2 Sm isotopes

For the Sm isotopes IBA calculations using a simplified Hamiltonian were performed by *Scholten et al.* [31]. In these calculations best fits for the even-even Sm isotopes with $N \geq 90$ were obtained using a value of $\chi = -\sqrt{7}/2$, placing those nuclei on the $U(5)$-$SU(3)$ leg of the symmetry triangle with $\theta = 0$. Thus the Sm isotopes are the most gamma-rigid well deformed nuclei considered in this study.

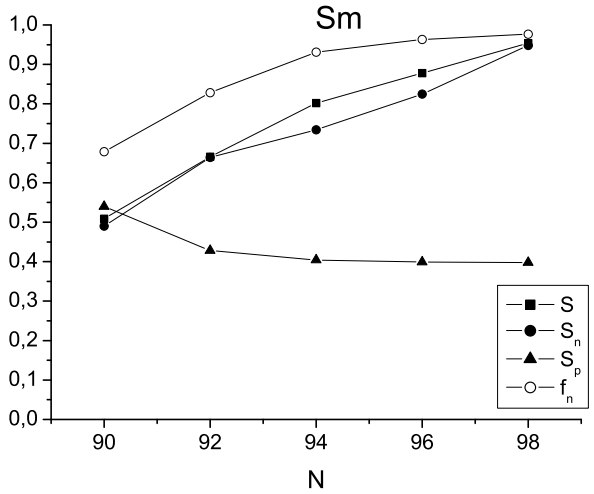

Figure 5.3: Distribution functions S_n and S_p for neutrons and protons, respectively, as a function of neutron number for well deformed even-even Sm isotopes together with the fraction f_n of neutrons in the wave-function of the 2^+_γ state and the distribution function S that does not distinguish between neutrons and protons.

The distribution of the wave function among the neutron basis states in Sm (see figure 5.3) changes its structure from an equal distribution of the wave function among many basis states to a dominance of few basis states leading to an increasing neutron distribution function S_n in figure 5.3. The protons show overall a very low proton distribution function S_p. At the same time one can observe a complete dominance of the neutrons in the wave-function of the 2^+_γ state with $f_n > 0.9$ for neutron numbers above N=92. This fact should be reflected in experimental electromagnetic reduced transition probabilities, potentially leading to strong M1 transitions from the 2^+_γ state to the 2^+_1 state. Indeed the extreme dominance of the neutrons is mainly responsible for the gamma rigidity of the Sm isotopes and determines the low values of the gamma correlation function Γ in figure 5.2.

5.3 Gd, Dy and Er isotopes

Within the IBA study of Ref. [16] the Dy and Gd isotopes evolve with increasing neutron number from intermediate angles around 20-30° for N=92, after crossing the transition from spherical to deformed phase, to larger angles close to 50° for N=98. At the same time the radial coordinate increases so that the O(6)-SU(3) leg of the symmetry triangle is reached near to the O(6) corner of the triangle. Thus these Dy and Gd nuclei show an increasing gamma-softness with increasing neutron number. However, one should keep in mind that these nuclei have a rotational $R_{4/2}$ value and thus are still quite far from a gamma-soft potential.

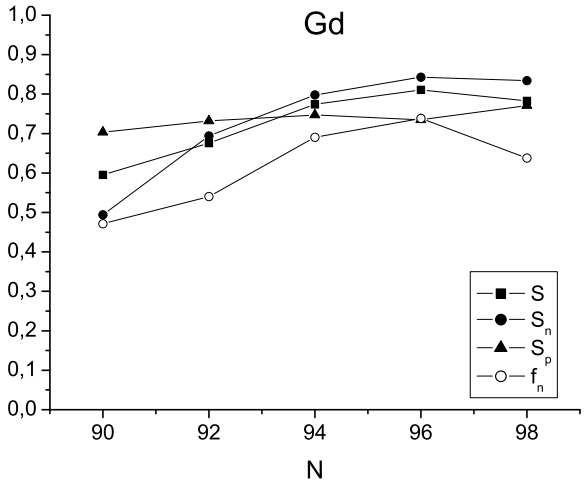

Figure 5.4: Same as figure 5.3 for Gd isotopes

In our calculation after the phase transition from spherical to deformed ($N > 90$) the Gd and Dy isotopes show the same structural evolution. The proton distribution function S_p in the figures 5.4, 5.5 stays for all isotopes on a relatively high level of about 0.7 indicating that the quasi-proton wave function is spread over only a few important basis states. Moving along the isotopic chain to higher neutron numbers the development among the neutron states changes their structure in Gd and Dy from an equal distribution of the wave function among many basis states to a dominance of few basis states leading to an increasing neutron distribution function S_n in figures 5.4 and 5.5. In this context the slope down of N=96 Gd in the plot of the gamma correlation function Γ might at first glance be confusing but one has to realize that Γ also incorporates beside S_n and S_p the wave function fractions f_p and f_n. The increasing dominance of the neutron states ($f_n \approx 0.75$) and hence the decreasing f_p values lead, despite the large S_n and S_p values to a reduction of

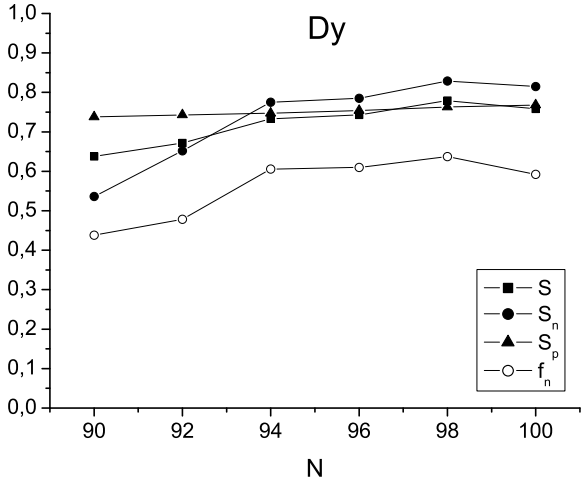

Figure 5.5: Same as figure 5.3 for Dy isotopes

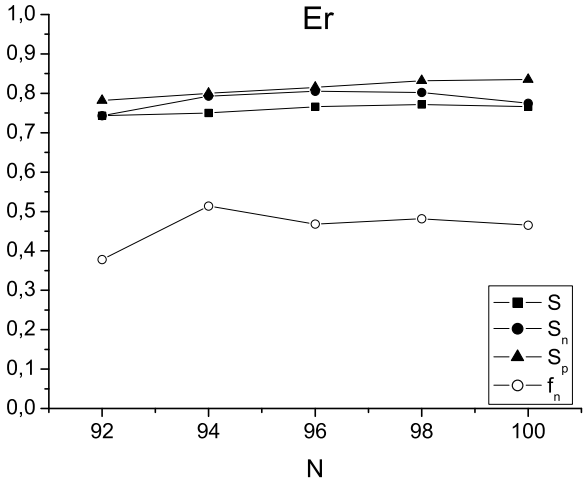

Figure 5.6: Same as figure 5.3 for Er isotopes

Γ. Considering the entire structural evolution it is apparent from our calculations that the Gd and Dy isotopes become gamma-soft for high neutron numbers.

All of the Er isotopes have nearly constant values of S_n and S_p (see figure 5.6) which are located at a rather high level comparable to the Gd and Dy isotopes and the wave function is except for ^{160}Er (N=92) perfectly balanced between neutrons and protons. Therefore all of the considered Er isotopes show a completely gamma-soft behavior with values for the gamma-correlation function Γ in figure 5.2 even higher

than those of the Gd and Dy isotopes. This result is consistent with the trajectory for the Er isotopes in the IBA triangle [16] which is lying somewhat above (higher angles) those trajectories of the Gd and Dy isotopes.

5.4 Yb and Hf isotopes

The Yb and Hf isotopes evolve quite differently in the IBA calculations [16], starting out at angles near 40° for N=92 down to angles below 20° for $N \geq 102$. Please note that for ^{170,172}Yb we used the χ-values obtained under the assumption that the second excited 0^+ state in these nuclei is the first excited collective 0^+ state. On first sight the trend of the two isotopic chains seems to be quite similar. On closer inspection one can, however, observe that the Yb isotopes stay at angles near 30° up to $N = 100$ and drops down to 20° for N=102 while θ drops for the Hf isotopes continuously from 30° at N=96 to 10° at $N = 102$, after which an increase in θ is observed to about 17°.

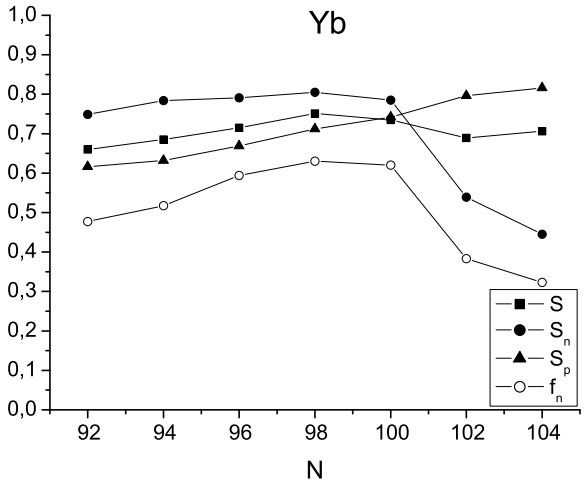

Figure 5.7: Same as figure 5.3 for Yb isotopes

In the present approach the different behavior of the proton distribution function S_p for the Yb and Hf isotopes in figures 5.7 and 5.8 is the main reason for the different evolution of Γ for these two isotopic chains, that is visible in figure 5.2. While the Yb isotopes start out with a trend towards gamma-softness (large Γ values) and drop suddenly to lower Γ-values at $N = 102$, the Hf isotopes start already at significantly lower Γ values of about 0.3 and drop to even lower values of about 0.15 at $N = 102$. For $N = 104$ the Γ-value increases again slightly only to drop back down for $N = 106$, for which unfortunately no IBA calculations were performed in [16] due to the large boson number.

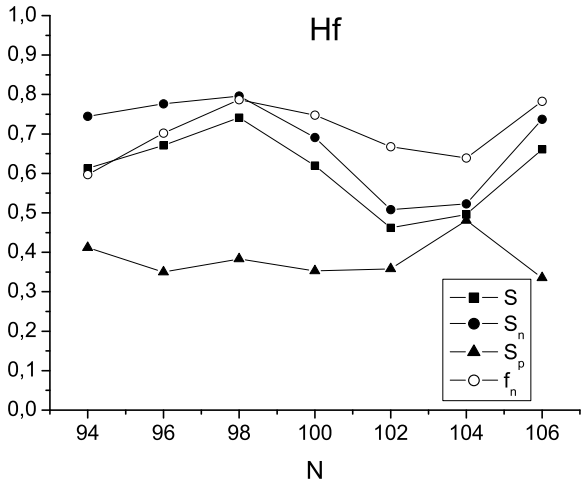

Figure 5.8: Same as figure 5.3 for Hf isotopes

For Yb the proton distribution function S_p is located at a level of about 0.7 increasing moderately with the neutron number meanwhile for Hf S_p is located at low values of about 0.4. For the Yb isotopes from $N = 92$ to $N = 100$ and for the Hf isotopes from $N = 94$ to $N = 98$ the neutron distribution function S_n stays nearly at the same level of about 0.77. This would imply a more or less constant behavior (of course at different levels for Yb and Hf) of the gamma correlation function Γ for those isotopes. However, in Yb the moderately increasing proton distribution function S_p leads to an increasing gamma-softness comparable in its rise with the rise of the Dy isotopes. For Hf isotopes the gamma correlation function Γ reveals even a slope down towards gamma-rigidity which is caused by the growing inequality in the distribution of the wave function on proton and neutron states. For the Yb isotopes from $N = 102$ to $N = 104$ the high value of the neutron distribution function S_n suddenly breaks away due to a change from a dominance of neutrons in the 2^+_γ wave function ($f_n \approx 0.5-0.6$) to a more dominant proton fraction ($f_p \approx 0.6-0.7$) that goes hand in hand with a change from a situation with few neutron quasiparticle states dominating the neutron wave-function ($S_n \approx 0.77$) to a more equal contribution of many neutron basis states to the neutron wave-function ($S_n \approx 0.5$) for $N > 100$. Therefore the isotopes go towards a more gamma rigid structure as the gamma-correlation function clearly shows. For the Hf isotopes from $N = 100$ to $N = 102$ exactly the same happens to the neutron states with the same intensity as in Yb leading to a further slope down of the new rating factor. Finally for $N = 104$ the Γ-value increases again towards gamma softness because of a sudden upward peak in S_p characterizing the proton state distribution. Despite the further growth of S_n for $N = 106$ the Γ drops down again. This is due partly to the increasing inequality of the distribution of the wave function among protons and neutrons and partly due to the return of S_p to its usual value for this isotopic chain.

5.5 Os and W isotopes

According to recent IBA Fits [17] the trajectories of the Os and W isotopes with 100, 102 and 104 neutrons lie quite close together, grouped very compactly close to the center of the triangle. The angle θ corresponds approximately to 19°.

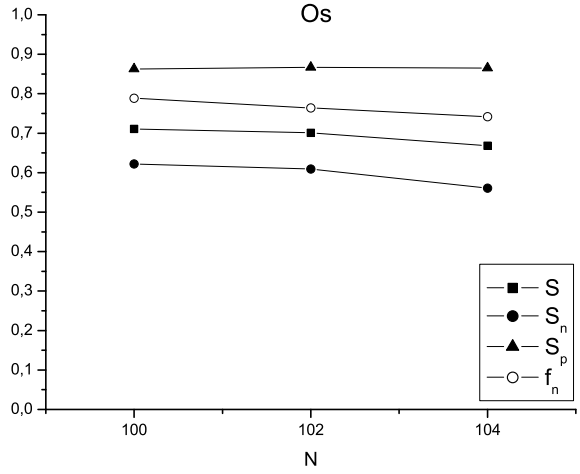

Figure 5.9: Same as figure 5.3 for Os isotopes

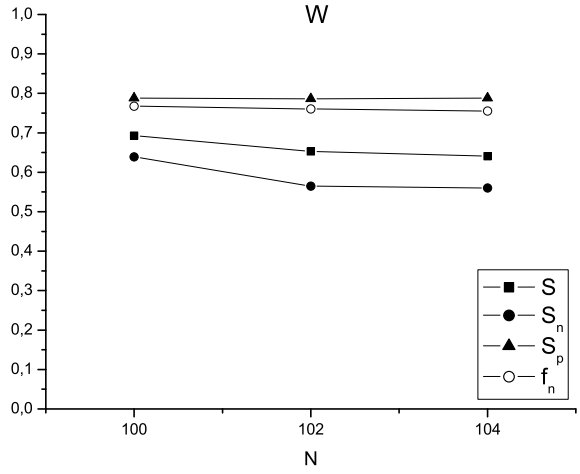

Figure 5.10: Same as figure 5.3 for W isotopes

In our calculations the distribution functions S_p and S_n as well as the neutron fraction of the wave function f_n do not change significantly along the short isotopic

chains for both elements. Furthermore Os and W show the same behaviour. The distribution function S_p is in both cases constant at a high level indicating that only a few orbital combinations contribute to the proton part of the wave function. The distribution function S_n for the neutrons also shows that there are only some few dominant neutron quasiparticle states. For Os and W the value of S_n is smaller than the value of S_p indicating that the neutron part of the wave function is spread over more orbital combinations in comparison to the proton part of the wave function. The relative low value of the gamma correlation function Γ corresponding to Gd and Dy isotopes with $N = 90$ is given because of the strong dominance of the neutrons in the entire wave function ($f_n \approx 0.8$) for all Os and W nuclei.

5.6 Pt isotopes

The structural evolution of the Pt isotopes from ^{172}Pt to ^{194}Pt has been recently re-investigated within the IBA [17, 18] using the same simple two-parameter Hamiltonian as applied for the rare earth region [16]. It was shown that their structure can be described by a smooth evolution *"from spherical with soft energy surfaces to deformed nuclei with increasingly γ-soft surface as N increases"* [18]. The structure of this isotopic chain ends in the classic O(6) nucleus ^{196}Pt [32].

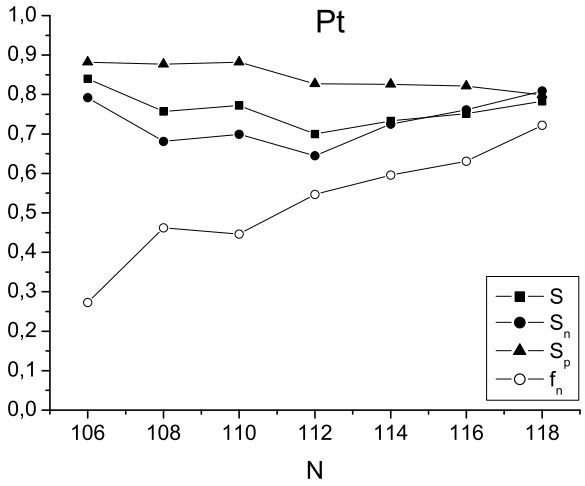

Figure 5.11: Same as figure 5.3 for Pt isotopes

In our current approach all of the Pt isotopes show an overall gamma-soft behavior with high neutron and proton distribution functions S_n and S_p of about 0.7 to 0.9 (see figure 5.11). The distribution of the wave function between neutrons and protons in general is also sufficiently balanced so that the values of the gamma-correlation function Γ for the Pt isotopes in figure 5.2 are relatively large and com-

parable to the highest values obtained for the neutron-rich Dy isotopes. The large values of Γ for the Pt isotopes relate well to the gamma-softness of the energy surfaces found in Ref. [18].

Despite the sensible results the calculations for the Pt isotopes yield in our model those results should be treated with caution. The Pt isotopes have only a slight deformation and the applied approximation in our approach (chapter 4.1) in calculating the interaction matrix elements is definitely not appropriate anymore. Our model and especially the further linear approach to relate the IBA angle to the values of the gamma-correlation function (see the following section 5.7) is only successful for well deformed nuclei. Applying it to the results for all Pt isotopes delivers IBA angles far above 60°.

5.7 Relation between Γ and Θ

So far we have discussed the behavior of the gamma-correlation function Γ for the various isotopic chains of even-even nuclei. It was possible to understand the evolution of Γ on the basis of the underlying dominant two-quasiparticle states.
Qualitatively, one can already see some similarities between the evolution of Γ and the angle Θ in the IBA triangle. In general large values of Γ relate to large angles Θ and vice versa.

In this section we would like to take this investigation one step further by trying to relate the gamma-correlation function directly to the angle θ which is proportional to the parameter χ in the simplified IBA Hamiltonian. However, besides Γ, one needs to take the energy of the 2^+_γ state explicitly into account, which also reflects directly the gamma-softness. We will do this using the energy ratio

$$R_{22} \equiv \frac{E(2^+_\gamma)}{E(2^+_1)}.$$

For example, for gamma-soft nuclei near the O(6) limit one finds $R_{22}^{-1} \approx 0.4$, while in the well deformed nuclei under investigation here, R_{22}^{-1} will take on much smaller values.

We have found that a linear combination of R_{22} and Γ is a reasonable starting point to reproduce the angles θ in the symmetry triangle. In order to obtain values for θ, we needed to introduce a baseline that was given by the Sm isotopes, that lie directly on the U(5) to SU(3) leg of the symmetry triangle and thus have $\theta = 0°$ (Ref. [31]). Therefore we have subtracted the Γ- and R_{22}-values for the Sm isotope with the same neutron number from the values for a given nucleus with proton number Z and neutron number N. Due to missing experimental data for Sm nuclei with $N > 98$ no calculations in the framework of our model could be made for these isotopes. Therefore we have used the Γ-value for the $N = 98$ isotope ^{160}Sm for

all Sm isotopes with $N > 98$. We end up with the following relation between θ in radians and the two dimensionless quantities R_{22} and Γ:

$$\theta = (\Gamma(Z,N) - \Gamma(62,N)) + R_{22}(O(6)) \cdot \left(R_{22}^{-1}(Z,N) - R_{22}^{-1}(62,N)\right) \qquad (5.3)$$

with $R_{22}(O(6))$ being the R_{22} value in the limit of the gamma unstable rotor. This relation works well for the Gd, Dy, Er, Yb and Hf isotopes.

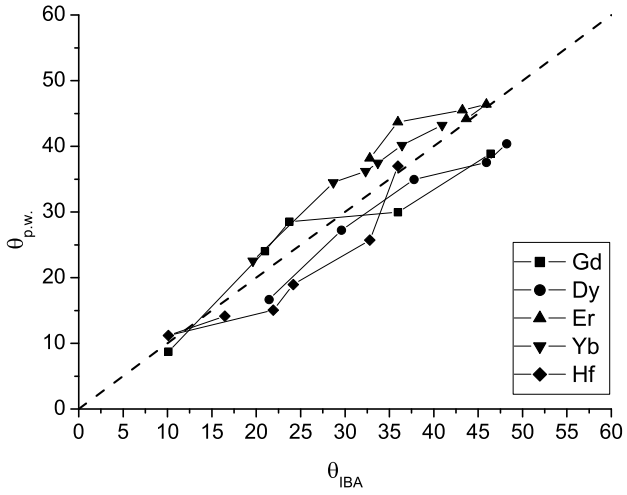

Figure 5.12: Angles $\theta_{p.w}$ calculated using equation (5.3) against angles obtained in the IBA fits. The dashed straight line indicates where the data points would lie in the case of a perfect correlation.

Figure 5.12 shows the angles $\theta_{p.w}$ from equation (5.3) against the angles θ_{IBA} obtained from the IBA calculations [16]. As one clearly sees, the θ-values calculated in our current approach correlate very well with those of the IBA fits. Unfortunately, the deeper theoretical connection leading to this equation escapes us at this point. Concerning this problem we make two remarks:

- It is obvious that the values $E_{2_\gamma^+}$ and Γ entering the formula (5.3) are not completely independent from each other. They are linked by the RPA equations describing the vibration. The energy of the vibrational state is somehow connected to the distribution of the contributing orbital combinations, but it was not possible to derive an explicit relation. This problem partly results from the many unknown small components which are part of the wave function.

- An approach to understand the relation between our calculations and the IBA values could be to create a kind of mapping of the IBA bosons that are affected

by the $d^\dagger d$ term[1] in the IBA quadrupole operator onto the corresponding deformed shell model states being important for the microscopical composition of the gamma-vibrational wave function. Perhaps this investigation would bring some insight why the phenomenological formula works, but this is clearly beyond the scope of this thesis.

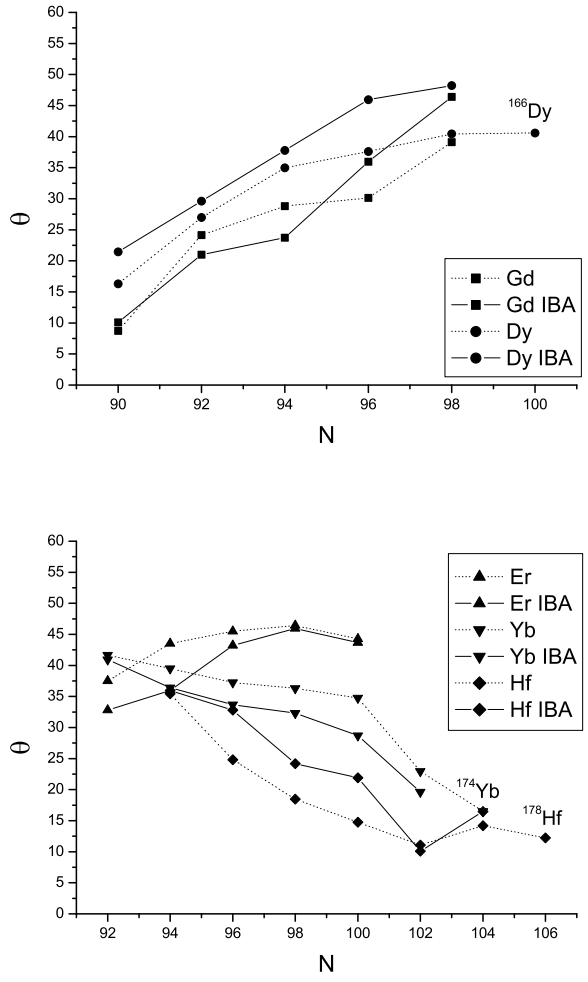

Figure 5.13: Another illustration of the correlation between equation (5.3) and the IBA angle is plotted in these figures. The horizontal axis denotes the neutron number N of the isotopes and the angle in degree is plotted on the vertical axis. The illustration also shows the predicted values resulting from equation (5.3) for the angle θ for Hf N=106, Yb N=104 and Dy N=100. Unfortunately for these isotopes no IBA fits are available.

[1] remember that χ and thus θ determines the strength of its contribution in the IBA quadrupole operator

In figure 5.13 another illustration of the correlation is shown. The solid lines indicate the IBA values and the dashed lines refer to our formula. Using the obtained data from our microscopical calculations for Hf with N=106, Yb with N=104 and Dy with N=100 it was also possible to predict IBA angles θ for these isotopes. For Hf with 106 neutrons the former rise towards gamma-softness for 104 neutrons decreases again yielding an angle of about 12°. The Dy isotope with 100 neutrons preserves the gamma-softness of Dy N=98. Finally for Yb with 104 neutrons we predict a further slope down of the gamma-softness to an angle of about 16°. Unfortunately because of the limitation of the boson number in the computer program used to obtain the IBA fits in Ref. [16] no fits for these isotopes were done.

Summarizing the previous discussion, equation (5.3) suggests the following "microscopical" definition of *gamma-softness* in well deformed rotational nuclei. Actually we have a linear combination of two conditions:

- Nuclei tend to gamma-softness if the neutron and proton part of the collective gamma-vibrational wave function is each dominated by only a few strongly contributing Nilsson states i.e. two quasi-particle excitations. Furthermore the wave function should be distributed in equal parts onto neutrons and protons[2].

- Nuclei with a relatively low lying energy of the gamma-vibrational state $E_{2^+_\gamma}$ in comparison to the energy of the 2^+ state of the ground-state rotational band also tend to a gamma-soft behaviour.

Our formula (5.3) was also applied to well-deformed Os and W isotopes with 100, 102 and 104 neutrons. The results are shown in figure 5.14. It is obvious that the IBA calculations [17] predict significantly lower values for the angle θ and also nearly the same angle for Os and W. Especially for Os the angle derived from our formula is about twice the value from the IBA fits. Moreover the behaviour of Os and W ist not similar.
A closer look at the paper of *McCutchan et al.* [17] reveals that in the fits for the Os and W isotopes the reproduction of the gamma-band was not satisfactory. The level of agreement for the location of the 2^+_γ state varies for different isotopes. It is generally overpredicted, in some cases by about 200keV. One other obvious discrepancy is the staggering in the γ-band for the W and Os nuclei. For the chosen parameters in the simplified Hamiltonian the IBA gives the sequence (2^+, 3^+)(4^+, 5^+) while experimentally a rather constant spacing with increasing spin is observed.

[2] We assume that neutrons and protons oscillate in a coherent manner (isoscalar) in the gamma-vibration: If only one kind of nucleon is able to carry out oscillations (due to available two quasiparticle excitations) the attractive neutron-proton interaction will lead to a significant suppression of the entire motion due to the strong coupling to the rigid nucleon component. Thus it is easier for a nucleus to oscillate if both neutrons and protons equally participate in the vibration leading to gamma-softness.

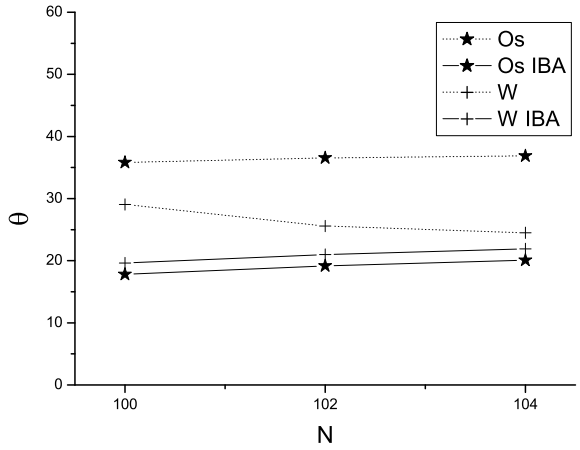

Figure 5.14: Additional application of equation (5.3) to the well-deformed Os and W isotopes. The vertical axis corresponds to the angle θ and the horizontal axis represents the neutron number (see figure 5.13). The IBA values for Os and W are taken from Ref. [17].

Indeed the energy of the 2^+_γ state and the staggering in the γ-band are explicitly connected with the gamma-softness and thus with the angle θ in the symmetry triangle. Gamma-soft nuclei show the sequence $(2^+)(3^+, 4^+)$ in the gamma-band while $(2^+, 3^+)(4^+, 5^+)$ indicates gamma-rigidity.
A further look at the ratio $R_\gamma \equiv \frac{B(E2:2^+_\gamma \to 0^+_1)}{B(E2:2^+_\gamma \to 2^+_1)}$ of reduced transition probabilities connected with the gamma-vibrational state shows that the experimentally known value of about 0.2 for ^{176}Os is not reproduced in the IBA fits [17] yielding a value of about 10 for all Os and W isotopes.
The reason for these discrepancies is that in the paper of *McCutchan et al.* [17] the major priority was laid on a correct reproduction of the ground-state band and the $K = 0$ band.

For the three Os isotopes using a modified version of the program *PHINT* written by *O. Scholten* we have performed our own IBA fits. It turns out that for an angle θ of about 36°, which coincides with the predictions of our calculations in formula (5.3), the experimental gamma-band values are well reproduced. The price we pay for this improvement is the fact that the agreement with the experimental $K = 0$ band is completely lost. But with regard to our microscopical model explicitly treating the gamma-vibration this approach to accurately reproduce the gamma-band seems to be reasonable. The results of our fits are shown in tables 5.2-5.4. It should be emphasized that the determined IBA fits are not optimized to deliver the best fits to the gamma-band that are possible. They only show that an angle of $\theta \approx 36°$ works.

^{176}Os	experimental value	IBA fit value	deviation in percent
2_1^+	135 keV	135 keV	0
4_1^+	395 keV	400 keV	1
6_1^+	742 keV	779 keV	5
$R_{4/2}$	2.93	2.96	–
2_γ^+	864 keV	843 keV	2
3_γ^+	1038 keV	1110 keV	7
4_γ^+	1224 keV	1207 keV	1
0_2^+	601 keV	946 keV	57
$2^+_{K=0\ band}$	742 keV	1272 keV	71
R_γ	0.20	0.17	–

Table 5.2: Our IBA Fit obtained for well-deformed ^{176}Os with the Hamiltonian parameters $\zeta = 0.70$ and $\chi = -0.53$ corresponding to $\theta \approx 36°$ and $N_{Bosons} = 12$. The ratio R_γ is the same as defined in the text.

^{178}Os	experimental value	IBA fit value	deviation in percent
2_1^+	132 keV	132 keV	0
4_1^+	398 keV	396 keV	0
6_1^+	761 keV	774 keV	2
$R_{4/2}$	3.02	3.00	–
2_γ^+	864 keV	897 keV	4
3_γ^+	1032 keV	1152 keV	11
4_γ^+	1213 keV	1258 keV	4
0_2^+	650 keV	1006 keV	55
$2^+_{K=0\ band}$	771 keV	1323 keV	72
R_γ	unknown	0.19	–

Table 5.3: Our IBA Fit obtained for well-deformed ^{178}Os with the Hamiltonian parameters $\zeta = 0.70$ and $\chi = -0.53$ corresponding to $\theta \approx 36°$ and $N_{Bosons} = 13$. The ratio R_γ is the same as defined in the text.

^{180}Os	experimental value	IBA fit value	deviation in percent
2_1^+	132 keV	132 keV	0
4_1^+	408 keV	389 keV	5
6_1^+	795 keV	751 keV	9
$R_{4/2}$	3.09	2.95	–
2_γ^+	870 keV	830 keV	5
3_γ^+	1023 keV	1091 keV	7
4_γ^+	1197 keV	1183 keV	1
0_2^+	736 keV	901 keV	22
$2^+_{K=0\ band}$	831 keV	1223 keV	47
R_γ	unknown	0.17	–

Table 5.4: Our IBA Fit obtained for well-deformed ^{180}Os with the Hamiltonian parameters $\zeta = 0.67$ and $\chi = -0.53$ corresponding to $\theta \approx 36°$ and $N_{Bosons} = 14$. The ratio R_γ is the same as defined in the text.

The fundamental underlying problem with the Os and W isotopes is given by the impossibiltiy to obtain a good description both of the gamma-band and the $K = 0$ band in the context of the simplified IBA Hamiltonian with only two-paramters. Thus it would be appropriate to take some further interaction term (which means more parameters) into account, but this would to some extend spoil the simple mapping of the nuclei into the IBA symmetry triangle. Anyhow, it is nice that the descrption for the Gd, Dy, Er, Hf and Yb isotopes in the context of a simplified IBA Hamiltonian works well, but this simple treatment should always be handled with care. In nuclei like Os and W other interaction terms could be of significant importance and must not be neglected.

Chapter 6

Summary and Outlook

In the present work we have shown a connection between the structural evolution of well-deformed even-even rare earth nuclei within the IBA symmetry triangle and the microscopic composition of the gamma-vibrational wave function in these nuclei. The relevant two quasi-particle components contributing to the vibration were determined in the framework of the Random Phase Approximation (RPA) based on the single-particle structure of the Nilsson model. The pairing residual interaction was also taken into account leading to a more complex ground-state with partial occupancies of levels around the Fermi surface and leading to the substitution of two quasi-particle excitations for particle-hole excitations.
It was possible to understand the evolution of the isotopic chains in the IBA triangle for different nuclei qualitatively on the basis of the gamma correlation function Γ and even quantitatively by additionally taking the R_{22} energy ratio into account (equation (5.3)).
Although the theoretical basis for equation (5.3) could not be derived, it was successfully applied to the Gd, Dy, Er, Hf and Yb isotopic chains showing that there is certainly an underlying relation between the evolution in the IBA symmtery triangle and the microscopical content of the gamma-vibrational wave function. Even without this analytical expansion, the relation between the two pictures is quite obvious. For Os and W the predicted values of the angle θ do not coincide with recent IBA fits [17]. This discrepancy is related to the fact that the IBA parameters used in these Os and W fits were not able to reproduce the gamma-band accurately. At least for the Os isotopes it was possible to show with further IBA fits determined in the present work that the gamma-band is much better reproduced for the angle θ predicted by equation (5.3).

In further investigations the crude approach of the present work should be refined by reducing the numerous simplifications. For example, if additionally the many small components of the wave function as well as the Coriolis Interaction were taken into account, our model would provide the possibility to calculate reduced transition

probabilities. This would be a decisive progress in the predictive power of the model. It could also be interesting to make additional calculations for further nuclei in the quasiparticle-phonon nuclear model (QPNM) [23] used by Soloviev et al. and compare the results with our predictions to continue the verification of our approach. There is no reason why our model should be restricted only to the rare-earth nuclei. An application to other deformed areas, e.g. in the transuranic region, is conceivable.

In most nuclei our calculations tend to a dominance of the neutrons. In some cases the neutron fraction of the wave function is extremely large e.g. for the neutron rich Sm isotopes or in ^{178}Hf (the neutrons make up ≈ 80 percent of the wavefunction). For those nuclei one could think of experiments to confirm these predictions. As already mentioned, the neutron dominance could lead to strong M1 transitions from the 2^+_γ state to the 2^+_1 state. A further reasonable experiment could be the measurement of the g-factor for those isotopes which is sensitive to the neutron and proton compositon of the wavefunction.
In order to get a direct insight into the two quasi-particle content of the gamma-vibration it is possible to determine the states of major importance to the wave function in single nucleon transfer reactions. This method is capable to deliver detailed information about the relative amplitudes of the contributing states. These experiments have been done for a number of nuclei, see for example Ref. [25, 26]. Further experiments may help to test our predictions.

Appendix A

Data tables for the rare earth nuclei

N	90	92	94	96	98
β_2	0,243	0,270	0,279	0,279	0,290
$E_{2_1^+}$	121,8	82,0	75,9	72,8	70,9
$E_{4_1^+}$	366,5	266,8	249,7	240,3	233,3
$E_{2_\gamma^+}$	1085,9	1440,1	1441,0	1441,0[a]	1441,0[a]
$R_{4/2}$	3,01	3,25	3,29	3,30	3,29
$R_{2/2}$	8,92	17,56	18,99	19,79	20,32

Table A.1: Experimental values of the ground state deformation parameter β_2, the energy levels $E_{2_1^+}$, $E_{4_1^+}$, $E_{2_\gamma^+}$ in keV and the energy ratios $R_{4/2} = \frac{E_{4_1^+}}{E_{2_1^+}}$, $R_{2/2} = \frac{E_{2_\gamma^+}}{E_{2_1^+}}$ for **Sm isotopes**.[a] indicates that no experimental data is available for these states. Therefore we use the know value for ^{156}Sm. All experimental values are taken from the National Nuclear Data Center [34] and the Raman compilation [29], respectively.

N	88	90	92	94	96	98
β_2	0,207	0,243	0,271	0,271	0,280	0,291
$E_{2_1^+}$	344,3	123,1	89,0	79,5	75,3	72,1
$E_{4_1^+}$	755,4	380,0	288,2	261,5	248,5	237,3
$E_{2_\gamma^+}$	1109,2	996,3	1154,2	1187,1	988,4	864,0
$R_{4/2}$	2,19	3,09	3,24	3,29	3,30	3,29
$R_{2/2}$	3,22	8,09	12,97	14,93	13,13	11,98

Table A.2: Experimental values of the ground state deformation parameter β_2, the energy levels $E_{2_1^+}$, $E_{4_1^+}$, $E_{2_\gamma^+}$ in keV and the energy ratios $R_{4/2} = \frac{E_{4_1^+}}{E_{2_1^+}}$, $R_{2/2} = \frac{E_{2_\gamma^+}}{E_{2_1^+}}$ for **Gd isotopes**. All experimental values are taken from the National Nuclear Data Center [34] and the Raman compilation [29], respectively.

N	88	90	92	94	96	98	100
β_2	0,207	0,235	0,262	0,272	0,281	0,292	0,293
$E_{2_1^+}$	334,6	137,8	98,9	86,8	80,7	73,4	76,6
$E_{4_1^+}$	747,0	404,2	317,1	283,8	265,7	242,2	253,5
$E_{2_\gamma^+}$	1027,1	890,5	946,3	966,2	888,2	761,8	857,2
$R_{4/2}$	2,23	2,93	3,21	3,27	3,29	3,30	3,31
$R_{2/2}$	3,07	6,46	9,57	11,13	11,01	10,38	11,19

Table A.3: Experimental values of the ground state deformation parameter β_2, the energy levels $E_{2_1^+}$, $E_{4_1^+}$, $E_{2_\gamma^+}$ in keV and the energy ratios $R_{4/2} = \frac{E_{4_1^+}}{E_{2_1^+}}$, $R_{2/2} = \frac{E_{2_\gamma^+}}{E_{2_1^+}}$ for **Dy isotopes**. All experimental values are taken from the National Nuclear Data Center [34] and the Raman compilation [29], respectively.

N	92	94	96	98	100
β_2	0,253	0,272	0,273	0,283	0,294
$E_{2_1^+}$	125,8	102,0	91,4	80,6	79,8
$E_{4_1^+}$	389,9	329,6	299,4	265,0	264,1
$E_{2_\gamma^+}$	854,4	900,7	860,3	785,9	821,2
$R_{4/2}$	3,10	3,23	3,28	3,29	3,31
$R_{2/2}$	6,79	8,83	9,41	9,75	10,29

Table A.4: Experimental values of the ground state deformation parameter β_2, the energy levels $E_{2_1^+}$, $E_{4_1^+}$, $E_{2_\gamma^+}$ in keV and the energy ratios $R_{4/2} = \frac{E_{4_1^+}}{E_{2_1^+}}$, $R_{2/2} = \frac{E_{2_\gamma^+}}{E_{2_1^+}}$ for **Er isotopes**. All experimental values are taken from the National Nuclear Data Center [34] and the Raman compilation [29], respectively.

N	92	94	96	98	100	102	104
β_2	0,225	0,264	0,274	0,284	0,295	0,296	0,287
$E_{2_1^+}$	166,9	123,3	102,4	87,7	84,3	78,7	76,5
$E_{4_1^+}$	487,6	385,6	330,5	286,6	277,4	260,3	253,1
$E_{2_\gamma^+}$	798,7	853,9	932,4	983,9	1145,7	1465,9	1634,0
$R_{4/2}$	2,92	3,13	3,23	3,27	3,29	3,31	3,31
$R_{2/2}$	4,79	7,01	9,11	11,26	13,59	18,63	21,36

Table A.5: Experimental values of the ground state deformation parameter β_2, the energy levels $E_{2_1^+}$, $E_{4_1^+}$, $E_{2_\gamma^+}$ in keV and the energy ratios $R_{4/2} = \frac{E_{4_1^+}}{E_{2_1^+}}$, $R_{2/2} = \frac{E_{2_\gamma^+}}{E_{2_1^+}}$ for **Yb isotopes**. All experimental values are taken from the National Nuclear Data Center [34] and the Raman compilation [29], respectively.

N	94	96	98	100	102	104	106
β_2	0,226	0,254	0,274	0,284	0,285	0,277	0,278
$E_{2_1^+}$	158,5	124,0	100,8	95,2	91,0	88,4	93,2
$E_{4_1^+}$	470,3	385,6	322,0	309,2	297,4	290,2	306,6
$E_{2_\gamma^+}$	810,1	875,4	961,3	1075,3	1226,8	1341,3	1174,6
$R_{4/2}$	2,97	3,11	3,19	3,25	3,27	3,28	3,29
$R_{2/2}$	5,11	7,06	9,54	11,30	13,48	15,17	12,60

Table A.6: Experimental values of the ground state deformation parameter β_2, the energy levels $E_{2_1^+}$, $E_{4_1^+}$, $E_{2_\gamma^+}$ in keV and the energy ratios $R_{4/2} = \frac{E_{4_1^+}}{E_{2_1^+}}$, $R_{2/2} = \frac{E_{2_\gamma^+}}{E_{2_1^+}}$ for **Hf isotopes**. All experimental values are taken from the National Nuclear Data Center [34] and the Raman compilation [29], respectively.

N	100	102	104
β_2	0,265	0,266	0,267
$E_{2_1^+}$	113,0	107,8	106,1
$E_{4_1^+}$	356,4	347,5	343,3
$E_{2_\gamma^+}$	1010,0	1040,0	1110,8
$R_{4/2}$	3,15	3,22	3,24
$R_{2/2}$	8,94	9,65	10,47

Table A.7: Experimental values of the ground state deformation parameter β_2, the energy levels $E_{2_1^+}$, $E_{4_1^+}$, $E_{2_\gamma^+}$ in keV and the energy ratios $R_{4/2} = \frac{E_{4_1^+}}{E_{2_1^+}}$, $R_{2/2} = \frac{E_{2_\gamma^+}}{E_{2_1^+}}$ for **W isotopes**. All experimental values are taken from the National Nuclear Data Center [34] and the Raman compilation [29], respectively.

N	100	102	104
β_2	0,246	0,247	0,238
$E_{2_1^+}$	135,1	131,6	132,1
$E_{4_1^+}$	395,3	397,7	408,6
$E_{2_\gamma^+}$	863,6	864,3	870,4
$R_{4/2}$	2,93	3,02	3,09
$R_{2/2}$	6,39	6,57	6,59

Table A.8: Experimental values of the ground state deformation parameter β_2, the energy levels $E_{2_1^+}$, $E_{4_1^+}$, $E_{2_\gamma^+}$ in keV and the energy ratios $R_{4/2} = \frac{E_{4_1^+}}{E_{2_1^+}}$, $R_{2/2} = \frac{E_{2_\gamma^+}}{E_{2_1^+}}$ for **Os isotopes**. All experimental values are taken from the National Nuclear Data Center [34] and the Raman compilation [29], respectively.

N	106	108	110	112	114	116	118
β_2	0,224	0,198	0,180	0,149	0,153	0,143	0,130
$E_{2_1^+}$	163,0	191,5	265,6	295,8	316,5	328,5	355,7
$E_{4_1^+}$	436,0	490,3	671,0	737,0	784,6	811,3	876,9
$E_{2_\gamma^+}$	648,8	607,2	605,7	597,6	612,5	622,0	688,7
$R_{4/2}$	2,67	2,56	2,53	2,49	2,48	2,47	2,47
$R_{2/2}$	3,98	3,17	2,28	2,02	1,94	1,89	1,94

Table A.9: Experimental values of the ground state deformation parameter β_2, the energy levels $E_{2_1^+}$, $E_{4_1^+}$, $E_{2_\gamma^+}$ in keV and the energy ratios $R_{4/2} = \frac{E_{4_1^+}}{E_{2_1^+}}$, $R_{2/2} = \frac{E_{2_\gamma^+}}{E_{2_1^+}}$ for **Pt isotopes**. All experimental values are taken from the National Nuclear Data Center [34] and the Raman compilation [29], respectively.

Appendix B

Nilsson Diagrams for neutrons and protons

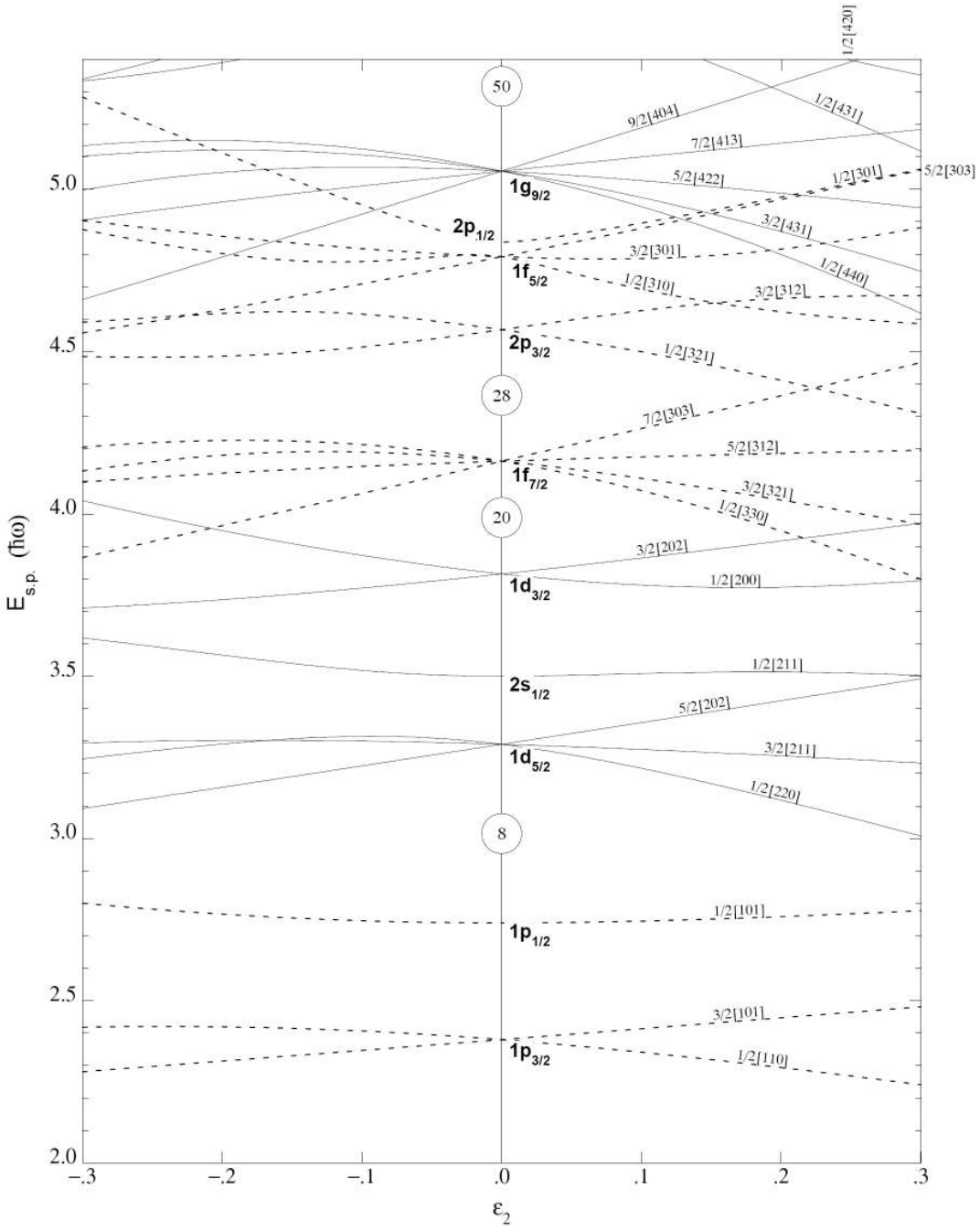

Figure B.1: Nilsson diagram for protons and neutrons, Z, N $\leq$ 50, taken from the Nuclear Data Sheets [33].

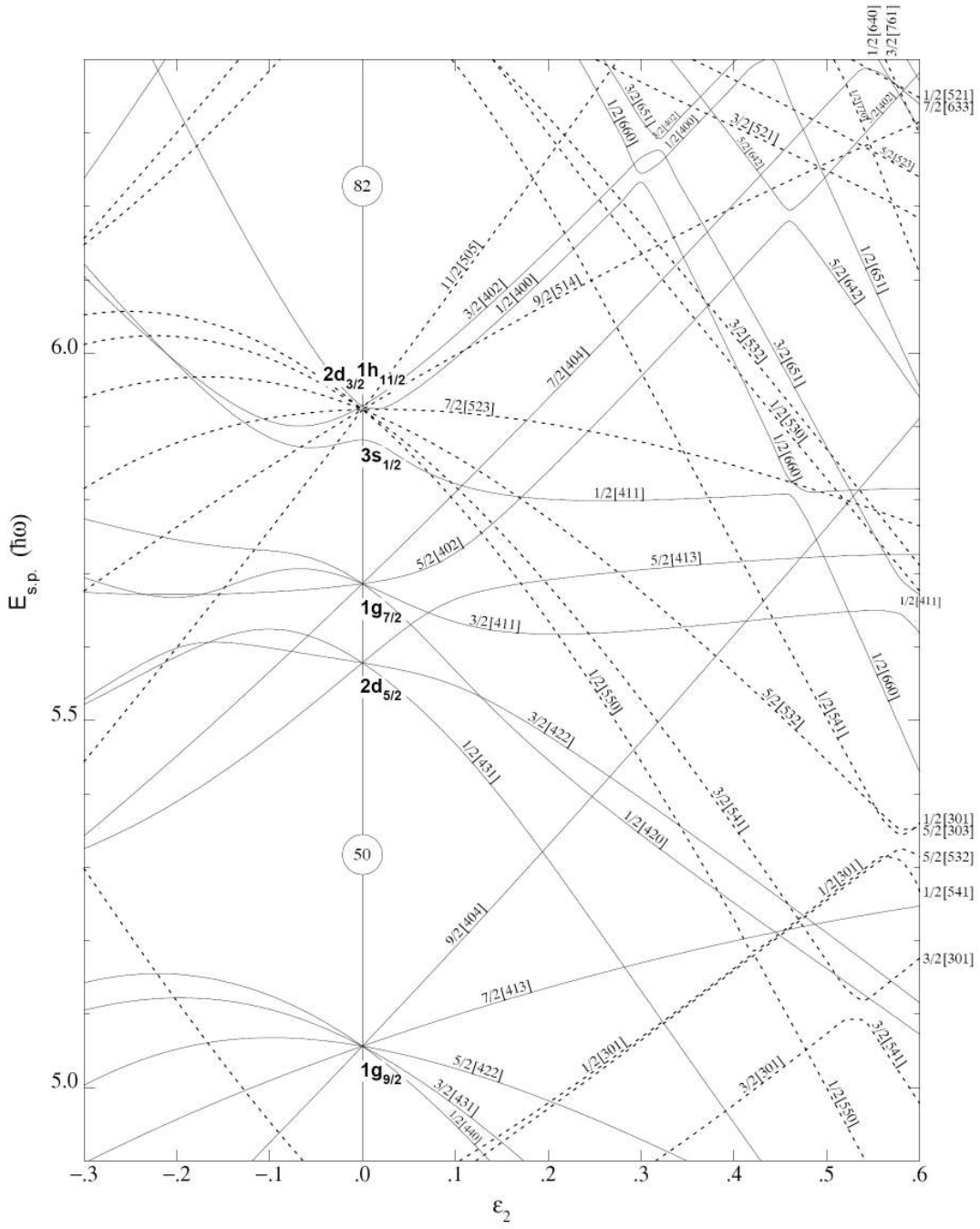

Figure B.2: Nilsson diagram for neutrons, $50 \leq N \leq 82$, taken from the Nuclear Data Sheets [33].

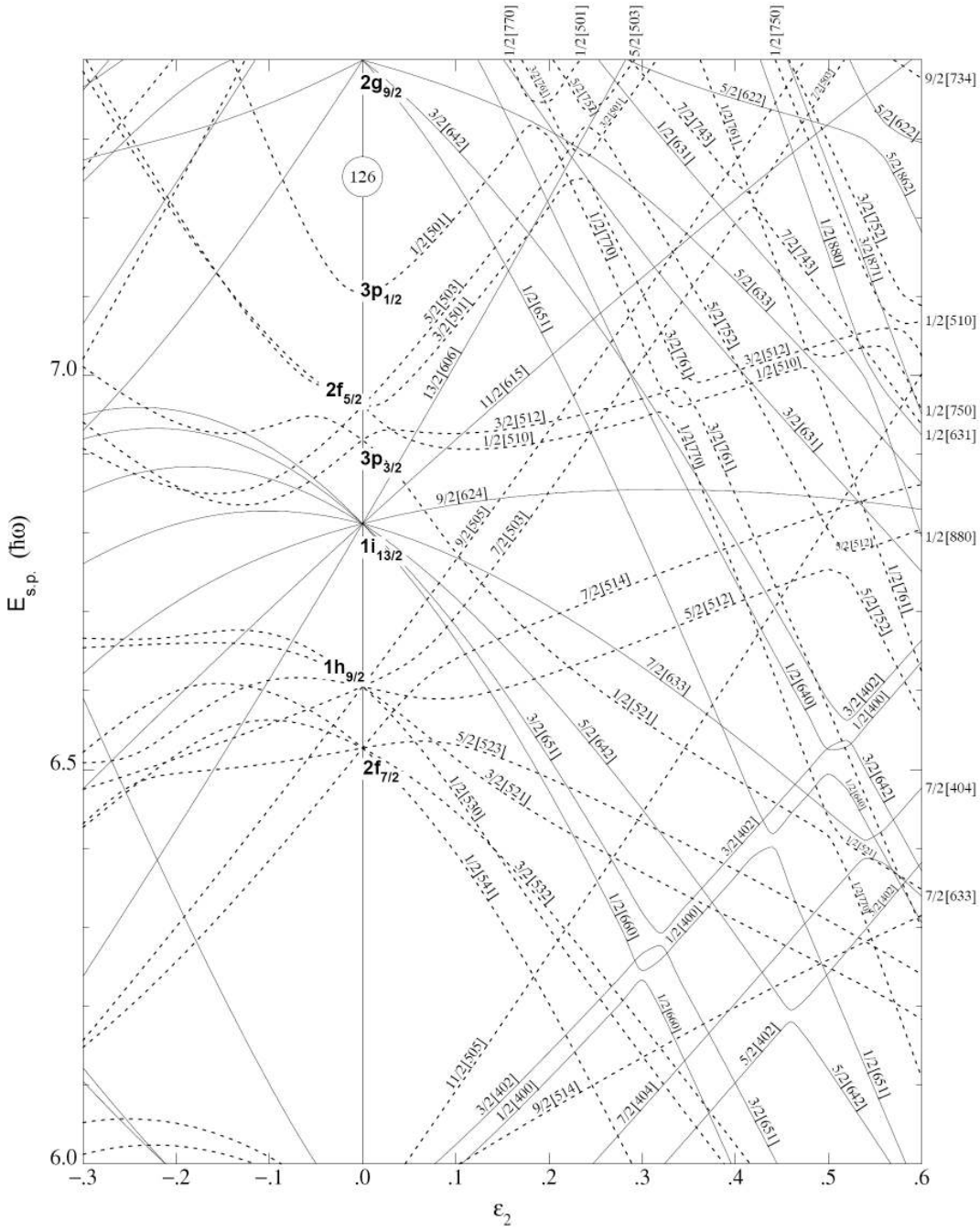

Figure B.3: Nilsson diagram for neutrons, $82 \leq N \leq 126$, taken from the Nuclear Data Sheets [33].

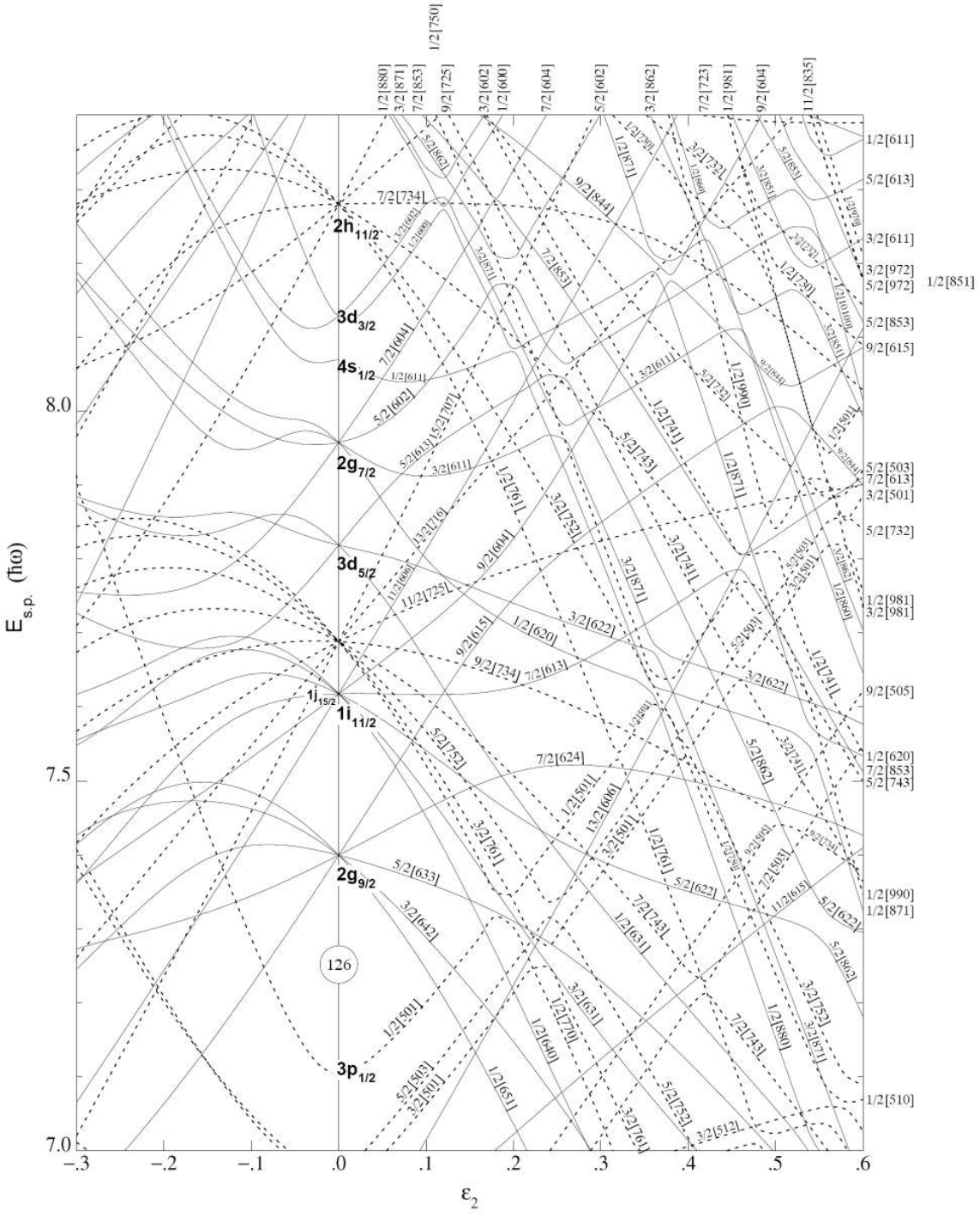

Figure B.4: Nilsson diagram for neutrons, N $\geq$ 126, taken from the Nuclear Data Sheets [33].

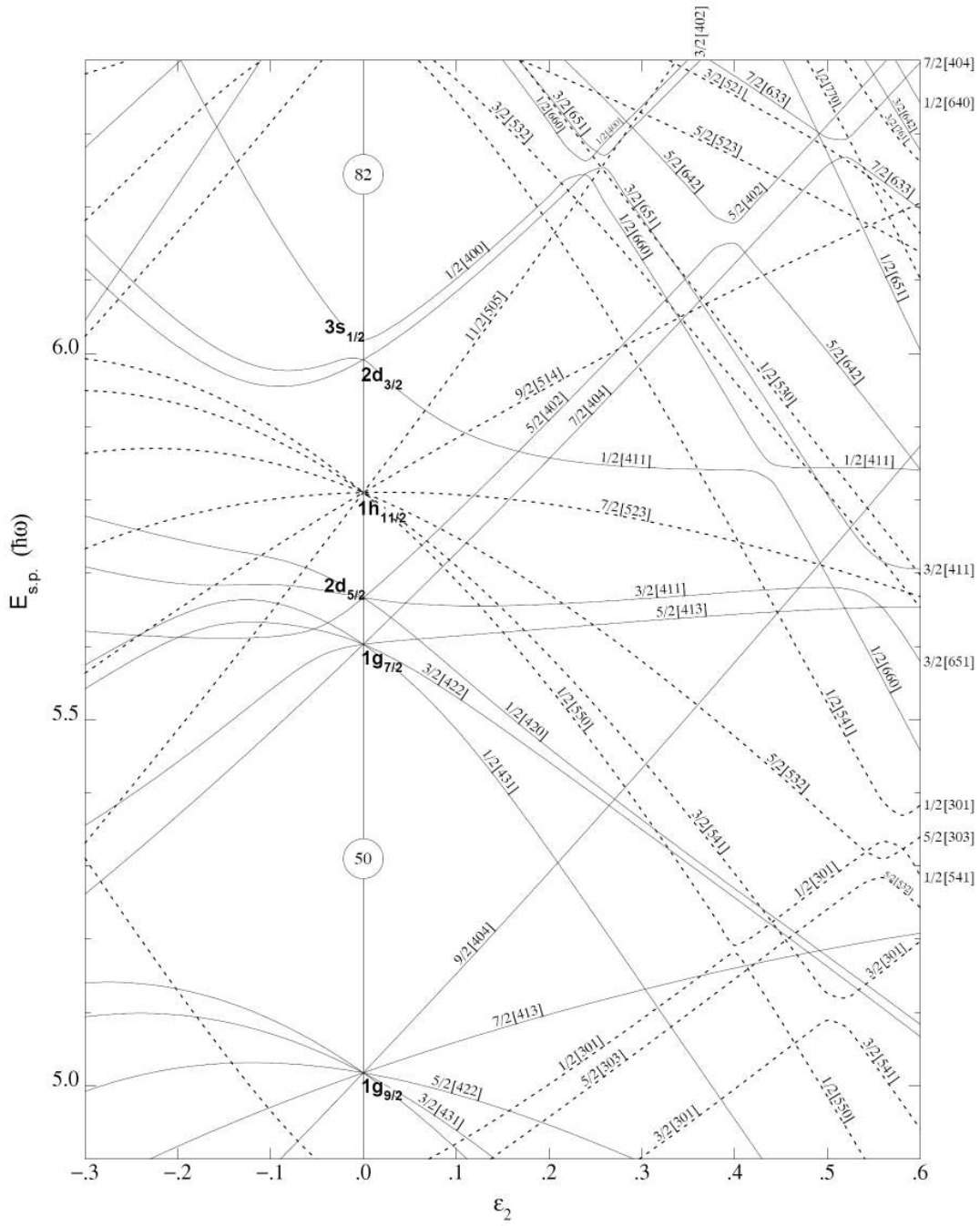

Figure B.5: Nilsson diagram for protons, $50 \leq Z \leq 82$, taken from the Nuclear Data Sheets [33].

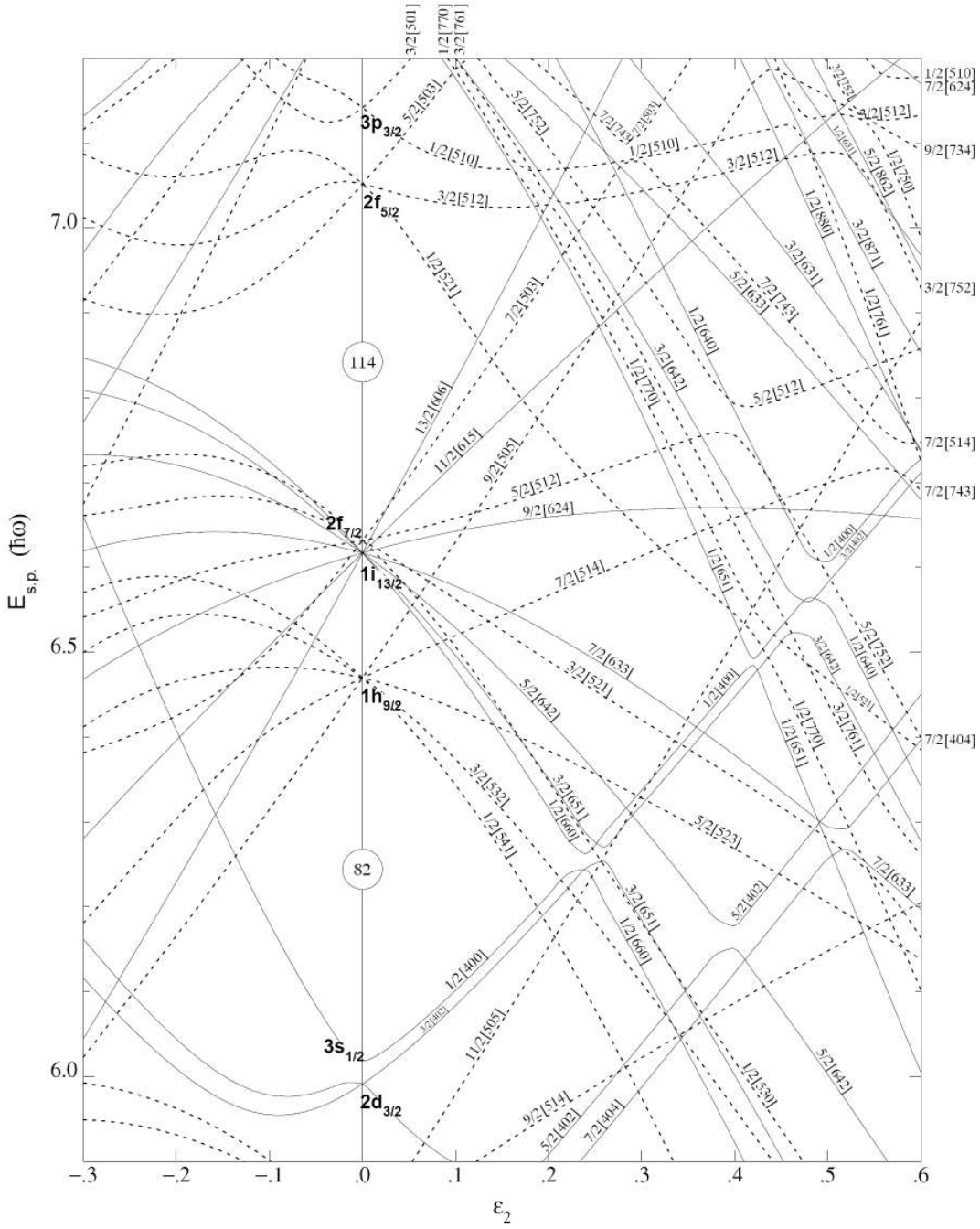

Figure B.6: Nilsson diagram for protons, Z $\geq$ 82, taken from the Nuclear Data Sheets [33].

Bibliography

[1] W. Greiner, J. Maruhn, "Kernmodelle", (1995), Verlag Harri Deutsch, Thun und Frankfurt am Main

[2] T. Mayer-Kuckuk, "Kernphysik", (2002), Teubner Verlag, Stuttgart Leipzig Wiesbaden

[3] Povh, Rith, Scholz, Zetsche, "Teilchen und Kerne", (2001), Springer Verlag, Berlin Heidelberg New York

[4] H. Frauenfelder, E.M. Henley, "Teilchen und Kerne", (1999), Oldenbourg Verlag, München und Wien

[5] R.F. Casten, "Nuclear Structure from a Simple Perspective", (2000), Oxford University Press

[6] S.C. Pieper, K. Varga, R.B. Wiringa, Phys. Rev. **C 66**, 044310 (2002).

[7] D. Vretenar, A.V. Afanasjev, G.A. Lalazissis, P. Ring, Physics Reports **409**, 101-259 (2005)

[8] M. Bender *et al.*, Reviews of Modern Physics, Volume 75, 121 January 2003

[9] Trieste Lectures 1969, "Theory of Nuclear Structure", (1970), International Atomic Energy Agency, 1969

[10] "Collective Phenomena in Atomic Nuclei", International Review of Nuclear Physics, Vol. 2, (1984), World Scientific, Singapore

[11] P. Ring, P. Schuck, in *The Nuclear Many Body Problem* (Springer, Heidelberg, 1980), pp. 200

[12] S.G. Nilsson, Mat. Fys. Medd. Dan. Vid. Selsk. **29** No. 16 (1955).

[13] A. Arima and F. Iachello, Phys. Rev. Lett. **35**, 1069 (1975).

[14] P.O. Lipas, P. Toivonen, and D.D. Warner, Phys. Lett. **155B**, 295 (1985).

[15] R.F. Casten, D. D. Warner, "The interacting boson approximation", Reviews of Modern Physics, Vol. 60, No. 2, April 1988

[16] E.A. McCutchan, N.V. Zamfir, and R.F. Casten, Phys. Rev. **C69**, 064306 (2004).

[17] E.A. McCutchan and N.V. Zamfir, Phys. Rev. C **71** 054306 (2005).

[18] E.A. McCutchan, R.F. Casten, and N.V. Zamfir, Phys. Rev. C **71** 061301 (R) (2005).

[19] R.F. Casten and D.D. Warner, in *Progress in Particle and Nuclear Physics*, edited by D. Wilkinson (Pergamon, Oxford, 1983), Vol. 9, p. 311.

[20] D.R. Bès, P. Federman, E. Maqueda, and A. Zuker, Nucl. Phys. **65**, 1 (1965).

[21] V.G. Soloviev, Sov. J. Part. Nucl **9**, 343 (1978).

[22] V.G. Soloviev, *Theory of the Nucleus. Quasiparticles and Phonons* (Institute of Physics, Bristol, England, 1992) [Russ. original, Energoatomizdat, Moscow, 1989].

[23] V.G. Soloviev, A.V. Sushkov, and N.Yu. Shirikova, Phys. Part. Nucl. **25**, 157 (1994).

[24] V.G. Soloviev, A.V. Sushkov, and N.Yu. Shirikova, Phys. Part. Nucl. **27**, 667 (1996).

[25] D.G. Burke, V.G. Soloviev, A.V. Sushkov, N.Yu. Shirikova, Nucl. Phys. **A 656**, 287 (1999).

[26] D.G Burke *et al.*, Nucl. Phys. **A 569**, 523 (1994).

[27] V.G. Soloviev, A.V. Sushkov, and N.Yu. Shirikova, Physics of Atomic Nuclei, **Vol. 60, No. 10**, 1599 (1997).

[28] A.J. Rassey, Phys. Rev. **109**, 949 (1958).

[29] S. Raman *et al.*, Atomic Data and Nuclear Data Tables 78, 1 (2001).

[30] Nucl. Data Sheets, through Vol. 94, Issue 4 (2001).

[31] O. Scholten, F. Iachello, and A. Arima, Ann. Phys. (N.Y.) **115** 325 (1978).

[32] J.A. Cizewski, R.F. Casten, G.J. Smith, M.L. Stelts, W.R. Kane, H.G. Börner, and W.F. Davidson, Phys. Rev. Lett. **40**, 167 (1978).

[33] Nilsson Diagrams from the Nuclear Data Sheets available online at the "Table of Superdeformed Nuclear Bands and Fission Isomers", McMaster University, Ontario, Canada *http://physwww.physics.mcmaster.ca/ balraj/sdbook/*

[34] National Nuclear Data Center at the Brookhaven National Laboratory *http://www.nndc.bnl.gov/*

Danksagung

Diese Diplomarbeit wäre nicht möglich gewesen ohne die Unterstützung einiger Menschen. Ich danke

- Reiner Krücken, der mir die Möglichkeit gab, an seinem Lehrstuhl an diesem Thema zu arbeiten, der mir stets mit Ratschlägen hilfreich zur Seite stand und der mir tatkräftig bei der Gestaltung der Diplomarbeit half.
- meinen Eltern ohne die das Studium der Physik überhaupt nicht möglich gewesen wäre.
- meinem Studienkollegen und guten Freund Dominik Bauer für seinen Beistand und seine Hilfe in schweren Zeiten.

Erklärung

Hiermit versichere ich, dass ich die vorliegende Arbeit ohne unzulässige Hilfe Dritter und ohne Benutzung anderer als der angegebenen Hilfsmittel angefertigt habe; die aus fremden Quellen direkt oder indirekt übernommenen Gedanken sind als solche kenntlich gemacht. Die Arbeit wurde bisher weder im Inland noch im Ausland in gleicher oder ähnlicher Form einer anderen Prüfungsbehörde vorgelegt.